

**Urban Growth and LULC Change Dynamics Using Landsat
Record of Region of Waterloo from 1984 to 2013**

by
Anqi Fu

A thesis
presented to the University of Waterloo
in fulfillment of the
thesis requirement for the degree of
Master of Science
in
Geography

Waterloo, Ontario, Canada, 2014

© Anqi Fu 2014

Author's Declaration

I hereby declare that I am the sole author of this thesis. This is a true copy of the thesis, including any required final revisions, as accepted by my examiners.

I understand that my thesis may be made electronically available to the public.

Abstract

Frequent human activities resulted by rapid urbanization lead to a variety of urban-related environmental and socio-economic issues. Therefore, for effective environmental management and urban planning, monitoring urban growth and detecting its resulting land use and land cover (LULC) change is very important. Most of the previous studies focused on bi-temporal or coarsely multi-temporal change detection to extract stationary change information over a time span. However, higher-order change information, for instance, acceleration or deceleration of urban growth, which would not be observed by bi-temporal method, is more meaningful information for policy makers to understand the urbanization process.

With the free access to the USGS Landsat archive and development of remote sensing techniques, detecting urban growth pattern (intensification or sprawl) and LULC change dynamics with temporally high frequent datasets become possible. In this study, bi-temporal, multi-temporal and long-term annual change detection were applied to the Region of Waterloo, Ontario, Canada, to identify the urban growth pattern and LULC change dynamics. Classification was performed for each scene to extract LULC information from 1984 to 2013.

This study demonstrates that machine learning classifiers, such as support vector machine (SVM), random forest (RF) and artificial neural network (ANN), perform better than classical maximum likelihood classifier (MLC), among which SVM performs the best. Total urban built-up area of the Region of Water increased from 30% in 1984 to 55% in 2013, replacing large area of vegetated area (agricultural lands and grassland. Outward (sprawl) and inward (intensification) growth patterns were detected both spatially and temporally. Within this time

span, built-up area experienced a relatively accelerating growth in 1990s and in early 2000s. In terms of long-term record, Kitchener had the fastest growing rate of low-density built-up (residential) area. The coverage of high-density built-up (commercial and industrial) area in Cambridge increased most dramatically. And the built-up area of Waterloo experienced the lowest growth rate. These important findings indicate that using long-term temporal-dense Landsat datasets enables monitoring of urban growth and LULC change dynamics. Such valuable long-term results can be used for better analysis of urban growth and LULC change patterns for planners and policy makers to comprehensively understand the urbanization process in the past and make better planning in the future.

Acknowledgements

First and foremost I offer my sincerest gratitude to my supervisor, Professor Dr. Jonathan Li, for his patience, motivation, enthusiasm, and immense knowledge. Through his valuable advice and support, I have learned how to study as a researcher and think in critical ways. Without his strong encouragement, I could not complete this thesis successfully.

Second, I would like to sincerely thank my Thesis Examining Committee members, Dr. Richard Kelly, Dr. Peter Deadman, and Dr. Joe Qian, for their encouragement, insightful comments, and hard questions.

Third, my thanks go to Haiyan Guan for her valuable suggestions on my programming work and for the stimulating discussions. Appreciation also goes out to the MAD's Technical Support Group for all their computer and technical assistance throughout my graduate program, and to Susie Castela and Diane Ridler, the office staff at the Department of Geography and Environmental Management for all the instances in which their assistance helped me along the way. I would also like to thank Chen Shang, Weigang Tang, Xu Sun for giving me valuable advice on my thesis, and thank my good friends, Qing Xiang, Junzhu Li, Lisha Zhou, for all the fun we have had in the past two and a half years.

Last but not least, I would like to extend my sincerest gratitude to my family for their constant source of love, support, and encouragement.

Table of Contents

Author’s Declaration.....	ii
Abstract	iii
Acknowledgements.....	v
List of Figures	viii
List of Tables	x
List of Abbreviations	xi
Chapter 1 Introduction	1
1.1 Urbanization of the Region of Waterloo.....	1
1.2 Motivations of the Study.....	2
1.3 Objectives of the Study	5
1.4 Structure of the Thesis	5
Chapter 2 Literature Review	7
2.1 Satellite Data for Monitoring Urban Dynamics.....	7
2.1.1 Overview of Earth Observation Satellites and Sensors	8
2.1.2 Introduction to USGS Landsat Archive Data	11
2.2 Urban Growth and LULC Change Detection	15
2.2.1 Overview of Widely Used Change Detection Methods.....	15
2.2.2 Detecting LULC Change and Monitoring Urban Growth Using Landsat Data: An Overview.....	19
2.3 Review of LULC classification Methods	25
2.3.1 Overview of Classification Techniques	25
2.3.2 Machine Learning Techniques.....	29
2.4 Chapter Summary	33
Chapter 3 Study Area and Data	34
3.1 Study Area	34
3.2 Data	37
3.2.1 Landsat Archive Data	38
3.2.2 Supplementary Data.....	39
3.3 Chapter Summary	40
Chapter 4 Methodology	41
4.1 Overview of Workflow	41

4.2 Data Preprocessing.....	42
4.3 Image Classification.....	45
4.3.1 Workflow of image classification module.....	45
4.3.2 Training Samples Selection	48
4.3.3 Classification Techniques	50
4.3.4 Accuracy Assessment	58
4.4 Change Detection Analysis.....	61
4.5 Urban Growth Analysis	62
4.6 Chapter Summary	65
Chapter 5 Results and Analysis	66
5.1 Classification.....	66
5.1.1 Class Separability.....	66
5.1.2 Comparison of Classifiers.....	67
5.2 Analysis of LULC Change.....	72
5.2.1 Bi-Temporal Change Detection Analysis	72
5.2.2 Multi-Temporal Change Detection Analysis	78
5.2.3 Time-Serial Change Dynamics Analysis	82
5.3 Urban Growth Analysis	85
5.3.1 Analysis of Urban Growth Pattern.....	85
5.3.2 Long-Term Processes of Population Growth and Urban Growth.....	87
5.3.3 Linear Regression analysis of Urban Growth.....	89
5.4 Chapter Summary	92
Chapter 6 Conclusions and Recommendations.....	94
6.1 Key Findings of the Study	94
6.1.1 Performance of Classifiers.....	94
6.1.2 LULC Change Dynamics of Urban Area of Region of Waterloo	95
6.1.3 Urban Growth Monitoring of the Region of Waterloo	96
6.2 Limitations and Uncertainties of This Study	97
6.3 Recommendations for Future Studies	99
References.....	100
Appendix I	114
Appendix II	115
Appendix III.....	116

List of Figures

Figure 2.1 Time scale of several remote sensing systems (Source: Patino & Duque, 2012)	11
Figure 2.2 Top 10 primary Landsat data uses (Source: USGS, 2013).....	12
Figure 3.1 Location of Region of Waterloo.....	35
Figure 3.2 Urban area of Waterloo Region (Source: ROP, 2010).....	36
Figure 3.3 Map of study area	37
Figure 4.1 Summarized workflow chart	41
Figure 4.2 Workflow chart of data preprocessing module	43
Figure 4.3 Workflow chart of image classification module	47
Figure 4.4 Concept of MLC algorithm (Source: JARS, 1999).....	51
Figure 4.5 An example of MLP neural network (Source: Yang, 2011)	52
Figure 4.6 Example of the optimal separating hyperplane between (a) separable sample and (b) non-separable samples (Adapted from Huang et al., 2002).....	54
Figure 4.7 Workflow chart of change detection analysis module	61
Figure 4.8 Workflow chart of urban growth analysis module.....	63
Figure 5.1 Classification maps of 2006 generated by (a) MLC, (b) ANN, (c) SVM, (d) RF, and (e) SVM with post-classification processing	68
Figure 5.2 Classification maps of (a) 1984 and (b) 2013	73
Figure 5.3 Examples of real scenes of several LULC types	74
Figure 5.4 Change map showing alteration from vegetated area to built-up area	75
Figure 5.5 Pie chart of LULC coverage of 1984 and 2013.....	76
Figure 5.6 Classification maps of (a) 1984, (b) 1990, (c) 1996, (d) 2002, (e) 2008, and (f) 2013	80
Figure 5.7 Normalized net change in municipality area by time period for each LULC class .	82
Figure 5.8 LULC dynamic change from 1984 to 2013.....	83
Figure 5.9 Map of the sprawl of urban built-up area	85
Figure 5.10 Examples of three urban growth patterns.....	87
Figure 5.11 Population growth and urbanization process during recent 30 years	88
Figure 5.12 Dynamic change of low-density urban built-up area of Waterloo, Kitchener, and Cambridge from 1984 to 2013.....	89
Figure 5.13 Dynamic change of high-density urban built-up area of Waterloo, Kitchener, and Cambridge from 1984 to 2013.....	90

Figure 5.14 Dynamic change of total urban built-up area of Waterloo, Kitchener, and
Cambridge from 1984 to 2013..... 90

List of Tables

Table 2.1 Most often used EO systems for urban area analysis	10
Table 2.2 Band designations for Landsat sensors	14
Table 2.3 Summary of most often used change detection methods.....	17
Table 2.4 Useful indices and their expressions.....	20
Table 2.5 Summary of classification techniques	28
Table 3.1 Landsat images used for classification	38
Table 4.1 Explanations of the classes and examples of training sites	49
Table 5.1 Class separability of training samples of 2006 image	67
Table 5.2 Accuracy assessment of classification maps generated by different classifiers	70
Table 5.3 “From-to” change confusion matrix	77
Table 5.4 Statistics of multi-temporal LULC net change	79
Table 5.5 Percentage of each class in municipality area for each year.....	84
Table 5.6 Growth rates of population and urban area.....	88
Table 5.7 Summary of regression coefficient and fit of linear regression model of urban built-up area over time from 1984 to 2013 for Waterloo, Kitchener, Cambridge.....	92

List of Abbreviations

ANN: Artificial Neural Network
BRBA: Band Ratio for Built-up Area
CVA: Change Vector Analysis
CTT: Canada's Technology Triangle
ETM+: Enhanced Thematic Mapper Plus
EO: Earth Observation
GIS: Geographic Information System
ISODATA: Iterative Self Organizing Data Analysis
LSMA: Linear Spectral Mixture Analysis
LULC: Land Use and Land Cover
MLC: Maximum Likelihood Classifier
MLP: Multi-Layer Perceptron
MNDWI: Modified Normalized Difference Water Index
MNF: Minimum Noise Fraction
MSS: Multi-Spectral Scanner
NAD83: North American Datum of 1983
NBAI: Normalized Built-up Area Index
NBI: New Built-up Index
NDBI: Normalized Difference Built-up Index
NDISI: Normalized Difference Impervious Surface Index
NDVI: Normalized Difference Vegetation Index
OBIA: Object-Based Image Analysis
OLI: Operational Land Imager
OOB: Out-Of-Bag
PCA: Principal Component Analysis
PCCD: Post-Classification Change Detection
RBF: Radial Basis Function
RF: Random Forest
RMSE: Root Mean Square Error
ROP: Regional Official Plan
SAVI: Soil Adjusted Vegetation Index
SVM: Support Vector Machine
TIRS: Thermal Infrared Sensor
TM: Thematic Mapper
USGS: U.S. Geological Survey
UTM: Universal Transverse Mercator
WGS84: World Geodetic System of 1984

Chapter 1 Introduction

1.1 Urbanization of the Region of Waterloo

To date, the entire world is continuously experiencing rapid urbanization (Kressler & Steinnocher, 1996; Ridd & Hipple, 2006). The Region of Waterloo, located in southern Ontario and comprised of cities of Waterloo, Kitchener, Cambridge, along with four rural townships (North Dumfries, Wellesley, Wilmot, and Woolwich), is one of the rapidest growing regions in Canada after its formation in 1973 (RGMS, 2006; Region of Waterloo, 2010). With its fast industrialization process, advanced technology and innovation in recent decades, the Region of Waterloo, also represented as Canada's Technology Triangle (CTT) (CTT, 2013), has attracted lots of investment and experienced rapid economic growth (Region of Waterloo, 2010). Consequently, numerous job opportunities, abundant social services and comfortable living environment appealed to more people to settle down here (RGMS, 2006). Based on census data from Statistics Canada (2011), population of urban area of Waterloo Region has increased by 5.7% to more than 470,000 from 2006 to 2011. With such tremendous population growth, urban area of Waterloo Region is now ranked as the 4th largest in Ontario and 10th largest in Canada (Statistics Canada, 2011).

In terms of constant and rapid population growth, the regional community keeps growing (RGMS, 2006). From environmental perspective, urban growth, mainly caused by population growth and frequent human activities, such as industrialization, migration from rural to urban area and resettlement (Bhatta, 2010; Ridd & Hipple, 2006), will inevitably lead to land use changes and landscape pattern alteration at local and regional scale (Yin et al., 2011; Gluch, 2002; Tan & Lim, 2010; Stefanov et al., 2001; Deng et al., 2009; Sundarakumar et al.,

2012). Those changes include losses of agriculture fields, water bodies, forest and other vegetated green spaces and non-vegetated fields (Yang, 2002; Sexton et al., 2013; Sundarakumar et al., 2012; Yin et al., 2011). Disturbance of natural environment by urban growth can bring about various urban environmental issues, such as climate change, urban heat island effect, water quality deterioration, vegetation degradation, increased flooding risk, decreased air quality and so on (Bhatta, 2010; Sexton et al., 2013; Li et al., 2011; Tan & Lim, 2010; Sundarakumar et al., 2012; Nong & Du, 2011; Thapa & Murayama, 2009). Additionally, increased population density, housing condition, education, employment, public facilities accessibility, infrastructure sufficiency, and quality of life and so on are important socio-economic issues accompanying urban expansion (Bhatta, 2010; Thapa & Murayama, 2009; Patino & Duque, 2013; Gluch, 2002).

To maintain sustainability and quality of life, effective and practical growth strategies and planning policies are requested by Regional Council of Region of Waterloo (RGMS, 2003). “Enhancing our natural environment and building vibrant urban places” are two foremost goals stated in final revised Regional Growth Management Strategy (RGMS) in 2003. More specific acts and planning policies were made and finalized in Regional Official Plan (ROP) in 2010 to ensure successful implementation of the strategy. Therefore, consistent monitoring of urban growth and land use and land cover (LULC) change at local and regional scale is an urgent need to planners and policy makers to understand change dynamics of urban area of the Region of Waterloo.

1.2 Motivations of the Study

With recent development of remote sensing technologies and increased remotely sensed data availability, identifying detailed spatial and temporal changes of urban areas and

monitoring urban growth and LULC change have become more cost-effective and successful (Thapa & Murayama, 2009; Patino & Duque, 2013; Lunetta et al., 2004). To date, various change detection methods have been explored and developed for detecting urban growth and LULC change analysis (Singh, 1989). From a technical perspective, image algebra (image differencing and image ratioing), principal component analysis (PCA), post-classification change detection (PCCD), direct multi-date classification, and change vector analysis (CVA) are most widely used methods for change detection (Singh, 1989; Almutairi & Warner, 2010; Coppin et al., 2004; Jensen, 2005). From an application perspective, most of the previous studies on urban growth and LULC change detection were based on bi-temporal and coarsely multi-temporal analyses.

Even though bi-temporal analysis and coarsely multi-temporal analysis have their own advantages of providing useful change information, they are unable to observe dynamic change patterns and higher-order complexities, such as acceleration, deceleration of specific LULC change within a long-term time span (Sexton et al., 2013). The dynamic change patterns include spatially and temporally complex changes in water, forest, agriculture, and urban built-up area caused by natural and anthropogenic processes (Sexton et al., 2013). Moreover, the impacts on ecosystems caused by frequent human activities exhibit nonlinearities, time lags, and legacy effects, and the change dynamics is only able to be detected by long-term repeatedly measurements (Sexton et al., 2013). Urban area development is a very complex process (Hodge & Gordon, 2008; Thapa & Murayama, 2009). Specifically, urban expansion and land use changes are driven by economic factors, restricted by policies preserving environmental sensitive and vulnerable areas, and oriented by zoning and taxation policies (Sexton et al., 2013; Hodge & Gordon, 2008). Therefore, for better monitoring regional

complex LULC change, more comprehensively understanding the causes and consequences of urban expansion, and more accurately identifying typical patterns and trends required by planners and policy makers for better future planning and environmental management (Hodge & Gordon, 2008), long-term time series dynamic LULC change analysis using satellite images spanning multiple decades with sufficient temporal resolution is needed (Sexton et al., 2013).

With the opening of Landsat archive from United States Geological Survey (USGS) in 2009 (Woodcock et al., 2008; Sexton et al., 2013; Wulder et al., 2011), the increased demand of long-term time-serial analysis of urban growth and LULC change dynamics can be met (Sexton et al., 2013, Hansen & Loveland, 2012). Therefore, with the free access of Landsat archive, processing dense datasets with high frequency will shift research focus from analyzing static bi-temporal change to comprehending more detailed long-term change dynamics in which planners, policy makers and resource managers are much more interested (Sexton et al., 2013).

In this study, bi-temporal, multi-temporal with 5-year interval and annual time-serial dynamic change detection methods were performed on Landsat images of urban area of Waterloo Region. Support vector machine (SVM) showed higher accuracy for extracting urban area LULC types than traditional maximum likelihood classifier (MLC) and other newly-developed machine learning classifiers, such as artificial neural network (ANN) and random forest (RF). Results were discussed to reveal the advantages and limitations of using datasets with different temporal resolutions. Other than static “from-to” change information, urban growth patterns and corresponding long-term dynamic LULC change information were also identified for better understanding of urbanization process in the past and for better planning by planners and policy makers in the future.

1.3 Objectives of the Study

The objectives of this study can be specified as follows:

- To compare several recently-developed machine learning classifiers including artificial neural network (ANN), support vector machine (SVM) and random forest (RF) to evaluate urban area LULC classification performance.
- To analyze LULC change dynamics of urban area of Region of Waterloo from 1984 to 2013 based on bi-temporal, multi-temporal and annually intensive Landsat datasets.
- To monitor and analyze long-term urban growth of Region of Waterloo and model the urban growth trend of City of Waterloo, City of Kitchener, and City of Cambridge respectively.

1.4 Structure of the Thesis

This thesis also consists of other five chapters.

Chapter 2 reviews a variety of previous studies and applications showing the capability of Landsat data for monitoring and detecting urban growth and LULC change.

Chapter 3 describes the study area and data acquisition; and points out the challenges of this study, especially for long-term dynamic LULC change analysis.

Chapter 4 explains specific approaches utilized to reach the study objectives; and explains considerations of the methodology designed from both technical and practical perspectives.

Chapter 5 presents and compares the major results obtained from different change detection schemes oriented by temporal resolutions. Urban growth and LULC change

dynamics are detected and monitored in great depth by annual interpretation of long-term Landsat records.

Chapter 6 draws a conclusion comprised of contributions of the study, considerations of uncertainties and limitations, and recommendations of future studies.

Chapter 2 Literature Review

Urbanization, caused by population growth, will lead to inward urban growth (intensification) and outward urban growth (sprawl) (Sexton et al., 2013). These processes inevitably result in LULC change which has great impacts on both natural ecosystems and human systems (Gillanders et al., 2008; Munthali & Murayama, 2011). Thus, detecting urban growth and its resulting LULC change is critical to planners, government agencies, hydrologists, ecologists, and so on. With the development of remote sensing technologies, reliable change detection results can be obtained. In this chapter, the applicability and availability of remotely sensed data, especially USGS Landsat archive, are introduced. Moreover, widely-used change detection methods and related previous studies are also reviewed here. In this study, LULC types were identified using a supervised classification method. Therefore, additionally, a variety of LULC classification methods are reviewed in this chapter.

2.1 Satellite Data for Monitoring Urban Dynamics

As information of distant objects can be gathered by remote sensing based on their reflected or emitted electromagnetic radiation (Patino & Duque, 2012; Jensen, 2007), LULC, urban morphology, vegetation distribution, and some other biophysical information can be extracted for planners and policy makers to analyze the urban environment (Pantino & Duque, 2012). There are several benefits that urban area analysis can get from remote sensing technology. As Yang (2011) summarized, remote sensing images can cover a large area of land surface which gives a full view of the landscape of the urban area for better analyzing interactions between human and environment. Also, as for some urban studies that researchers

do field surveys to collect sampling data, using remote sensing data is more cost-effective and unbiased; and electromagnetic information gives researchers more knowledge about the study area than human visual perception (Tang et al., 2008; Tian et al., 2011; Yang, 2011). Additionally, retrospective measurements of land surface enable long-term time-series analysis of urban area to examine process of urbanization or human activities (Sexton et al., 2013). Moreover, remote sensing can be integrated with geographic information systems (GIS) incorporating other human variables for more spatio-temporal analyses to help understand the drivers of changes of urban area (Tang et al., 2008; Tian et al., 2011; Yang, 2011).

Therefore, in terms of its superiority to traditional research methods, remote sensing technology has been widely used and proved to be effective and reliable for monitoring urban growth and detecting LULC change (Munthali & Malawi, 2011; Sexton et al., 2013; Patino & Duque, 2013; Hansen & Loveland, 2012; Sundarakumar et al., 2012; Tian et al., 2011; Nong & Du, 2011; Tan & Lim, 2010; Gluch, 2002). Based on their availability and capability of urban area analysis, a variety of remote sensing sensors and their products will be introduced in this section, especially for Landsat archive data used in this study.

2.1.1 Overview of Earth Observation Satellites and Sensors

The beginning of remote sensing technology can be considered as the first aerial photographs taken in 1860s by Felix Tournachon (Patino & Duque, 2012). Since the late 1950s, aerial images have been used for urban area analyses. However, with the launch of several earth-orbiting satellites, the focus of studies has shifted from using aerial images to satellite-based images because of their lower costs, wider area coverage, and frequent image updates (Patino & Duque, 2012). Since the earliest satellite Landsat 1 with Multispectral Scanner (MSS) was launched in 1972, many satellites with various sensors in different spectral, spatial

and temporal resolutions were launched in the past four decades (Patino & Duque, 2012; Jensen, 2007; ITC, 2013). Based on the review of Patino and Duque (2012), Earth-orbiting satellite sensors, such as Landsat 5 Thematic Mapper (TM), Landsat 7 Enhanced Thematic Mapper Plus (ETM+), SPOT 1 to 5, QuickBird, IKONOS, NASA Terra Advanced Spaceborne Thermal Emission and Reflection Radiometer (ASTER) and Indian Remote Sensing (IRS-1C), are most often used earth observation (EO) systems in urban area studies. Specific characteristics of these EO systems are summarized in Table 2.1. Those characteristics include satellites, sensors, resolutions, life time on service, and organization.

Table 2.1 Most often used EO systems for urban area analysis

Satellites	Sensors	Spectral Resolution	Spatial Resolution (m)	Temporal Resolution (Days)	Launched in	Out of Service Since	Organization
Landsat 1	MSS	5 bands	80 for visible and infrared bands 240 for thermal infrared band	18	1972	1978	NASA-USA
Landsat 2					1975	1983	
Landsat 3					1978	1983	
Landsat 4	MSS; TM	7 bands for TM	30 for visible and infrared bands 60 for thermal infrared band	16	1982	2001	
Landsat 5					1984	2013	
Landsat 7	ETM+	9 bands	30 for visible and infrared bands 60 for thermal infrared bands 15 for panchromatic band	16	1999		
Landsat 8	OLI; TRIS	11 bands	30 for visible and infrared bands 100 for thermal infrared bands 15 for panchromatic band	16	2013		
SPOT 1	HRV	4 bands	20 for visible and infrared bands 10 for panchromatic band	26	1986	2002	
SPOT 2					1990	2009	
SPOT 3					1993	1996	
SPOT 4	HRVIR	5 bands	20 for visible and infrared bands 10 for panchromatic band	26	1998	2013	
SPOT 5	HRVIR	5 bands	20 for mid-infrared band 10 for visible and near infrared bands 2.5-5 for panchromatic band	26	2002		Astrium
SPOT 6	NAOMI	5 bands	6 for visible and near infrared bands 1.5 for panchromatic band	26	2012		
Terra	ASTER	14 bands	15 for visible bands 30 for infrared bands 90 for thermal infrared bands	16	1999		NASA-USA
IRS-1C	LISS-III	5 bands	23.5 for multispectral bands 5.8 for panchromatic band	5 to 24	1995	2007	ISRO-India
IKONOS	IKONOS	4 bands	4 for multispectral bands 1 for panchromatic band	3	1999		DigitalGlobe
QuickBird	QuickBird	5 bands	2.4 for multispectral bands 0.6 for panchromatic band	3	2001		DigitalGlobe

Spatial resolution was considered as the most important factor for urban area analysis using remotely sensed data (Jensen & Cowen, 1999). However, based on characteristics listed below in Table 2.1, most of the images that are often used for identifying urban attributes successfully are with moderate spatial resolutions. Patino and Duque (2012) also stated that the moderate spatial resolution images are appropriate for detecting LULC change and monitoring urban growth trends, because historical images can be used dating back to 1970s. To illustrate the lengths of the archives of listed remote sensing systems, a time scale figure, showed as Figure 2.1, was generated by Patino and Duque (2012).

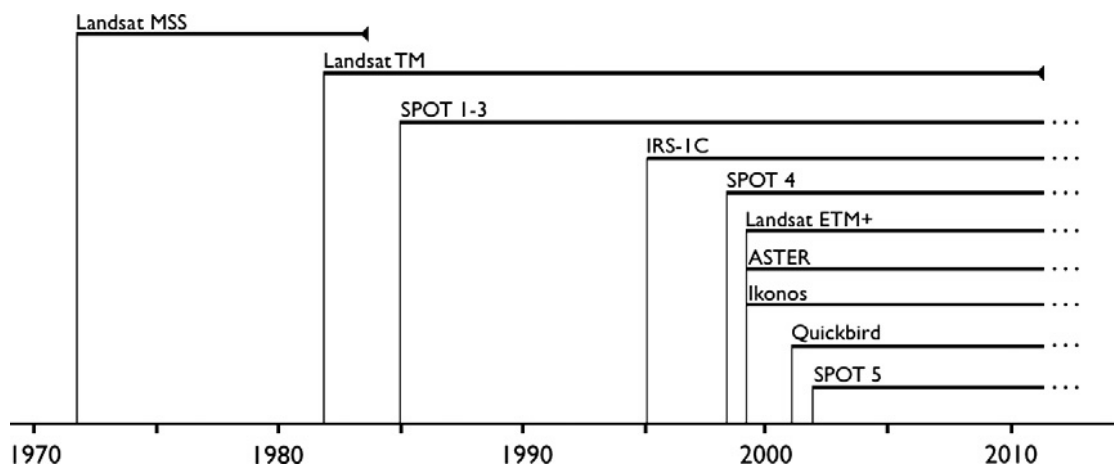


Figure 2.1 Time scale of several remote sensing systems (Source: Patino & Duque, 2012)

2.1.2 Introduction to USGS Landsat Archive Data

Landsat project is the oldest satellite project in the United States for land-surface observation (Jensen, 2007). Landsat Project, initiated by National Aeronautics and Space Administration (NASA) and USGS, has launched 8 satellites to collect data of Earth surface to provide resources for people who manage regional development, who manage natural resources, and who do research in various environmental fields throughout the United States and worldwide (USGS, 2013). Based on Landsat Project Statistics on USGS website (2013), the most primary use of Landsat data is detecting LULC change, showed as Figure 2.2. As

established to routinely gather Earth resource information from space, Landsat satellites had very well performance during their missions, expect for Landsat 6 (USGS, 2013). To date, long-term record of global landscape information has been acquired since the first Landsat satellite launched in 1972 (USGS, 2013). To continue the mission of Landsat Project of observing land-surface information, Landsat 8, providing higher quality data, was recently launched on February 11, 2013 (USGS, 2013).

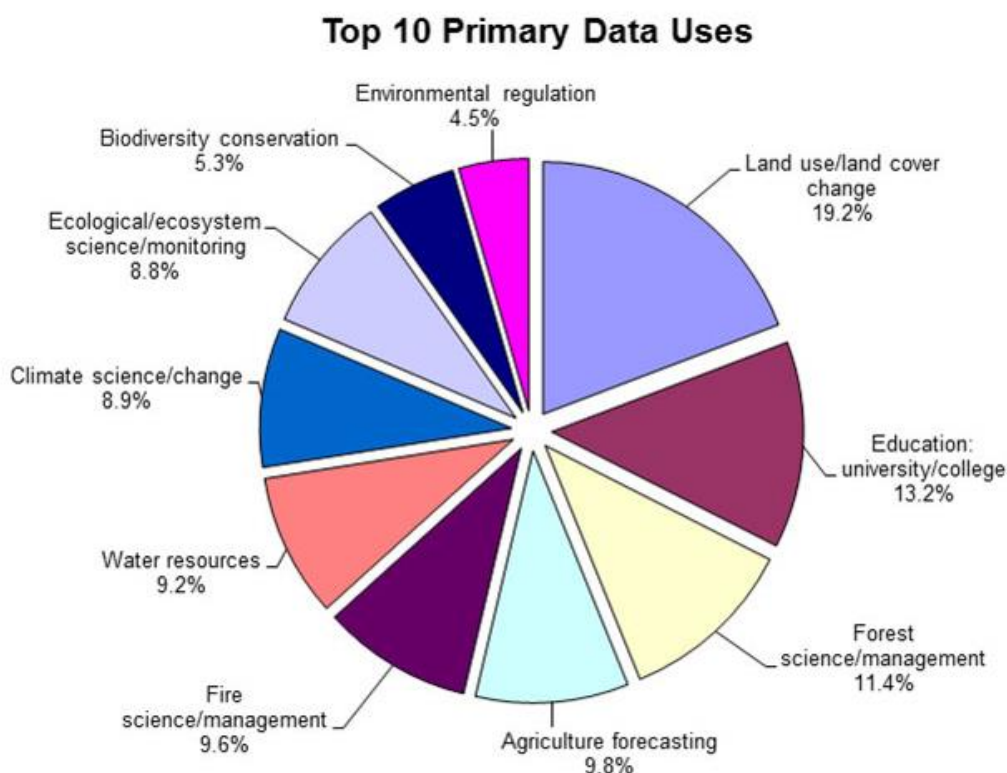


Figure 2.2 Top 10 primary Landsat data uses (Source: USGS, 2013)

With technology development, sensors onboard Landsat satellites have been improved as well. Spectral and spatial information retrieved from USGS (2013) of each Landsat sensor are specified in Table 2.2. Landsat Multispectral Scanner (MSS) was the primary sensor placed on Landsat 1, 2, and 3. MSS have four multispectral bands from green to near-infrared (IR) with 80m resolution and one thermal band with 240m resolution only onboard Landsat 3. Thematic Mapper (TM) sensors were placed on Landsat 4 and 5 with two added shortwave infrared (SWIR) and one thermal band. Resolutions have been increased to 30m for visible and infrared bands and to 120m for thermal band. Enhanced Thematic Mapper Plus (ETM+) onboard Landsat 7 had one more panchromatic band in 15m resolution; and thermal band increased to 60m resolution. As for the newly launched Landsat 8, Operational Land Imager (OLI) sensor has eight spectral bands in 30 m resolution, adding one deep blue band and one cirrus band, and one panchromatic band in 15m resolution; and Thermal Infrared Sensor (TIRS) has two thermal bands with 100m resolution (USGS, 2013).

In 2009, USGS opened Landsat archive data to the public for free access (Woodcock et al., 2008; Sexton et al., 2013; Wulder et al., 2011), enabling more studies can be conducted at local, regional, even global scale within a long time span (Hansen & Loveland, 2012). In this study, Landsat archive data were chosen to detect LULC change and monitor urban growth of Waterloo Region. Free access to Landsat archive makes it possible to obtain satellite images with no cost comparing to other commercial satellite images, such as IKONOS and QuickBird. More importantly, the longest record of Landsat archive data allows this study to detect long-term trend of LULC change and monitor urban growth pattern.

Table 2.2 Band designations for Landsat sensors

Sensor	Spectral Bands		Wavelength (μm)	Resolution (m)
	Landsat 1,2,3	Landsat 4,5		
MSS	4 – green	1– green	0.5 – 0.6	80
	5 – red	2– red	0.6 – 0.7	80
	6 – near-IR	3– near-IR	0.7 – 0.8	80
	7 – near-IR	4– near-IR	0.8 – 1.1	80
	8 – thermal (Landsat 3)		10.4 – 12.6	240
TM & ETM+	1 – blue – green		0.45 – 0.52	30
	2 – green		0.52 – 0.60	30
	3 – red		0.63 – 0.69	30
	4 – near-IR		0.76 – 0.90	30
	5 – SWIR 1		1.55 – 1.75	30
	6 – thermal		10.40 – 12.5	120; 60 (ETM+)
	7 – SWIR 2		0.98 – 2.35	30
	8 – panchromatic (ETM+)		0.52 – 0.90	15
OLI & TIRS	1 – coastal/ aerosol		0.43 – 0.45	30
	2 – blue		0.45 – 0.51	30
	3 – green		0.53 – 0.59	30
	4 – red		0.64 – 0.67	30
	5 – near IR		0.85 – 0.88	30
	6 – SWIR 1		1.57 – 1.65	30
	7 – SWIR 2		2.11 – 2.29	30
	8 – panchromatic		0.50 – 0.68	15
	9 – cirrus		1.36 – 1.38	30
	10 – thermal 1		10.60 – 11.19	100
	11 – thermal 2		11.50 – 12.51	100

(USGS, 2013; Jensen, 2005)

2.2 Urban Growth and LULC Change Detection

LULC change is the major component of global change that significantly influences the global climate and environment (Jensen, 2007; Yin et al., 2011). Therefore, monitoring and evaluating LULC changes has become one of the most important applications in remote sensing field (Almutairi & Warner, 2010; Alphan, 2011). In this section, most widely used digital change detection methods were introduced; and several applications of detecting LULC change and monitoring urban growth were reviewed as well.

2.2.1 Overview of Widely Used Change Detection Methods

As Singh (1989) defined, “change detection is the process of identifying differences in the state of an object or phenomenon by observing it at different times”. Changes can be detected because the radiance values of the objects also change along with LULC alterations (Singh, 1989). To effectively monitoring landscape change by observing satellite data, a variety of change detection methods have been developed and applied in many studies (Singh, 1989; Jensen, 2005; Lu et al., 2004). Four important aspects of monitoring changes were suggested and summarized by Macleod and Congalton (1998), which are determination of whether or not the changes happened, identification of the nature of the changes, detection of the areal extent of the changes, and analysis of the change patterns. In terms of different purposes and objectives of applications, selecting an appropriate change detection method is very critical to obtain reliable results (Jensen, 2005; Lu et al., 2004). To illustrate and compare the key characteristics, advantages and disadvantages of the most often used change detection methods, Table 2.3 was generated in terms of some previous review works (Singh, 1984; Jensen, 2005; Lu et al., 2004; Coppin et al., 2004; Alphan, 2011; Lunetta & Elvidge, 1998).

The methods listed in Table 2.3 have been proved to be effective for detecting changes in various applications. Image algebra method can be used for monitoring forest canopy change (Hayes & Sader, 2001), monitoring irrigated crops (Manavalan et al., 1995), detecting land cover change (Kleynhans et al., 2011; Kaufmann & Seto, 2001), detecting mining process and land use change (Prakash & Gupta; 1998), and monitoring landscape change of coastal area (Alphan, 2011). Using PCA method, land cover change (Byrne et al., 1980; Parra et al., 1996; Fung, 1990), forest conversion (Jha & Unni, 1994) can be detected. CVA is also can be used in vegetation degradation detection (Lunetta et al., 2004), desertification monitoring (Dawelbait & Morari, 2012), LULC change detection (Kontoes, 2008; Song & Cheng, 2011), and so on. As for PCCD method, thematic maps and valuable “from-to” change information can be obtained by PCCD (Jensen, 2005). Therefore, many applications focusing on LULC change and urban growth employed PCCD method to identify specific categories of LULC, and thus explore the change pattern and change effect on surrounding environment (Abd El-Kawy et al., 2011; Zhou et al., 2011; Yuan et al., 2005; Sundarakumar et al., 2012; Peiman 2011; Tan et al., 2010).

Table 2.3 Summary of most often used change detection methods

Methods		Characteristics	Advantages	Disadvantages	Key Considerations
Write Function Memory (WFM)		Visual interpretation by inserting three individual bands from multiple dates into Red, Green, and Blue planes to highlight the change area.	Quick visual interpretation of the change at two and even three dates; Normally not necessary to have atmospheric correction.	No quantitative information; No “from-to” change class information.	Determine appropriate bands.
Image Algebra	Image Differencing	Subtract one image of one date from another image of second date.	Simple and quick method to identify change/no change information; Normally not necessary to have atmospheric correction.	No “from-to” change class information; Difficult to determine the threshold to distinguish change/no change information.	Determine appropriate bands; Threshold should be identified carefully.
	Image Regression	Identify the linear relationship between images from two dates. Subtract the first image from the regressed image.	Impacts of atmospheric effect and sun angle effect can be reduced.	No “from-to” change class information; Need to establish accurate regression model.	Develop regression model; Determine appropriate bands and threshold.
	Image Ratioing	Calculate the ratio of two images from two dates, band by band.	Simple and quick method to identify change/no change information; Normally not necessary to have atmospheric correction.	No “from-to” change class information; Difficult to determine the threshold to distinguish change/no change information.	Determine appropriate bands; Select appropriate threshold.
	Vegetation Index Differencing	Calculate vegetation index for two dates before using image differencing method.	Difference of spectral features can be enhanced; Reduce impacts of topographic effects.	Enhance random noise and coherent noise;	Determine appropriate vegetation index; Select appropriate threshold.

Table 2.3 (Continued)

Methods	Characteristics	Advantages	Disadvantages	Key Considerations
Principal Component Analysis (PCA)	Put bands from two dates into one single dataset. Perform PCA and analyze minor component which represents change information.	Data redundancy can be reduced; Change can be visually interpreted from minor component; Normally not necessary to have atmospheric correction.	Difficult to label change classes; Threshold is needed to identify change/no change information.	Need skills to identify the component which represents the change information; Select appropriate threshold.
Multi-date Composite Classification (MCC)	Put bands from two or more dates into one single dataset. Supervised or unsupervised approach is used to extract change information.	Requires only one classification.	Data redundancy; Difficult to select training sites because of many change classes.	Need thorough examination of the images to label the change classes.
Change Vector Analysis (CVA)	Direction and magnitude of change from one date to another date are generated. Direction vector determines the change types. Magnitude vector determines whether the change happens.	Have ability to process any number of spectral bands; Detailed change information can be provided.	Difficult to identify change trajectories.	Determine direction of change; Identify threshold for magnitude of each change vector.
Post Classification Change Detection (PCCD)	Change information is obtained by comparing independently classified thematic maps.	No atmospheric correction required; Provides “from-to” information;	Requires two classifications; Accuracy of change information heavily relies on the accuracy of classification results.	Sufficient training sample for classification.

(Jensen, 2005; Lu et al., 2004; Lu et al., 2005)

2.2.2 Detecting LULC Change and Monitoring Urban Growth Using Landsat Data:

An Overview

Even though urban areas are quite small when looking down on the global landscape, their expansion is the primary cause of transformation of LULC types and is significant factor that has great influence on biodiversity, ecosystems, hydrology, and climate at local, regional, and global scales (Yang, 2011). Since the first Landsat satellite launched in 1972, observing the regional and global land surface and LULC change became possible throughout the United States and worldwide (USGS, 2013). Subsequently, a large number of applications and studies focusing on LULC change detection and urban growth emerged using Landsat data. With the significantly increased remote sensing data availability in recent two decades, for instance, the commercial satellite imagery with higher spatial resolution has evoked new studies and applications in urban area because it is possible to identify much finer objects in the complex urban systems (Patino & Duque, 2013). However, even today, Landsat data in medium spatial resolution is still a satisfactory data source for large regional LULC change detection and urban growth monitoring due to their longest historical record and global coverage (Hansen & Loveland, 2012). According to previous studies and applications, the usefulness of detecting LULC change and monitoring urban growth of a variety of methods has been proved using Landsat data.

In remote sensing studies, impervious built-up land, which precipitation cannot penetrate through, is considered as an important indicator of urban land use (Sexton et al., 2013; Xu, 2007; Slonecker et al., 2001), including buildings, roads, parking lots, sidewalks, etc. (Slonecker et al., 2001). Since built-up land dominates urban area land cover, studies of monitoring urban expansion requires useful method to extract built-up area efficiently and

accurately (Xu, 2007). Because different land cover types show different spectral characteristics based on Landsat multispectral bands, some useful built-up indices have been developed to increase separability between built-up area and other land cover types (Waqar et al., 2012). Index-based built-up area extraction is a popular approach that many studies applied it to monitor growth of urban built-up areas (Jensen, 2005). In Table 2.4, several useful indices for extracting built-up areas derived by Landsat TM bands are listed.

Table 2.4 Useful indices and their expressions

Index	Computed as
NBI (new built-up index)	$TM3 * TM5 / TM4$
NDVI (normalized difference vegetation index)	$(TM4 - TM3) / (TM4 + TM3)$
NDBI (normalized difference built-up index)	$(TM5 - TM4) / (TM5 + TM4)$
SAVI (soil adjusted vegetation index)	$(1 + L) (TM4 - TM3) / (TM4 + TM3 + L)$ (L is a correction factor that adjust soil brightness variations)
MNDWI (modified normalized difference water index)	$(TM2 - TM5) / (TM2 + TM5)$
NBAI (normalized built-up area index)	$(TM7 - TM5 / TM2) / (TM7 + TM5 / TM2)$
BRBA (band ratio for built-up area)	$TM3 / TM5$
NDISI (normalized difference impervious surface index)	$[TM6 - (WI + TM4 + TM5) / 3] / [TM6 + (WI + TM4 + TM5) / 3]$ (WI is a water index)

By setting NDVI threshold, binary built-up/non-built-up map can be extracted (Slonecker et al., 2001). Zhao and Chen (2005) and Zha et al. (2003) used the same method but employed NDBI to extract built-up lands. Masek et al. (2000) observed simple NDVI differencing map with ancillary unsupervised classification map for second date to distinguish true urban growth from vegetation phenological change of Washing DC metropolitan area. Chen et al. (2007) compared NBI, NDVI, and NDBI to discover that NBI shows better separation of built-up areas and other land cover types. To increase the accuracy of built-up area extraction, Xu (2007) used SAVI, NDBI, and MNDWI simultaneously and tested the

performance of these three indices by applying PCA, supervised classification, and logic calculation approaches. Simple “if-then-else” logic calculation approach and PCA approach provided results with accuracy higher than 93%. This method reduced data redundancy and data correlation, and increased separation of land cover types when combining these three index bands (Xu, 2007). To more effectively estimate built-up area, some new indices were developed, such as NBAI, BRBA, NDISI, etc (Xu, 2010; Waqar et al., 2012). Index-based built-up area extraction method is very simple and rapid method for mapping urban area and sequentially monitoring urban expansion. Those Landsat derived built-up indices are useful features, which enhancing the urban area, to help data users perceive urban information at their first glances. However, urban growth area cannot be identified accurately unless an appropriate threshold is used (Waqar et al., 2012). Moreover, reviewing the results from those studies, only binary built-up/non-built-up maps were generated. Urban growth can be monitored by their spatial characteristics, but no specific LULC change information will be provided. However, it is important to detect resulting LULC change because it reveals valuable information of interactions between urban growth and ecosystems (Tan & Lim, 2010).

To monitor nation-wide LULC change of the U.S. and evaluate and manage the consequences of change, USGS developed a Land Cover Trends (LCT) project to detect LULC change at ecoregional scale for the 1972 – 2000 period using Landsat data (USGS, 2013). PCCD method was employed to obtain specific “from-to” information (which LULC classes are changing, what they are changing to, and how much they change) and monitor LULC change dynamics (Sleeter et al., 2012). The study of Mojave Basin and Range Ecoregion is a typical example of LULC change detection. Since Las Vegas is one of the fastest growing cities in the U.S., significant urban growth in place of grassland is detected. The most rapid

growth happened during 1986 to 1992. In 2011, Huang et al. applied PCCD method using the Iterative Self Organizing Data Analysis (ISODATA) classifier to analyze urbanization process and its effect on irrigation districts of the Lower Rio Grande Valley in the south of Texas. Using the same PCCD method, Tan and Lim (2010) evaluate the impact of land surface temperature by monitoring urban expansion based on LULC maps classified by MLC in Penang Island, Malaysia. For spatial progressive urban growth mapping of Atlanta metropolitan area, Yang (2003) designed a change detection scheme based on multi-temporal map-by-map comparison. Similarly, Yin et al. (2011), in order to evaluate how Shanghai metropolitan area conformed to the “reform and opening-up” policy, detected urban growth dynamics applying multi-temporal change detection scheme as well. In addition, Yin et al. (2011) generated radar graphs to illustrate spatial orientation of LULC change. Moreover, other studies, conducted by Yuan et al. (2005), Sundarakumar et al. (2012), Tang et al. (2008), Afify (2011), and Abd El-Kawy et al. (2011), also proved that PCCD is a very useful and popular approach for LULC change detection and urban growth monitoring.

Classification processes involved in the above reviewed studies are all conducted at pixel level. However, Landsat multi-spectral bands are in 30m spatial resolution, some pixels are mixed pixels that represent as a mixture of different LULC types (Slonecker et al., 2001). Linear spectral mixture analysis (LSMA) was then proposed by some studies to increase mapping accuracy of built-up area at sub-pixel level (Lu et al., 2011; Lu et al., 2004; Lu & Weng, 2004; Powell et al., 2007). The basis of this method is the assumption that reflectance measured at one pixel is a linear combination of reflectance of all components (endmembers which assumed to represent the purest pixels) within the pixel (Lu & Weng, 2006; Powell et al., 2007). Powell et al. (2007) applied a pure pixel index (PPI) to collect endmembers, while in

some other studies (Lu & Weng, 2004; Lu & Weng, 2006; Lu et al., 2011), endmembers were selected from feature spaces formed by components from minimum noise fraction (MNF) transformation. After spectral unmixing, some approaches, such as direct classification (Lu & Weng, 2006; Lu et al., 2004), regression tree model (Yang et al., 2003), and decision tree (Lu & Weng, 2004), were conducted on fraction images to identify LULC classes. Even though LSMA method is a suitable technique to characterize urban LULC types and estimate built-up area, there are still some limitations and uncertainties when using this method (Yang et al., 2003; Weng, 2012). The key aspect of LSMA is to select appropriate endmembers to generate fraction images successfully (Lu et al., 2011; Somers et al., 2011; Lu et al., 2004; Lu & Weng, 2006). Carefully identifying number and type of endmembers and reducing correlation between image bands are two key factors for obtaining high quality fraction images (Somers et al., 2011; Lu et al., 2004).

Other than per-pixel and sub-pixel approaches, object-based image analysis (OBIA) is also useful for processing remote sensing data for change detection analysis (Walter, 2004; Im et al., 2008). Instead of pixel by pixel, OBIA approach identifies objects by analyzing not only spectral but also spatial homogeneity of groups of pixels (Yang, 2011). Since objects of interest should be larger than the ground resolution, OBIA is more applicable to high spatial resolution data (Yang, 2011; Im et al., 2008; Jensen, 2005).

As for study object which has persistent but irregular change mode during different time periods, for instance, urban growth, determination of temporal frequency is especially important (Lunetta et al., 2004; Gillanders et al., 2008). According to previous studies, most of the urban area change detection analyses were conducted based on bi-temporal scheme (Song & Cheng, 2011; Afify, 2011) or coarsely multi-temporal scheme (Abd El-Kawy et al., 2011;

Yuan et al., 2005; Sundarakumar et al., 2012; Peiman, 2011; Tian et al., 2011). With data availability increasing recently, more and more studies used multi-temporal datasets to detect change dynamics of urban area. However, as Sexton et al. (2013) mentioned, in order to understand the causes and consequences of urbanization, coarsely multi-temporal datasets are still insufficient. To detect the spatially and temporally complex change of LULC of North Carolina Piedmont from 1984 to 2007, Sexton et al. (2013) derived LULC information from a dense time-serial Landsat dataset using supervised classification approach. To monitoring urban expansion and observe the change pattern (acceleration or deceleration), Sexton et al. (2013) developed a regression tree model to detect impervious surface of the Washing D.C. - Baltimore metropolitan area from 1984 to 2010 using normalized Landsat images at high temporal frequency. The results clearly illustrated the change dynamics, and well depicted the trajectories of each LULC type spanning a long-term period. Such long-term detailed change information has great potential for planners, policy makers, social scientists and ecologists to better understand the complicated urbanization process and human-natural systems (Sexton et al., 2013).

In this study, in order to detect LULC change dynamics and observe urbanization pattern of Waterloo Region, supervised classification will be conducted for the urban area from 1984 to 2013 with a dense-temporal Landsat dataset. Per-pixel method will be adopted because (1) this study requires large amount of classification capacity and the per-pixel approach uses relatively less steps to obtain satisfactory LULC maps than sub-pixel approach, and (2) it is not easy to generate consistent high quality fraction images for every year because uncertainties are bound to be introduced during endmember selection process. The effectiveness of this change detection technique is mainly reply on the accuracy of each classification maps (Sexton

et al., 2013). Therefore, choosing an appropriate classifier is very important in this study. Classification techniques will be reviewed in the following section.

2.3 Review of LULC classification Methods

The key factor of acquiring satisfactory change detection results based on PCCD method is producing highly accurate classification maps (Lu et al., 2004). Many statistical pattern recognition techniques have been developed and applied to multispectral remotely sensed data to extract LULC information (Jensen, 2005). This section gives an overview of a variety of classification techniques and introduces several newly developed machine learning techniques.

2.3.1 Overview of Classification Techniques

Since accurate classification results are useful information for many environmental and socio-economic applications, image classification is still a popular topic among various remote sensing researches, and many scientists and practitioners put great efforts in exploring new classifiers to increase classification accuracy (Lu & Weng, 2007). Generally, classification techniques can be grouped or categorized by parametric and nonparametric, supervised and unsupervised, hard and soft (fuzzy), or per-pixel, sub-pixel, and object-based (Jensen, 2005; Lu & Weng, 2007). Table 2.5 summarizes the characteristics of each category. Since each method has its own merits, it is hard to determine which method is best (Lu & Weng, 2007). As Jensen (2005) stated, classification algorithm selection is determined by the nature of classification problem, biophysical complexity of the landscape, distribution of remote sensing data, and prior knowledge of the classes.

With the first Landsat satellite launched in 1972, numerous classification techniques have been developed for LULC classification (Huang et al., 2002). In spite of its limitation due

to data assumption of normal distribution, MLC is still one of the most widely used classifiers (Huang et al., 2002; Rogen & Chen, 2004). In a variety of urban area studies using Landsat data, MLC provided satisfactory LULC classification results for successful urban area change detection analysis (Deng et al., 2009; Yuan et al., 2005; Afify, 2011; Rogen & Chen, 2004). In addition to a single classification, Sundarakumar et al. (2012) applied unsupervised ISODATA classifier first to understand the distribution of pixels and then applied MLC to acquire the final classification maps. Moreover, Rozenstein & Karnieli (2011) compare classification results obtained by unsupervised ISODATA algorithm, supervised MLC algorithm, and a hybrid method that used ISODATA first and MLC second to improve the spectral signature set. Results indicated that the hybrid method obtained more accurate classification results. Similarly, Thapa and Murayama (2009) compared ISODATA, MLC, fuzzy classification method using a membership function, and a combination of the advantages of these methods with GIS overlay function. They concluded that the hybrid approach worked better than either single approach.

In order to improve classification accuracy, new advanced classification algorithms continuously emerged in recent years (Lu & Weng, 2007). Machine learning classifiers, such as, ANN, SVM, RF, decision tree, expert systems etc. have been used effectively in a variety of LULC classification studies (Rogen & Chen, 2004; Huang et al., 2002). Almost in all studies, these non-parametric machine learning classifiers performed much better than traditional statistical classifiers (e.g. MLC) (Bischof et al., 1992; Rogen & Chen, 2004; Jensen, 2005; Lu & Weng, 2007; Estes et al., 2012). These non-parametric classifiers have superiority of LULC classification in complex landscape, and thus commonly used for solving urban area change detection problems (Rogen & Chen, 2004; Lu & Weng, 2007; Estes et al., 2012). More

studies of several machine learning classifiers and their applications will be introduced in the next section.

Table 2.5 Summary of classification techniques

Criteria	Category	Characteristics	Examples
Whether parametric statistics are used or not	Parametric	Normally distributed; need prior knowledge of class density functions; produce noisy results when landscape is complex; cannot integrate ancillary spatial, contextual and non-statistical information into classification process.	MLC, unsupervised classification etc.
	Nonparametric	No assumption of the data; not normally distributed; suitable for incorporating non-statistical information into classification process.	Nearest-neighbor classifiers, fuzzy classifiers, ANN, SVM, RF, decision tree classifiers, expert system etc.
Whether training samples are needed or not	Supervised	LULC classes need to be defined; select training samples for each known class; thematic maps are generated based on the signatures obtained from the training samples.	MLC, minimum distance, parallelepiped, nearest neighbor classifier, ANN, SVM, RF etc.
	Unsupervised	Used when there is no prior knowledge of the classes; pixels are grouped into unique clusters based on their spectral similarity determined by some criteria.	ISODATA, K-means clustering etc.
Which pixel level the classification is conducted at	Per-pixel	Process the image pixel by pixel; ignore mixed pixel problems.	Most of the classifiers, such as MLC, ANN, SVM, RF etc.
	Sub-pixel	The spectral information of each pixel can be considered as linear or nonlinear combination of endmembers; membership of each pixel of each endmember will be assigned.	Fuzzy set classifiers, spectral mixture analysis
	Object-based	Group pixels into objects and classify the objects based on their spectral and spatial homogeneity.	Supervised classifiers
Whether the LULC type is definitive or not	Hard	Assign each pixel into a single class.	Most of the classifiers, such as MLC, ANN, SVM, RF etc.
	Soft	Assign membership for each pixel of each class based on the degree of similarity for each class.	Fuzzy set classifiers, spectral mixture analysis

(Jensen, 2005; Lu & Weng, 2007)

2.3.2 Machine Learning Techniques

Supervised machine learning algorithms can be used to predict future instances based on hypotheses that made by reasoning from provided instances (Kotsiantis, 2007). A concise model, which also can be called as a classifier, will be built after the learning process to assign class labels to the future instances where the predictor features are known (Kotsiantis, 2007). In terms of the classification capability of machine learning techniques, they have been widely attempted for LULC mapping in remote sensing field, and proved to be superior to conventional statistical classifiers in many studies (Bischof et al., 1992; Rogen & Chen, 2004; Jensen, 2005; Lu & Weng, 2007; Estes et al., 2012). The most commonly used machine learning algorithms include ANN, SVM, RF, decision trees, expert systems etc. (Lu & Weng, 2007). In this review, focus will be narrowed to ANN, SVM, and RF techniques.

ANN can be considered as an artificial intelligence system that works like a massively parallel distributed processor consisting of many simple units to simulate the capabilities for knowledge acquisition and problem solving of human brain (Bischof et al., 1992; Yang, 2011). In addition to no assumption of the data distribution, the adaptive learning process enables ANN to handling nonlinear and complex situation (Jensen, 2005; Yang, 2011). Also, it has outstanding performance under noisy environment with incomplete and ambiguous data (Bischof et al., 1992; Rogen & Chen, 2004; Yang, 2011; Song et al., 2012). Practitioners began to use ANN in remote sensing field for classification in late 1980s (Yang, 2011). The most widely used ANNs in LULC classification studies are the multilayered perceptrons (MLP) feed-forward networks trained with a back propagation learning process due to their robustness (Huang et al., 2002; Frohn & Arellano-Neri, 2005; Kotsiantis, 2007; Lu & Weng, 2007). Bischof et al. (1992) compared ANN and MLC for classification of Landsat data at per-pixel

level, demonstrating that ANN outperformed MLC for multi-class classification and incorporating texture information in ANN improved the overall accuracy. Frohn and Arellano-Neri (2005) also used ANN and integrated texture information to improve LULC classification results, showing that ANN has capability of incorporating non-spectral features into classification process and obtained a thematic map with much higher accuracy than USGS land cover data. ANNs also have some limitations. It is difficult to configure ANN, because ANN is very sensitive to various parameter settings which will influence classification performance (Yang, 2011). Moreover, the learning process through which the output is obtained is difficult to explain comprehensively (Jensen, 2005). Therefore, a neural network is usually considered as a “black box” (Jensen, 2005).

In addition to ANN, SVM has also been successfully applied in many pattern recognition tasks (Huang et al., 2002; Nemmour & Chibani, 2010; Song et al., 2012). SVM is based on statistical learning theory, and used structural risk minimization method proposed by Vapnik (1995) to discriminate class members (Nemmour & Chibani, 2010; Song et al., 2012). Thus, a minimal generalization error can be obtained by minimizing the probability of misclassification of the unseen data points. SVM was initially designed for binary classification; but now has been extended for solving multi-class problems (Nemmour & Chibani, 2010). According to previous studies, SVM has showed superior performance in handling high dimensional dataset, such as hyperspectral images (Huang et al., 2002; Nemmour & Chibani, 2010). It also has been proved to be applicable for multispectral image classification (Huang et al., 2002). Pal and Mather (2005) designed an experiment to test the classification performance of SVM, MLC, and ANN using Landsat data and hyperspectral data. No matter for multispectral data or hyperspectral data, SVM obtained more accurate results,

even when the training data set is small (Pal & Mather, 2005). Similarly, Nemmour and Chibani (2010) applied SVM as well as ANN to detect LULC change of Algerian capital using Landsat data. Classification results also demonstrated that SVM performed better than ANN for identifying all LULC types. In terms of the superior performance of SVM, Estes et al. (2012) applied it for LULC mapping to identify the causes for population growth and LULC change in the protected area of greater Serengeti ecosystem from 1984 to 2003 using Landsat data. As the same disadvantage of ANN, the effectiveness of SVM is determined by the user-defined parameters, including kernel functions and associated parameters (Huang et al., 2002; Pal & Mather, 2005).

Many previous studies demonstrated that using combination of multiple classifiers can produce more accurate classification results than using one single classifier (Pal, 2005). Some studies showed that an ensemble classifier by using bagging or boosting method based on a decision tree increased accuracy for LULC classification (Pal, 2005; Gislason et al., 2006). RF classifier, proposed by Breiman in 2001, assigns an unknown pixel to a class by generating a great number of trees (classifiers) and conducting unweighted voting to combine their results (Pal, 2005; Gislason et al., 2006). These decision trees are created involving randomly choosing a set of features and selecting samples from training data using bootstrap sampling method (Pal, 2005; Mellor et al., 2013). Pal (2005) compared the performance of RF and SVM using Landsat data; and concluded that RF performed equally well to SVM. A study, which was conducted by Gislason et al. (2006), integrated Landsat multispectral bands, elevation, slope and aspect data together for classification of a mountainous area in Colorado. Mellor et al. (2013) incorporated Landsat multispectral bands, texture information, topographic variables, and climate variables for forest mapping. RF was proved to be effective tool to learn the

complex and nonlinear relationships between forest land cover types and biophysical variables (Mellor et al., 2013). Moreover, RF is capable of dealing with outliers and nonparametric and noisy data (Mellor et al., 2013). In addition to the good classification performance of RF, importance of variables can be estimated by this algorithm (Gislason et al., 2006; Mellor et al., 2013). Therefore, RF can be a useful tool applied in other studies such as feature selection for multisource data classification (Gislason et al., 2006). The advantage of RF is that fewer parameters need to be determined comparing to SVM. Number of features selected for each split and number of trees are two parameters that need to be predefined before training (Pal, 2005; Gislason et al., 2006).

In summary, ANN, SVM, and RF are advanced nonparametric machine learning classifiers that have been proved to be superior to traditional classifier for LULC classification in many remote sensing studies. Their superiority can be represented as the capability of handling data in complex landscape with no data assumption, capability of dealing with missing or noisy data, and capability of integrating continuous, categorical, binary, and other multisource data in classification procedure (Huang et al., 2002; Pal, 2005; Frohn and Arellano-Neri, 2005; Gislason et al., 2006; Kotsiantis, 2007; Benediktsson et al., 2007; Mellor et al., 2013). In this study, MLC, ANN, SVM, and RF will be applied on one Landsat image for the built-up area of Region of Waterloo; and the classifier with highest classification accuracy will be selected for classification of images obtained on other dates.

2.4 Chapter Summary

Since the Landsat 1 was launched in 1972 as the first land-surface observation satellite, satellite data have been widely used for urban area analysis. Landsat archive data with longest record and global coverage allowed a great number of studies to detect long-term LULC change and urban expansion. With the open of Landsat archive data, detect long-term change dynamics is the trend of change detection analysis of complex systems. Numerous change detection methods were applied in previous studies. The most widely used one is PCCD method which can generate thematic map for each date and provide specific “from-to” change information. The key factor of producing high quality change detection results is producing accurate individual thematic map. Selecting an appropriate classification technique is critical to generate accurate classification maps. According to numerous studies, newly developed advanced machine learning classifiers outperformed the traditional classifiers and widely adopted in classification of complex landscape.

Chapter 3 Study Area and Data

3.1 Study Area

The Region of Waterloo, located in southern Ontario, has become a prosperous and fast growing region after its formation in 1973 (RGMS, 2006). The location of Region of Waterloo is shown in Figure 3.1. Three urban municipalities, Waterloo, Kitchener, and Cambridge, and four rural townships, North Dumfries, Wellesley, Wilmot, and Woolwich, make up this region (Region of Waterloo, 2013). The region is 1369 km² in size and the Region's population was 507,079 as of the 2011 census (Region of Waterloo, 2013). As the main goal of this study is to monitor urban growth and detect its resulting change dynamics, the study area can be narrowed to the urban area of Waterloo Region. According to visual observation of Landsat image acquired in 1984, urban built-up areas located within municipal boundaries of the three cities. However, with the rapid urban sprawl in recent decades, urban built-up areas have exceeded the cities' municipal boundaries.

The latest map of official-defined urban area retrieved from the Regional Official Plan (ROP) is shown as Figure 3.2. Urban area is represented as the purple zone within the dashed line. One part of the urban built-up area expanded out of cities' municipalities is adjacent to the northernmost part of City of Waterloo along Weber Street and King Street. Another part is the expansion of the built-up area along the eastbound railway, which is known as East Side Lands designated for employment uses (ROP, 2010). Even though both of these two areas belong to the Township of Woolwich, they are of great significance to explore the nature of the urban growth and should be included. As a result, the study area, shown in Figure 3.3, is determined as the union of the municipal area of the cities and the official-defined urban area. The

geographic extents are from $43^{\circ}31'53.71''\text{N}$ to $43^{\circ}19'56.81''\text{N}$ and from $80^{\circ}37'32.94''\text{W}$ to $80^{\circ}14'57.79''\text{W}$. The total area is approximately 328 km^2 .

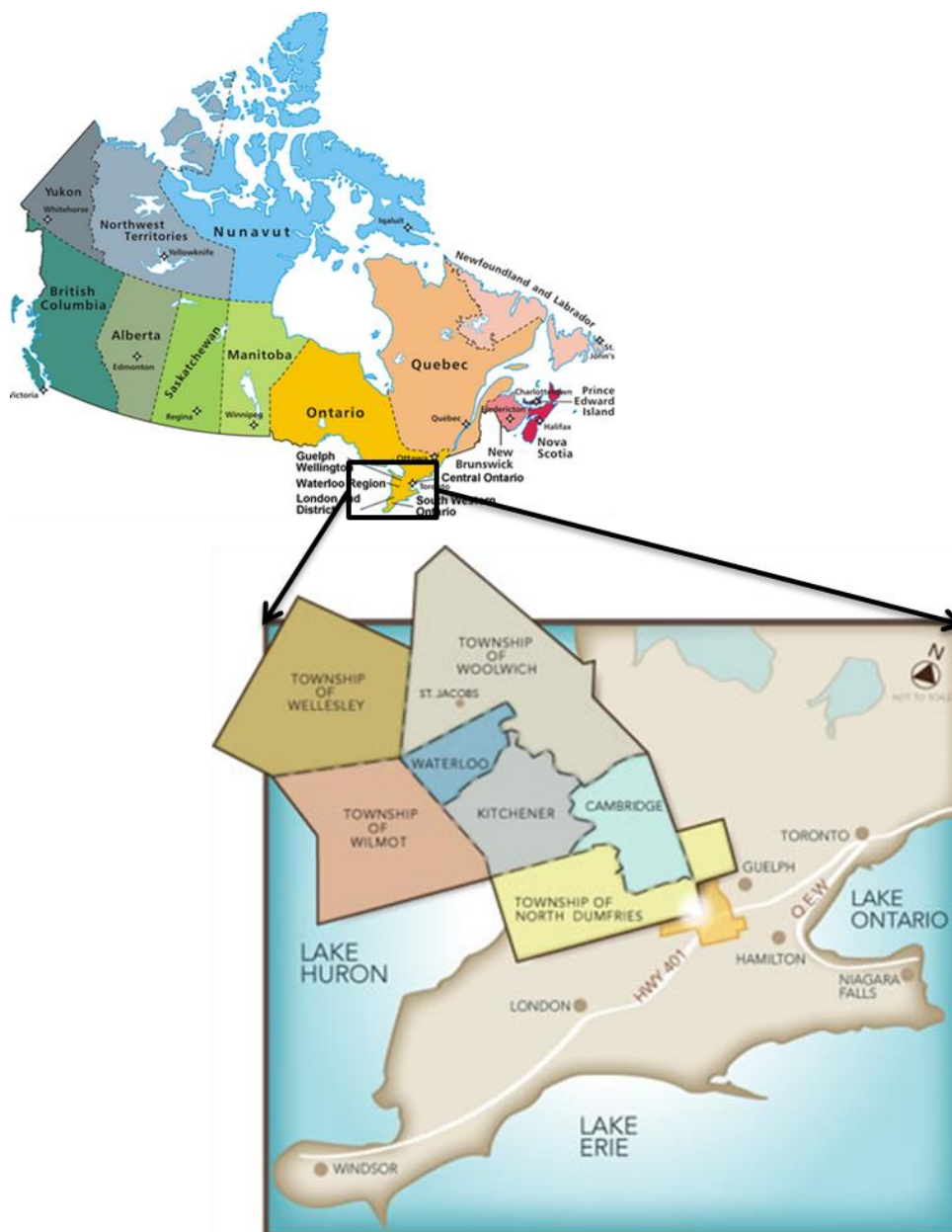


Figure 3.1 Location of Region of Waterloo

As an overview, within this study area, urban built-up area is one of the most typical land cover types, including low-density urban use area (e.g. single/multiple family houses, local roads, etc.) and high-density urban use area (e.g. commercial and industrial areas, high-

density residential areas, etc.). Another typical land cover type is vegetation, such as agriculture area and grassland (e.g. pastures, golf courses, parks, etc.). Forest land, considered as very important land cover type, occupies relatively small area in general. This study area also covers some water bodies, such as part of Grand River and Laurel Creek Reservoir. Moreover, there are small areas of exposed lands, including natural barren land and building sites.

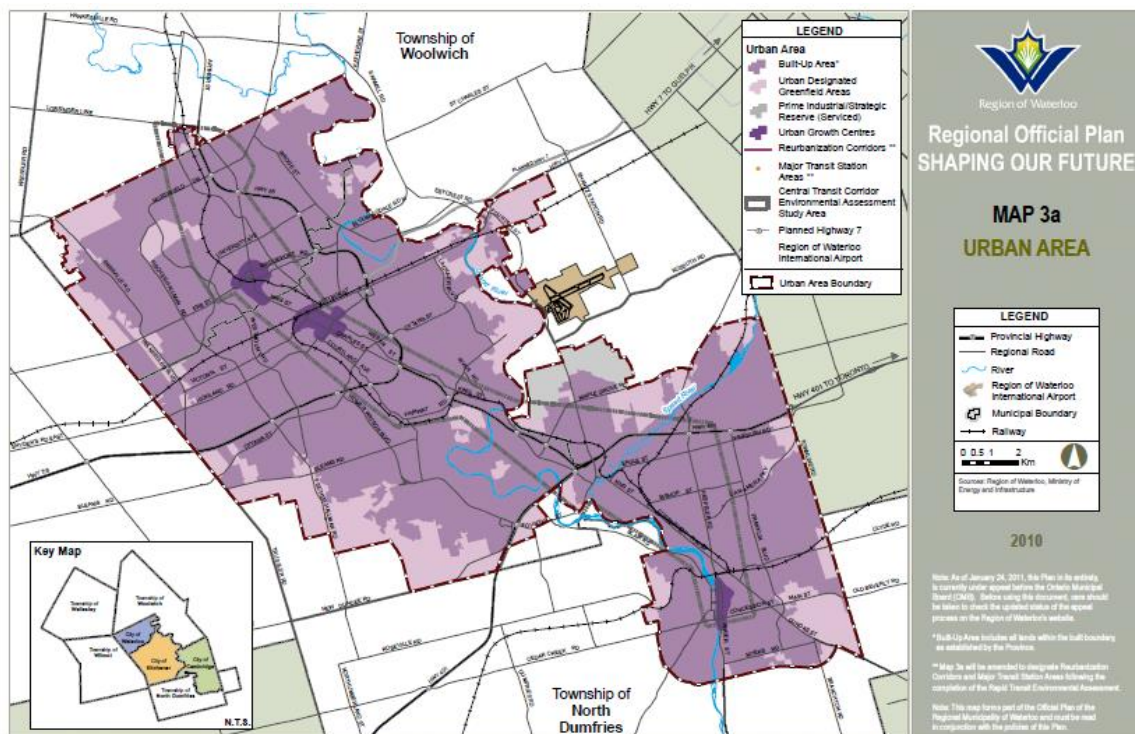


Figure 3.2 Urban area of Waterloo Region (Source: ROP, 2010)

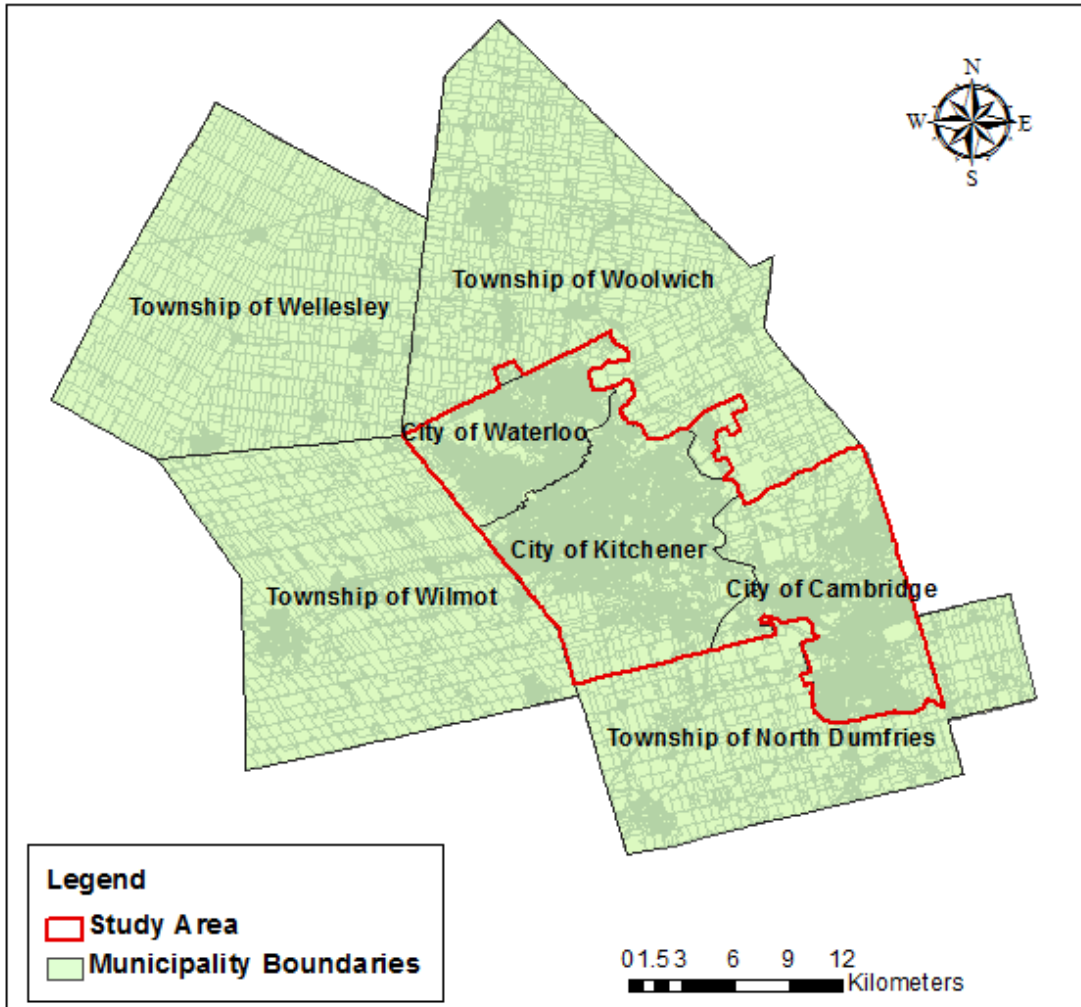


Figure 3.3 Map of study area

3.2 Data

Sufficient and appropriate datasets are very critical to reach the objectives of this study. As is stated in Section 2.1.2, free access of long-term Landsat archive data provide opportunity to detect time-serial change dynamics at regional scale. In this study, Landsat archive data are the core data of extracting urban LULC information. Population data is useful supplementary data for analyzing urbanization process of this Region. In addition, some other ancillary data are utilized as reference during Landsat data processing and accuracy assessment.

3.2.1 Landsat Archive Data

Table 3.1 Landsat images used for classification

Year	Sensor system	Date (mm/dd)	Year	Sensor system	Date (mm/dd)
1984	Landsat 5 TM	06/13	1999	Landsat 7 ETM+	09/03
1985	Landsat 5 TM	09/20	2000	Landsat 5 TM	08/28
1986	Landsat 5 TM	06/03	2001	Landsat 5 TM	08/15
1987	Landsat 5 TM	09/10	2002	Landsat 7 ETM+	08/01
1989	Landsat 5 TM	06/11	2003	Landsat 5 TM	06/02
1990	Landsat 5 TM	09/02	2005	Landsat 5 TM	08/26
1991	Landsat 5 TM	07/19	2006	Landsat 5 TM	08/13
1992	Landsat 5 TM	08/22	2007	Landsat 5 TM	06/29
1993	Landsat 5 TM	08/09	2008	Landsat 5 TM	09/03
1994	Landsat 5 TM	10/15	2009	Landsat 5 TM	05/17
1995	Landsat 5 TM	07/30	2010	Landsat 5 TM	05/20
1996	Landsat 5 TM	05/29	2011	Landsat 5 TM	06/08
1997	Landsat 5 TM	07/19	2013	Landsat 8 OLI & TIRS	09/17
1998	Landsat 5 TM	05/19			

Path and Row Worldwide Reference System (WRS) is designated for locating Landsat scenes for any area on Earth (Jensen, 2007). The entire study area can be covered by the WRS-2 path-18/row-30 scene. Images are projected in Universal Transverse Mercator (UTM) coordinates based on World Geodetic System of 1984 (WGS84) datum. Since the time span of this study is from 1984 to 2013, one scene of each year is needed. To obtain high quality data, images with no cloud and no haze were selected. Data for 1988, 2004, and 2012 were eliminated due to large cloud obstructed area. In order to minimize the phenological effect during change detection analysis, data acquired in summer season were preferred. Most of the data are obtained from June to September. All used Landsat data were retrieved from USGS Global Visualization Viewer (GloVis) interface (<http://glovis.usgs.gov/>). Specific data acquisition information is listed in Table 3.1.

3.2.2 Supplementary Data

To clip out the study area from Landsat images, a shapefile representing the study area boundary should be generated first. This shapefile can be considered as the revision of the shapefile representing municipal boundaries of Waterloo Region based on the urban area map from ROP. The Region of Waterloo boundary shapefile was obtained from the University of Waterloo Geospatial Centre. The urban area map was retrieved from the Region of Waterloo official website.

To help select training samples of the supervised classification and reference samples for accuracy assessment, two full-colour digital orthoimages with 12cm spatial resolution were acquired from University Geospatial Centre. These two orthoimages cover the entire area of Waterloo Region in 2006 and 2010 respectively. With 12cm spatial resolution, the orthoimages are projected in UTM coordinates and are stored in MrSID image format, accompanying SDW world files (Morgan, 2012). The datum used is the North American Datum of 1983 (NAD83) (Morgan, 2012). Another data that can be used for aiding choosing training samples is a land use shapefile of Waterloo Region in 2007, also obtained from the University of Waterloo Geospatial Centre. This shapefile parcels the study area into polygons based on different land use types. Additionally, Google Maps, providing high spatial resolution aerial or satellite images of the world, is an auxiliary source for training samples selection and accuracy assessment. Selecting appropriate training samples is very critical for satisfactory classification results. Even though there is no reference data for every year, the two orthoimages, the land use shapefile, and images from Google Maps are effective reference data for understanding the land surface information of this study area.

In this study, population growth in recent decades is incorporated to help understand the urbanization process of Waterloo Region. A census of population is taken every five years in Canada (Statistics Canada, 2013). The earliest available census data of Waterloo Region can be dating back to 1991. Data taken since 1991 were recorded and edited by the geographic area. Because the population of non-permanent residents is a growing segment of the Canadian population, Statistics Canada covered both permanent and non-permanent residents since 1991 census (Statistics Canada, 2013). Population information used in this study is for 1991, 1996, 2001, 2006, and 2011, respectively. The shapefiles containing census statistics were retrieved from the University of Waterloo Geospatial Centre.

3.3Chapter Summary

Scenes of the long-term Landsat archive data were selected from 1984 to 2013 for each year with no cloud for classification. Supplementary orthoimages, land use shapefile, and images from Google Maps were useful reference data for training sample selection and accuracy assessment. Census data were incorporated for analyzing urbanization process. Details of data processing and analysis methods will be explained in next chapter.

Chapter 4 Methodology

After study area determination and data acquisition, a sequence of processes was adopted to obtain the desired results. The major modules include data preprocessing, image classification, change detection analysis, and urban growth analysis. This chapter begins with an overview of the methods applied, clearly summarized by a workflow. Then specific steps of each module will be explained sequentially.

4.1 Overview of Workflow

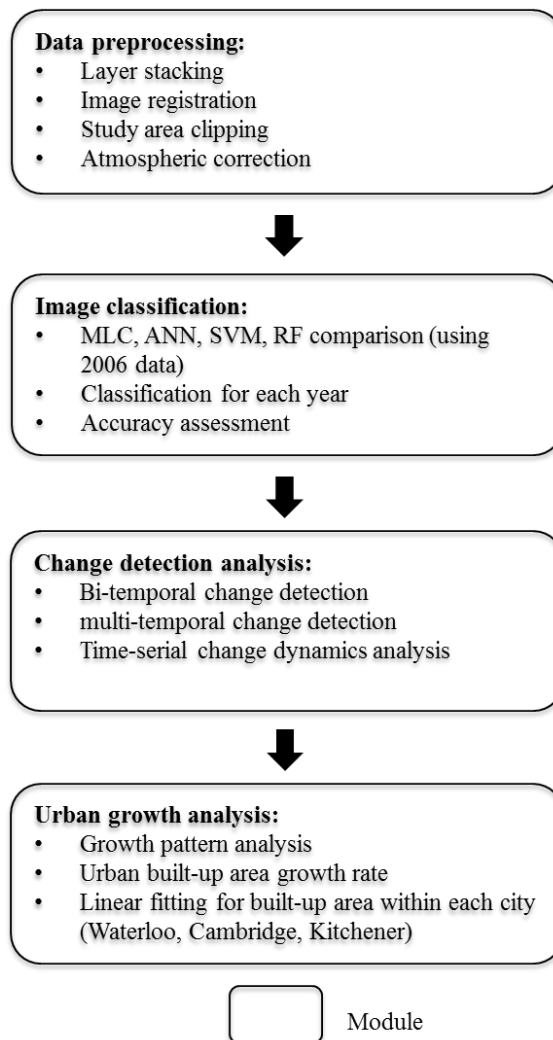


Figure 4.1 Summarized workflow chart

The methodology can be divided into four modules, which are data preprocessing, image classification, change detection analysis and urban growth analysis, illustrated in Figure 4.1. The first module is data preprocessing. After layer stacking for each year, image registration issue was considered. Then study area was clipped out for all images. Atmospheric correction was conducted sequentially for each image based on specific characteristics of data acquisition. After data preprocessing, consistent calibrated images for each year were prepared for LULC information extraction in next module. To determine which classifier would be used for classification of all images, MLC, ANN, SVM, and RF classifiers were compared using 2006 data. The classifier which can obtain the highest classification accuracy was selected for classifying other images. The quality of classification maps was indicated by the results of accuracy assessment. LULC information can be extracted from classification maps for further post-classification analysis. In the third module, change detection analysis is performed in terms of classification maps comparison based on different temporal resolutions ----- bi-temporal, coarsely multi-temporal, and annually time-serial resolutions. Furthermore, in last module, urban built-up area was extracted individually to analyze urban growth pattern. Moreover, a simple linear model was applied to fit the built-up area using all built-up area estimation results. Then development rates for each city (Waterloo, Cambridge, and Kitchener) were acquired. The detailed processes and related image processing principles will be explained in the following sections.

4.2 Data Preprocessing

Data preprocessing is an important part that is prerequisite to generate consistent calibrated images for classification and change detection analysis. Specific processes are shown in Figure 4.2.

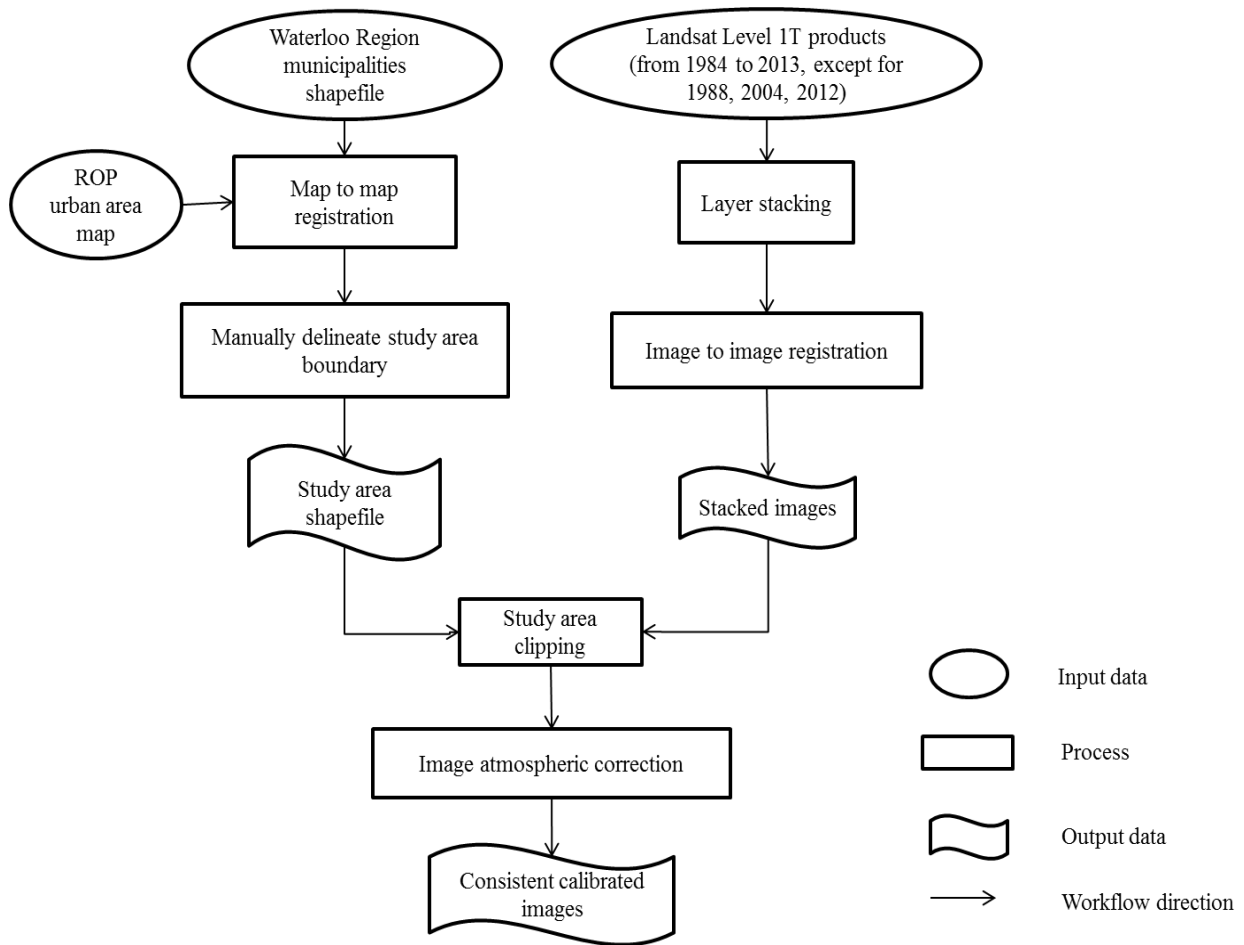


Figure 4.2 Workflow chart of data preprocessing module

Downloaded Landsat archive data were all in GeoTIFF format for each individual band layer. The layers acquired on the same date were stacked into one dataset using ENVI software. All Landsat scenes used in this study were processed to Standard Terrain Correction (Level 1T), which has provided systematic, radiometric, and geometric accuracy (USGS, 2013). However, image registration issue still needs to be considered before performing change detection analysis, because subtle differences caused by spatial offset have direct impact on change detection result. Image registration degree can be visually observed by linking the images for different dates geographically. By checking the overlapping of some easily located

features, such as intersection of roads or corner of a building, all images have already been well co-registered.

To clip out the study area from all Landsat scenes, a shapefile representing the union of ROP urban area and city municipalities needs to be generated. Taking the shapefile which represents Waterloo Region municipalities as the base map, the urban area map can be georeferenced using Georeferencing Tool under ArcGIS software. Study area boundary was generated by extending cities municipal boundaries towards the urban area boundary based on manually delineation. Then study area was clipped out for each Landsat images.

Before electromagnetic radiation emitted from the Earth's surface is observed by satellite sensors, it undergoes interaction with the atmosphere when propagated through the atmosphere (Jensen, 2007; Hadjimitsis et al., 2010). Absorption and scattering of radiation are two major effects of atmosphere. Atmospheric correction is the process of eliminating the atmospheric and terrain effects to obtain the true ground reflectance of the land surface (Geomatica, 2013). In this study, PCI Geomatica ATCOR module was used to conduct atmospheric correction. Atmospheric conditions and some data acquisition information which can be retrieved from metadata file were entered into the ATCOR module to accomplish the correction, such as data acquired date and time, sensor type, coordinates of the image central, atmospheric definition area, and atmospheric condition. Atmospheric definition area was set up as "urban" area. Atmospheric condition was determined as "mid-latitude summer" for images taken prior to October, otherwise as "fall".

4.3 Image Classification

4.3.1 Workflow of image classification module

Image classification is the most important process for obtaining accurate LULC information. To generate consistent classification results, an appropriate classification algorithm needs to be determined first. Thus, this module was comprised of two parts. Detailed workflow is illustrated in Figure 4.3.

Part A was to compare several classifiers that were suitable for urban area classification. Training samples were selected for training process before classification. Some supplementary data, such as 2007 LULC shapefile and 2006 orthoimage, were used to assist in identifying appropriate training samples for 2006 image. A separability report was generated to indicate the spectral separability of the training samples. After the training samples were determined, MLC, ANN, SVM, and RF classifiers were applied on 2006 image to generate classification maps. These classification maps were compared not only by visual observation, but also by conducting statistical accuracy assessment. SVM classifier was superior to other classifiers in this study, and thus was selected to classify other Landsat images.

Part B was classification for all images using SVM classifier. Classification process was the same as Part A. Since the shadows in urban area can be misclassified into water class, post-classification processing of the classification maps was performed to remove the casting shadow by the tall buildings. The real water area has very low value based on mid-infrared and thermal bands. Therefore, shadow areas can be removed by observing their corresponding values from mid-infrared and thermal bands. Then a 3×3 majority filter was applied to the classification maps to reduce the “salt and pepper” noise. Finally accuracy assessment was performed for all classification maps.

During classification process, results accuracy is controlled by the quality of training samples and the classifier used. In the following sections, classification algorithms, training samples selection method, and accuracy assessment method will be explained specifically.

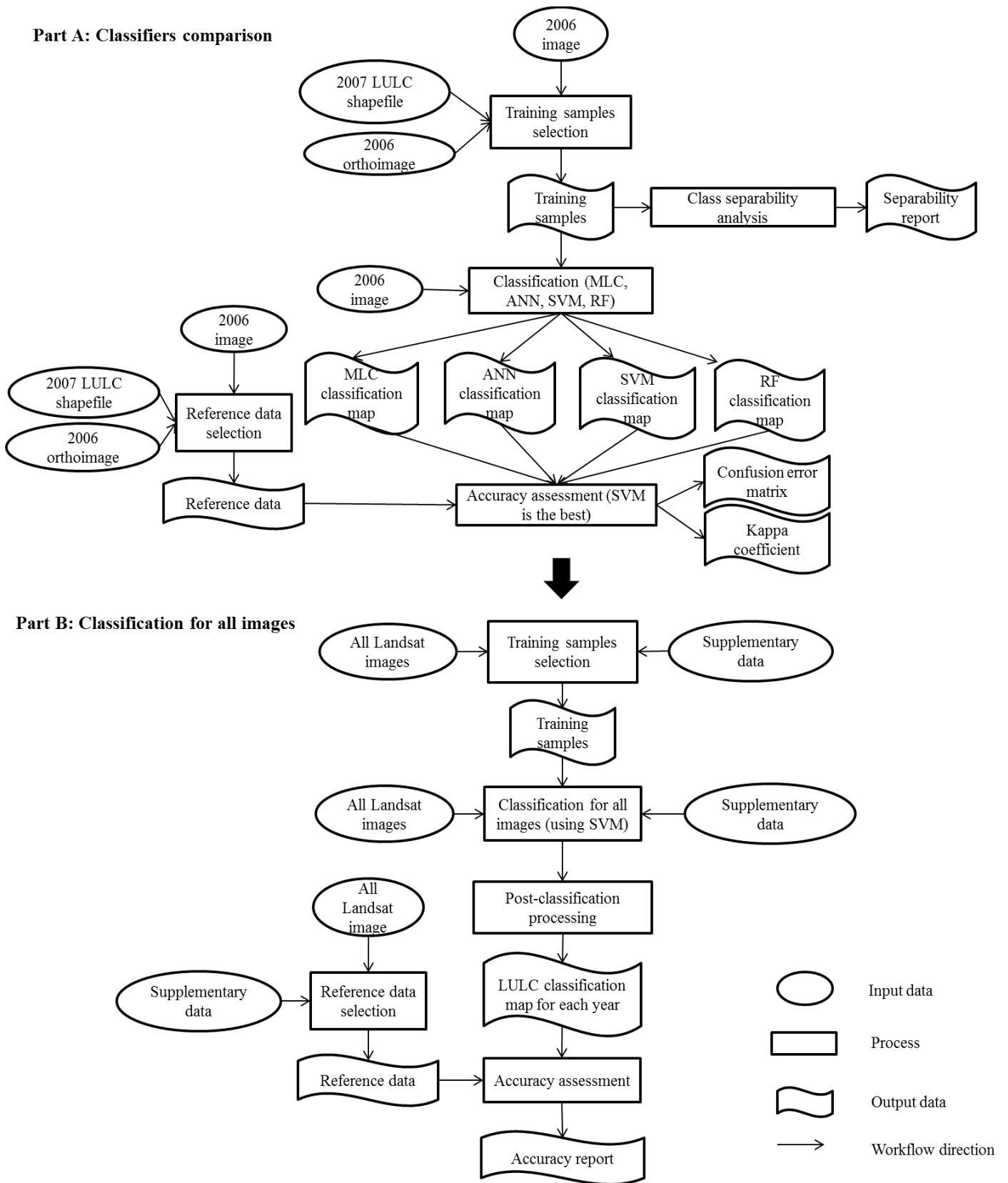


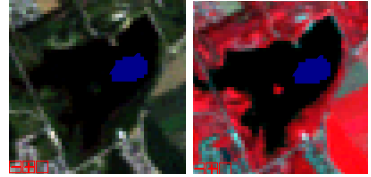
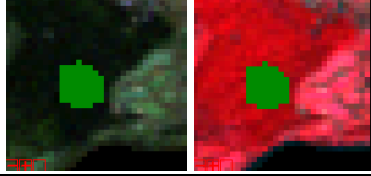
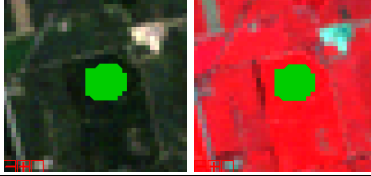
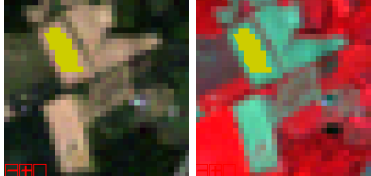
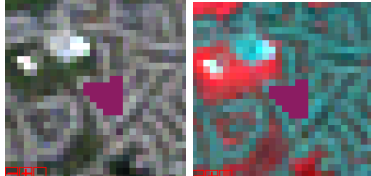
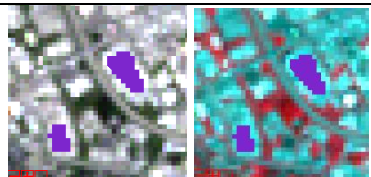
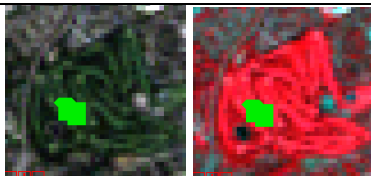
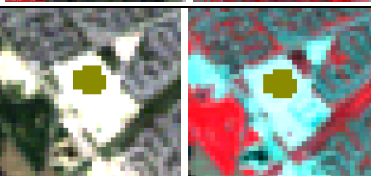
Figure 4.3 Workflow chart of image classification module

4.3.2 Training Samples Selection

An appropriate classification system and sufficient representative training samples are very critical for a successful classification (Lu & Weng, 2007). As referring to USGS “Land-Use/Land-Cover Classification System for Use with Remote Sensor Data” (Anderson et al., 1976), classification design in this study was determined at a mixed USGS Level I/II based on the consideration of spectral and spatial resolution of Landsat image. With visual interpretation and analysis of the satellite images and supplementary data, eight classes were determined, which were water, forest land, agricultural land I (green cropland), agricultural land II (fallow), low-density urban built-up area, high-density urban built-up area, grassland, and barren land. Explanations of the classes and examples of training sites are shown in Table 4.1. Examples are displayed in RGB by true colour composite (Bands 1, 2, 3) and false colour composite (Bands 2, 3, 4) of 2006 image.

One of the key factors of training samples selection is identifying relatively homogeneous pixels of each class from the satellite images. Different classes can be distinguished by their different color, shape, textures, tones, and spectral signatures. Training sites can be selected by visual observation of Landsat images and higher resolution orthoimages, and by distinguishing spectral characteristics of each LULC type. As for the number of samples, a minimum of $10n$ to $100n$ pixels should be selected for each class, where n (is 6 in this study) is the number of spectral bands that used for classification. The total number of training samples is approximately 8000 for each image in this study. Moreover, training samples were distributed dispersedly over the study area to obtain sufficient representative samples. Classification can be conducted after training sample selection.

Table 4.1 Explanations of the classes and examples of training sites

Class Type	Explanation	Examples
Water	Rivers, lakes, reservoirs, streams	
Forest land	Coniferous, deciduous, and mixed forest land	
Agricultural land I (green cropland)	Growing green crop fields	
Agricultural land II (fallow)	Harvested crop fields	
Low-density urban built-up area	single/multiple family houses, roads, yards, small open spaces	
High-density urban built-up area	Commercial and industrial complexes, high-density residential areas	
Grassland	Pastures, golf courses, parks, lawns	
Barren land	Construction/transitional area, sandy area, quarries, bare exposed rock	

4.3.3 Classification Techniques

As reviewed in Chapter 2, MLC is the most widely used classifier in various remote sensing studies. ANN, SVM, and RF are newly developed advanced classifiers that can deal with more complex situation. To determine which classifier would be used in this study, the four classifiers were conducted on 2006 image and then compared their results accuracies. Principles of these classifiers are explained in this section.

4.3.3.1 Maximum Likelihood Classifier

Maximum Likelihood Classifier (MLC) is based on the concept of probability. MLC assumes that the statistics of each class in each band are in normal (Gaussian) distribution, and pixels are assigned to a specific class for which has the highest probability (Jensen, 2005). Taking Figure 4.4 as an example, after calculation of probability density of class A and B, pixel X is assigned to class B because it has higher probability of being a member of class B. This diagram shows a bivariate example as pixel X is distributed in a two dimensional feature space built up by band 1 and band 2. Since Landsat image, which has multispectral bands, is considered as a multivariate dataset, the probabilities can be calculated by an n-dimensional multivariate probability density function based on mean vector and covariance matrix estimated from training data for each class (Jensen, 2005). Since there is no prior knowledge of probability of the classes using Landsat images in this study, an assumption of considering each class has an equal probability of occurring in the study area can be made.

The probability density function can be calculated by:

$$p_i = \frac{1}{2} \log_e |V_i| - \left[\frac{1}{2} (X - M_i)^T V_i^{-1} (X - M_i) \right] \quad (4.1)$$

where M_i mean vector for class i , V_i is the covariance matrix of class i for all bands, V_i^{-1} is the inverse of V_i (Jensen, 2005). And the unknown measurement vector X is in class i if, and only if, $p_i \geq p_j$ for all i and j out of 1, 2, ... m possible classes (Jensen, 2005). The measurement vector X for each unknown pixel has n elements, where n is the number of bands used in classification (Jensen, 2005). To assign an unknown pixel to a specific class, p_i of the measurement vector X of that unknown pixel for each class is calculated (Jensen, 2005). The unknown pixel will be assigned to the class that has the highest probability value (Jensen, 2005). In this study, no probability threshold was set up. All pixels were classified to a specific class. Classification was conducted in ENVI 4.8.

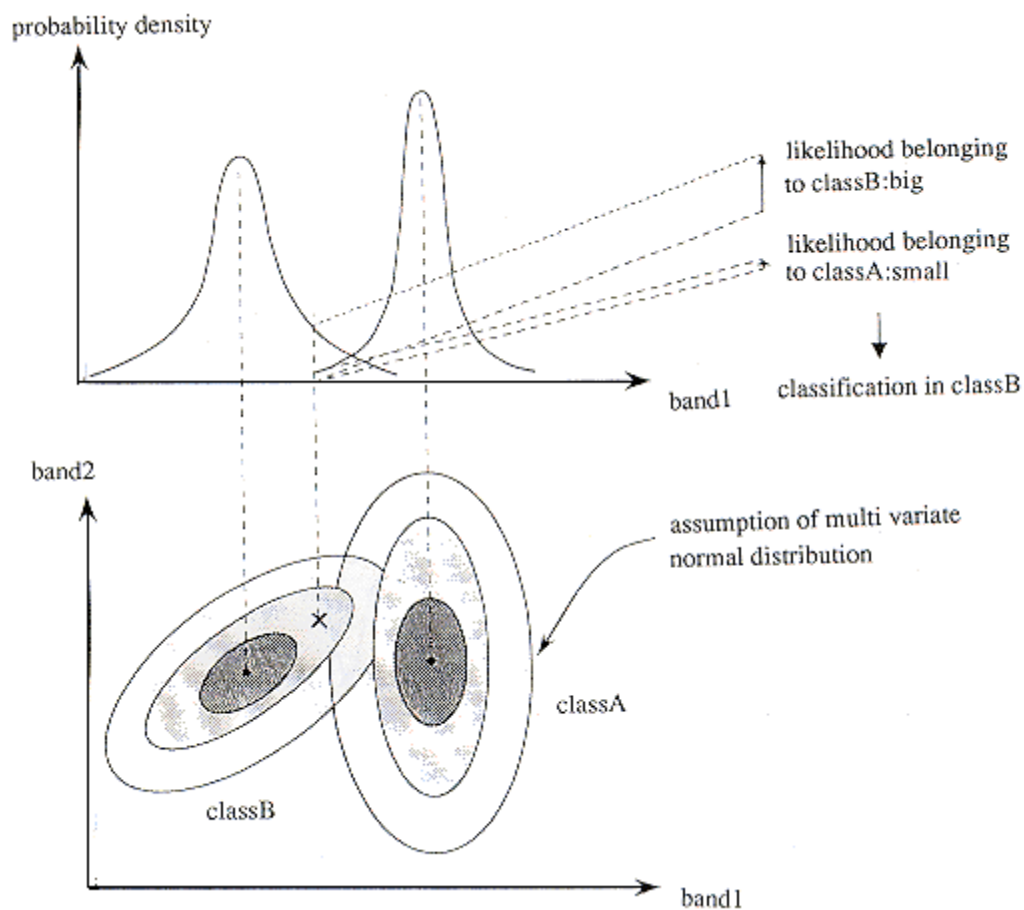


Figure 4.4 Concept of MLC algorithm (Source: JARS, 1999)

4.3.3.2 Artificial Neural Network (ANN)

Feed-forward networks and recurrent networks are the two fundamentally different types of neural networks (Yang, 2011). The multilayer perceptron (MLP) feed-forward networks are the most popular neural networks used in image classification because of its technological robustness (Lu & Weng, 2007; Yang, 2011). As shown in Figure 4.5, MLP neural network is arranged in input-hidden-output layered structure with distributed neurons and weighted links (Yang, 2011). ANN has the capability of dealing with statistics with non-linear relationship, so that the inputs can be various types of data, such as spectral reflectance, slope, elevation, aspect, etc. Then data propagate through the neurons and the weighted links in a forward direction. Each neuron has an activation function that can deal with complex problems individually; and the weighted links determine the data flow direction and the effect of the neuron ahead to the neuron behind (Yang, 2011). Finally, thematic map classes are generated in the output layer.

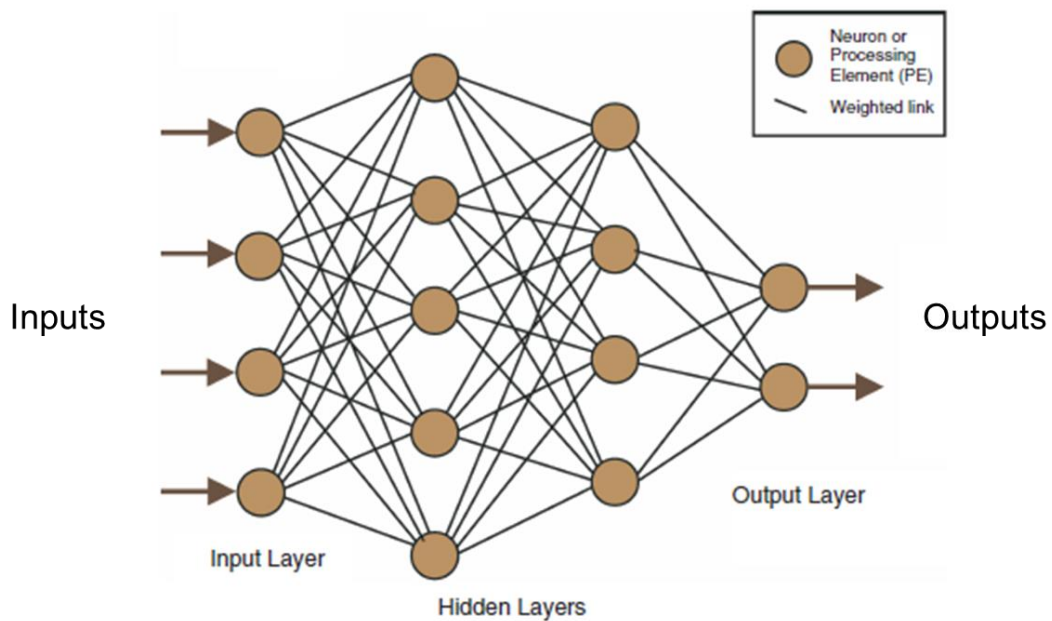


Figure 4.5 An example of MLP neural network (Source: Yang, 2011)

Except for training samples, an error measure and a learning algorithm are needed to accomplish the learning process when using ANN. The learning process aims to acquire an optimal network by adjusting the connection weights (Yang, 2011). The most commonly used error measure is the root mean square error (RMSE); and the widely used learning algorithm is back-propagation method (Yang, 2011). This algorithm used an iterative learning method that on each iteration the direction and magnitude of the weights are adjusted to minimize the RMSE by propagating the computed error backward through the network (Yang, 2011; Song et al., 2012). Then the network can be optimized through the iterations.

In this study, ANN classification was conducted using ENVI 4.8. Several topological parameters and training parameters need to be defined before the training and learning processes. Topological parameters include number of hidden layers, type of activation function, and training threshold, while training parameters include learning rate, momentum and number of iterations (Yang, 2011). To evaluate the sensitivity of MLP neural network for image classification in relation to the parameter settings, Yang (2011) designed an experiment to classify a Landsat ETM+ image of the northern Atlanta metropolitan area with different parameters combinations. The rule of the experiment was to allow one parameter to alter at one time while keeping others unchanged. The results demonstrated that the most accurate classification map was generated by setting one hidden layer, using logistic-sigmoid activation function, and by setting training threshold as zero, learning rate as 0.1, momentum as 0.8, and iteration time as 1300. Since the experiment has been conducted on a Landsat image which had similar urban landscape as this study, same parameter settings were used in this study to save time of tuning the parameters to acquire accurate classification result. Training RMSE exit criterion is another parameter that needs to be defined using ENVI package. Default value (0.1)

of this parameter was used. Learning process will stop when either RMSE exit criterion is reached or all iterations are finished.

4.3.3.3 Support Vector Machine

Support Vector Machine (SVM) is another advance non-parametric statistical learning method that has been successfully applied to LULC classification (Huang et al., 2002; Pal & Mather, 2005; Song et al., 2012). SVM employs optimization algorithms to decide the location of optimal boundaries that can best separate the classes (Huang et al., 2002; Pal & Mather, 2005). Taking a two-class problem as an example (shown as Figure 4.6), if the two classes are linearly separable in two dimensional feature space, a linear boundary can be determined with a greatest margin which leaves maximal space between two classes (Pal & Mather, 2005). This linear boundary can be called as a hyperplane. The margin is determined by the sum of distances from the closest data points to the central hyperplane. Those closest data points are the support vectors (Pal & Mather, 2005).

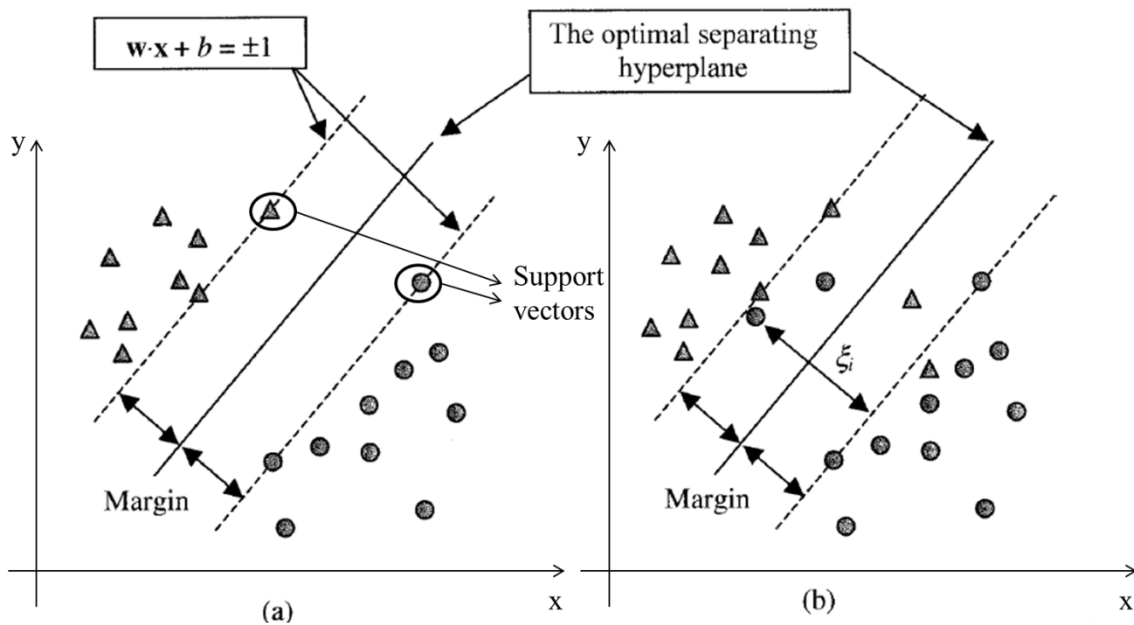


Figure 4.6 Example of the optimal separating hyperplane between (a) separable sample and (b) non-separable samples (Adapted from Huang et al., 2002)

The hyperplane is represented as:

$$\mathbf{w} \cdot \mathbf{x} + b = 0 \quad (4.2)$$

where \mathbf{w} represents the normal vector to the hyperplane, \mathbf{x} are vectors on hyperplane, b is the parameter that determines the offset of hyperplane from the origin by calculating $\frac{b}{\|\mathbf{w}\|}$ ($\|\mathbf{w}\|$ is the Euclidean norm of \mathbf{w}) (Huang et al., 2002). The two linearly separable classes can be separated by two hyperplanes that are parallel to the central optimal hyperplane, shown as Figure 4.6 (a). Then an assumption can be made that each pixel is classified and labeled by $y_i = +1$ or $y_i = -1$ (Huang et al., 2002). The criteria of the classification can be described by:

$$\begin{aligned} \mathbf{w} \cdot \mathbf{x}_i + b \geq 1, \text{ then } y_i = +1 \text{ (} i = 1, 2, 3, \dots, n, n \text{ is the number of samples) or} \\ \mathbf{w} \cdot \mathbf{x}_i + b \leq -1, \text{ then } y_i = -1 \end{aligned}$$

However, in the real world, situations are more complex that there are rarely cases that data samples are well linearly separable. To deal with non-linearly separable cases, except for finding the optimal hyperplane that maximize the margin, misclassification errors should be minimized (Pal & Mather, 2005). Therefore, positive slack variables ξ_i and a penalty parameter C are introduced to solve this problem (Huang et al., 2002). Then the criteria of the classification become as:

$$\begin{aligned} \mathbf{w} \cdot \mathbf{x}_i + b \geq 1 - \xi_i, \text{ then } y_i = +1 \text{ or} \\ \mathbf{w} \cdot \mathbf{x}_i + b \leq -1 - \xi_i, \text{ then } y_i = -1 \end{aligned}$$

The maximized margin can be obtained by using standard quadratic programming (QP) optimization techniques which try to find the minimum value of the following formula (Huang et al., 2002; Pal & Mather, 2005).

$$\frac{\|\mathbf{w}\|^2}{2} + C \sum_{i=1}^n \xi_i \quad (4.3)$$

SVM has been extended to deal with non-linear problem by projecting the sample data onto a high-dimensional feature space using a kernel function and then generate the optimal hyperplane in that feature space (Huang et al., 2002; Pal & Mather, 2005). In this study, SVM classification was conducted using ENVI 4.8. There are four kernel functions that can be used, which are linear, polynomial, radial basis function (RBF), and sigmoid. RBF is the most widely used kernel function (Nemmour & Chibani, 2010; Song et al., 2012) which can be represented by:

$$\mathbf{K}(\mathbf{x}_i, \mathbf{x}_j) = e^{-\gamma(x_i - x_j)^2} \quad (4.4)$$

A γ parameter is introduced that should be defined by users. In terms of a series of trials, the parameter was set as the inverse of the number of bands used in the classification process in this study, which is 0.167; and parameter C is 100.

SVM was initially developed for dealing with two-class problems, and now has been extended for multi-class problems (Huang et al., 2002; Pal & Mather, 2005; Nemmour & Chibani, 2010). n classifiers are generated. And n classes are compared in pairwise way. Each classifier is trained based on only two out of n classes. Each data vector will be tested by all classifiers and given a vote to the winning class (Pal & Mather, 2005). Then the data vector can be assigned to specific class with most votes (Pal & Mather, 2005).

4.3.3.4 Random Forest

Random Forest (RF), which was proposed by Breiman (2001), has become another effective machine learning algorithm to improve classification accuracy significantly in terms of its robustness of dealing with noisy data (Liaw & Wiener, 2002; Pal, 2005; Gislason et al., 2006; Akar & Güngör, 2012; Immitzer et al., 2013; Mellor et al., 2013). RF, which also can be known as a voting based ensemble classification method, creates many classifiers (trees) and

then classifies the data points into the specific class using a voting method based on their predictions (Breiman, 2001; Liaw & Wiener, 2002; Akar & Güngör, 2012). Each classification tree is generated independently using a different bootstrap sample of the dataset with replacement to construct a classifier (Breiman, 2001; Liaw & Wiener, 2002). The selected samples are used for training and the rest of them are used for estimating the error of the tree. The data not in the bootstrap sample is called “out-of-bag” (OOB) data (Breiman, 2001). For each node in a random forest, the best split is determined based on the randomly selected features (or variables) (Breiman, 2001). The trees are grown without pruned (Breiman, 2001). Final prediction of the OOB data can be determined due to the majority votes by aggregating the results of the trees (Breiman, 2001). When a forest is constructed, an OOB estimate of error rate can be calculated to evaluate the performance of the classifiers generated by the training samples (Breiman, 2002).

In this study, RF classification was conducted using “randomForest” package available in R software. R is a free software programming language that used for statistical analysis. The functions available in that package were written by Breiman and Cutler (2002). RF is a user-friendly machine learning method because there are only two parameters that need to be defined and usually classification results are not very sensitive to the values of the parameters (Liaw & Wiener, 2002). These two parameters are the number of variables used to split each node and the number of trees in the forest, which are represented as m_{try} and n_{tree} in R respectively. Breiman (2002) suggested that generally optimum results can be obtained by setting m_{try} equal to the square root of the number of all variables. As for the parameter n_{tree} , generally more trees will obtain more accurate results but take much more time (Breiman, 2002). In this study, a sequence of trials was conducted and m_{try} and n_{tree} were set to be 3 and

500 respectively in terms of the lowest OOB estimate of error rate. The R script can be found in Appendix I.

4.3.4 Accuracy Assessment

Even though each classification algorithm has its own advantages, it is difficult to determine which algorithm is the best due to complex real world situation. In order to select the most appropriate classifier for classification of all Landsat images of this study area, accuracy assessment was performed on classification maps of 2006 image using the four classification methods described above. In addition to compare different classification results, accuracy assessment was also conducted on subsequent classification maps of the rest images.

Accuracy assessment requires unbiased design, strict sampling procedures, and rigorous analysis of the classification results to make the accuracy itself reliable (Congalton & Green, 1999). Some factors and issues need to be considered when performing accuracy assessment, which are reference data selection, sample size, sampling schemes, assessment techniques (confusion error matrix, Kappa analysis), etc. (Congalton, 1991). Reference data were selected on Landsat images based on visual interpretation of the high resolution orthoimages to identify the pixel type. As for the sample size, it should be minimized to reduce the cost and time, and also should be large enough to generate an appropriate error matrix (Congalton & Green, 1999). A general guideline is to collect a minimum of 50 samples for each land cover type (Congalton & Green, 1999). In this study, a more reliable sample size determination method introduced by Thompson (1992) was used. When investigating the accuracy of multi-class classification map, sample size can be calculated by:

$$N = \frac{B\Pi_i(1-\Pi_i)}{b_i^2} \quad (4.5)$$

where N is the sample size; Π_i is the proportion of the i th class out of all classes that has the proportion closest to 50%; b_i is the desired precision; B is determined from the chi-squared (χ^2) table that B is the upper $(\alpha/k) \times 100^{\text{th}}$ percentile of the χ^2 distribution with one degree of freedom; α is the allowable probability of error; and k is the number of classes. When determine the sample size before performing accuracy assessment, the allowable probability of error α should be determined first (Thompson, 1992). $100\%(1-\alpha)$ is called the confidence interval. Confidence interval is a very important parameter of estimating the sample size, because generally it shows the reliability of an estimation (Thompson, 1992). In this study, α and b_i was set to be 0.05 and 0.05 respectively. χ^2 value that used to determine B was $1 - \frac{\alpha}{k} = 0.99375$. Then B was obtained as 7.568 from the chi-squared table. Since the values of Π_i varied from image to image of different years, 2006 classification map was taken as an example here. The value of Π_i was 39%. Then sample size can be determined as 720.

Sampling scheme is another important factor that needs to be considered before accuracy assessment. Stratified random sampling scheme was employed in this study to ensure that sufficient samples can be selected for each class. This method considers classes as strata; then certain number of sample points can be selected randomly without bias within each stratum (Thompson, 1992). Since there were 720 samples totally and eight classes, 90 samples were selected for each class of 2006 classification map.

After reference samples have been selected, reference data were compared to their corresponding classified data to generate the confusion error matrix. This matrix is another important component of accuracy assessment. It is a square array of numbers representing the number of sample points classified into a specific category compared to their actual category based on the reference data (Congaton, 1991). All off-diagonal numbers are considered as

failures (Rossiter, 2004). The confusion matrix can provide much information on a classification. It provides the overall and per-class accuracy. Some descriptive statistics can be derived from the error matrix, such as overall accuracy, user's accuracy, and producer's accuracy. Overall accuracy can be calculated by dividing the total value of diagonal numbers by total number of pixels (Congaton, 1991). Producer's accuracy, also called as omission error, obtained by dividing the number of pixels classified correctly by total number of pixels of that category from the reference data (Congaton, 1991). As for user's accuracy, also the commission error, the denominator is the total number of pixels that classified in one category (Congaton, 1991). Overall accuracy reflects the accuracy of entire thematic map. Producer's accuracy represents how well a certain area can be classified, while user's accuracy indicates the probability that a pixel classified on the map can actually represent the category on the ground (Congalton, 1991).

Another useful statistic of measurement of agreement in accuracy assessment is Kappa coefficient (Congaton, 1991). Kappa statistic is a more sophisticated measure of interclassifier agreement, and provides better interclass discrimination than overall accuracy (Fitzgerald & Lees, 1994). It can be calculated by:

$$K = \frac{N \sum_{i=1}^r x_{ii} - \sum_{i=1}^r (x_{i+} \times x_{+i})}{N^2 - \sum_{i=1}^r (x_{i+} \times x_{+i})} \quad (4.6)$$

where r is the number of rows in the matrix; x_{ii} is the diagonal numbers; x_{i+} and x_{+i} are the marginal total of row i and column i respectively; N is the total number of the samples (Congalton, 1991).

Confusion error matrix and Kappa coefficient were obtained for each classification map in this study to demonstrate the quality of classification maps. Then the useful LULC information can be extracted for change detection analysis and urban growth monitoring.

4.4 Change Detection Analysis

The change detection method used in this study is post-classification change detection. LULC information of each year was extracted to detect changes. To fully understand the change occurred in recent three decades, bi-temporal, multi-temporal (in six-year interval), and time-serial change analyses were performed. The logic of change detection analysis module and some major outputs are illustrated in Figure 4.7.

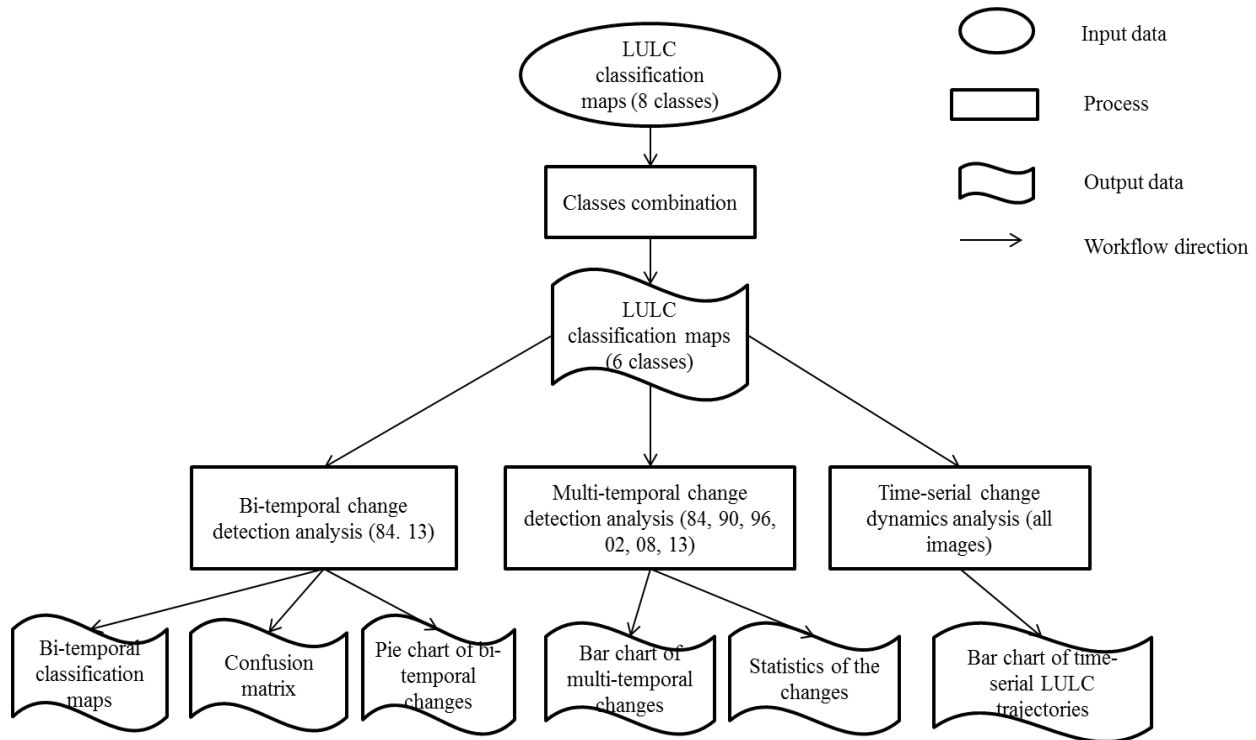


Figure 4.7 Workflow chart of change detection analysis module

In order to minimize the vegetation phenological effect and periodic cultivation cycle of agricultures in suburban and rural area, green cropland, fallow, and grassland were combined into one category, which is called “vegetated area”. Forest land was not combined into the new class because forest is important natural resource that needs to be considered individually. Other classes also remained the same. Then LULC information was extracted for

change detection analyses. Analyses were conducted both qualitatively and quantitatively. Bi-temporal analysis compared the classification maps of 1984 and 2013. Multi-temporal analysis detected changes based on classification maps in six-year interval, which were 1984, 1990, 1996, 2002, 2008, and 2013 classification maps. Time-serial analysis used all images to illustrate the trajectories of each LULC type change dynamics over these three decades. Various graphics and tables were created to help interpret and analyze the results shown in Figure 4.7. For example, change maps demonstrating significant spatial change of LULC types can be obtained; and confusion matrix showing very detailed statistical “from-to” information of each class can be generated.

4.5 Urban Growth Analysis

Changes detected in this study area were primarily caused by urban growth. More specific urban growth analysis was conducted in this module. The logic and processes are clearly illustrated in Figure 4.8. The urban built-up area for each year can be obtained from the LULC classification maps. Spatial growth pattern was analyzed based on the entire built-up area extracted from 1984, 1990, 1996, 2002, 2008, and 2013 maps. An urban sprawl map then can be obtained by overlaying the built-up area detected from those maps. This map was generated based on the assumption that the built-up area existing in previous years would not change to other land cover types. To investigate the relationship between population growth and urban growth, total population of 1991, 1996, 2001, 2006, and 2011 in the municipality area and total built-up area of each corresponding year were used. Since the urban areas belong to the three cities and nearby townships, in order to monitor the urban growth of the cities, built-up areas extracted for each city were analyzed separately.

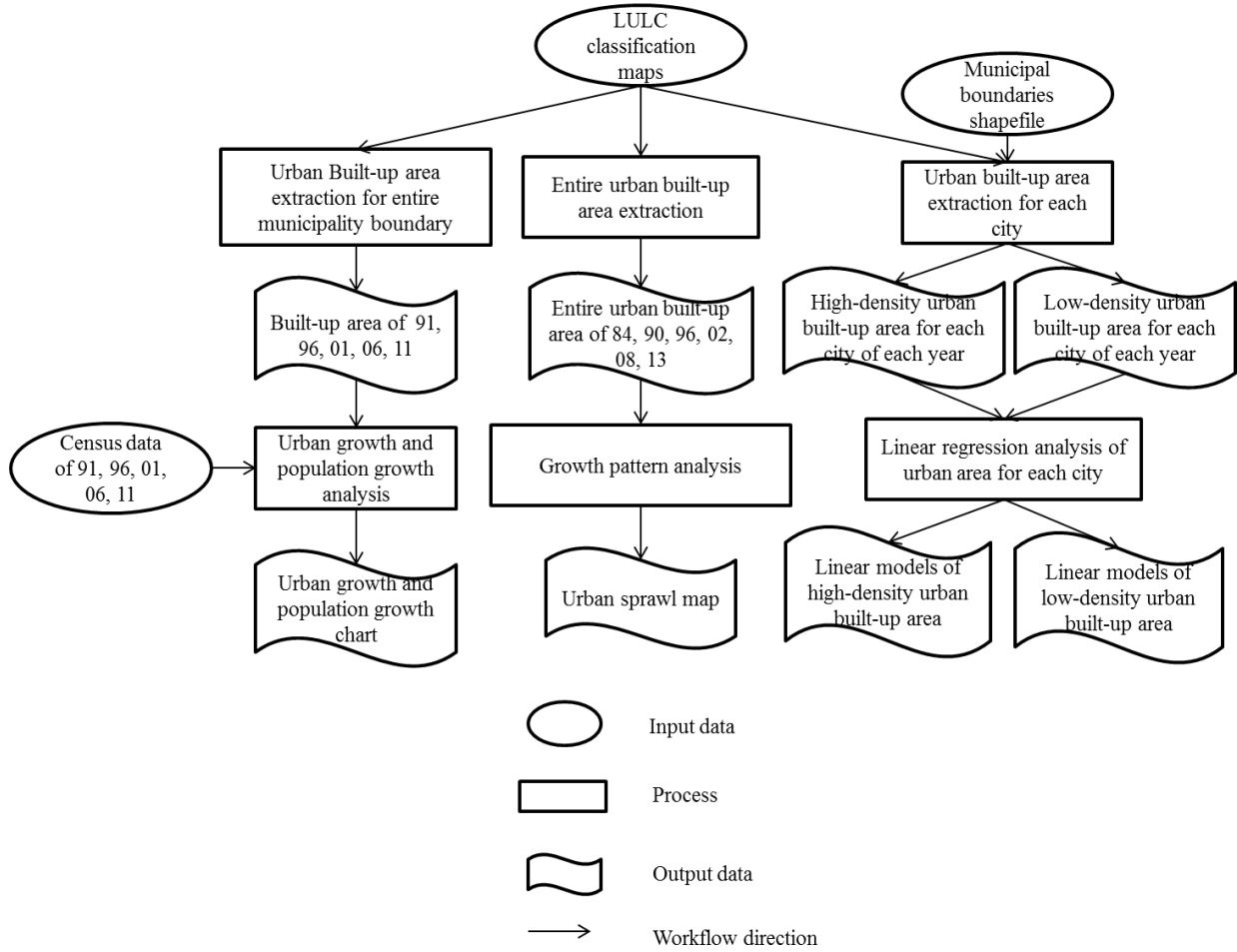


Figure 4.8 Workflow chart of urban growth analysis module

A simple linear regression model was fitted for urban built-up area based on least squares method to show the relationship between the area of built-up areas and corresponding year. Least squares method finds the least sum of squared residuals which are the differences between the observed values and the values provided by the model (Meyers et al., 2006). The sum of squared residuals can be represented by:

$$\sum_{i=1}^n \hat{\varepsilon}_i^2 = \sum_{i=1}^n (Y_i - \hat{Y}_i)^2 \quad (4.7)$$

where n is the number of observations; Y_i is the i th observed value; \hat{Y}_i is the model estimated value; $\hat{\varepsilon}_i$ is the residual between Y_i and \hat{Y}_i . Thus, after finding the minimum value of $\sum_{i=1}^n \hat{\varepsilon}_i^2$.

The regression line generated based on the values representing the area of built-up areas can be expressed as:

$$Y_i = \beta_0 + \beta_1 X_i \quad (4.7)$$

where Y_i represents the area of built-up area of the i th year; X_i represents the i th year; β_0 is value of the Y intercept when X equals 0; β_1 is regression coefficient, which is also known as the slope of regression line (Meyers et al., 2006; Walpole et al., 2012). In this study, coefficient β_1 also can be considered as the annual urban growth rate. Standard error of each estimated coefficient was also calculated. The equations are listed in Appendix I.

To measure the strength of linear relationship between Y_i and X_i , the coefficient of determination, denoted as R^2 , was used in this study. This indicator is widely used to represent the total proportion of variation which can be explained by the regression (Meyers et al., 2006; Walpole et al., 2012). The value ranges from 0 to 1. A value close to 0 indicates little association between X_i and Y_i while a value close to 1 indicates strong relevance (Meyers et al., 2006; Walpole et al., 2012). Calculation process of R^2 is also illustrated in Appendix I. p-value, an indicator showing the significance of the relationship of X_i and Y_i , was also provided in this study. The lower the value, the more significant the relationship is (Meyers et al., 2006; Walpole et al., 2012).

The linear models were generated for high-density urban area and low-density urban area of each city respectively based on the information extracted from time-serial classification maps. In this way, urban growth rate for each city can be obtained. The linear regression analysis was conducted by using SPSS software.

4.6 Chapter Summary

This chapter gives an overall and comprehensive explanation of the methods that used in this study. This methodology consists of four modules, which are data preprocessing, image classification, change detection analysis, and urban growth analysis. All Landsat images needed to be checked and preprocessed to calibrated consistent images for classification process. Classifiers, such as MLC, ANN, SVM, and RF, were compared based on the classification results. Algorithm of each classifier was explained here. The most appropriate classifier with the highest classification accuracy was selected for classification of all images. After obtaining the LULC classification maps for each year from 1984 to 2013, change detection analysis was performed in terms of different temporal resolutions. Furthermore, urban built-up area was extracted individually for urban growth analysis. The trend of urban development can be detected and analyzed.

Chapter 5 Results and Analysis

Following the methodology specified in Chapter 4, results of this study were obtained. Classification maps of 2006 image generated by the four classifiers, ANN, MLC, SVM, and RF, were compared to select the most appropriate one for all image classification. Subsequent change detection and urban growth analysis were based on the annual classification results. Change detection analysis was conducted from different temporal resolutions perspective. Urban growth situation of each city was monitored using high-frequent classification results. In this chapter, major results are provided and analyzed. Analyses focus on dynamic LULC change detection analysis and urban growth monitoring.

5.1 Classification

5.1.1 Class Separability

Training sample selection is a very important process for obtaining accurate and reliable classification results. For 2006 image classification, pairwise spectral separability values of different classes of training samples are shown in Table 5.1. Values range from 0 to 2. The closer to 2, the more separable training samples have been selected (ENVI Help, 2010). Values greater than 1.9 represent that class pairs have good separability, while values lower than 1 represent that the class pairs should be combined into one single class (ENVI Help, 2010). Observing the values shown in Table 5.1, most of the class pairs are well separated from each other with values greater than 1.9. Grassland and green cropland have relatively lower value (1.657); and class separability value of pair of high-density urban built-up area and barren land (1.412) is also relatively lower than other pairs. However, no class has to be combined into others because all values are greater than 1. The selected training samples are

satisfactory to be used for classification. After determining the training samples, classification using four classifiers can be conducted. Classification results will be illustrated in the following context.

Table 5.1 Class separability of training samples of 2006 image

Separability values	Water	Forest land	Green cropland	Fallow	Low-density urban area	High-density urban area	Grassland	Barren land
Water	——	1.999	1.999	2.000	1.999	2.000	1.999	2.000
Forest land	——	——	1.898	2.000	2.000	2.000	1.995	2.000
Green cropland	——	——	——	2.000	1.999	2.000	1.657	2.000
Fallow	——	——	——	——	1.999	1.999	2.000	1.999
Low-density urban area	——	——	——	——	——	1.985	1.999	1.999
High-density urban area	——	——	——	——	——	——	2.000	1.412
Grassland	——	——	——	——	——	——	——	2.000
Barren land	——	——	——	——	——	——	——	——

5.1.2 Comparison of Classifiers

Classification was conducted on 2006 image using four different classifiers, which were MLC, ANN, SVM, and RF. The classification maps are illustrated in Figure 5.1. Analyzing the classification maps from Figure 5.1 (a) to (d) visually, maps generated by three machine learning classifiers appear to be very similar. All classification maps have intraclass “salt and pepper” noise. This situation of MLC classification map is more obvious than others. Additionally, some pixels which represent shadow areas that are casted by tall buildings are classified into “water”. However, in general, by rough observation, all classifiers can generate useful LULC maps and produce consistent classification results.



Figure 5.1 Classification maps of 2006 generated by (a) MLC, (b) ANN, (c) SVM, (d) RF, and (e) SVM with post-classification processing

In addition to visually observing the classification maps, accuracy assessment was also conducted on the classification maps to compare the performance of these classifiers quantitatively. User's accuracy and producer's accuracy of each category and overall accuracy and Kappa coefficient of each classification map are demonstrated in Table 5.2. According to the result, in general, classification using SVM has highest overall accuracy and Kappa coefficient, which are 89.58% and 0.88 respectively, while MLC generates the least accurate classification map with 81.11% overall accuracy and 0.78 Kappa coefficient. Classification maps generated by ANN and RF have much higher overall accuracy (88.36% and 88.47% respectively) than MLC, but relatively slightly lower than SVM.

Table 5.2 Accuracy assessment of classification maps generated by different classifiers

Class	MLC		ANN		SVM		RF		SVM (with post-classification processing)	
	UA (%)	PA (%)	UA (%)	PA (%)	UA (%)	PA (%)	UA (%)	PA (%)	UA (%)	PA (%)
Water	100.00	95.56	100.00	98.89	100.00	100.00	100.00	96.56	100.00	100.00
Forest land	85.94	61.11	97.65	92.22	93.48	95.56	95.24	88.89	91.67	97.78
Green cropland	75.00	60.00	68.70	87.78	77.45	87.78	83.52	84.44	79.05	92.22
Fallow	93.02	88.89	92.22	92.22	89.58	95.56	93.33	93.33	92.55	96.67
Low-density urban area	100.00	97.78	98.89	98.89	100.00	97.78	96.67	96.67	100.00	100.00
High-density urban area	88.57	68.89	90.67	75.56	88.75	78.89	85.54	78.89	96.30	86.67
Grassland	56.93	86.67	85.92	67.78	92.31	80.00	79.21	88.89	93.42	78.89
Barren land	69.23	90.00	73.33	85.56	77.66	81.11	76.84	81.11	86.02	88.89
Overall accuracy (%)	81.11		87.36		89.58		88.47		91.94	
Kappa coefficient	0.78		0.86		0.88		0.87		0.91	

(UA = user's accuracy; PA = producer's accuracy)

Be more specific, to detect performance of the classification of each category, user's accuracy (UA) and producer's accuracy (PA) should be analyzed as well. These values are important for indicating the value of LULC information extracted from the classification maps. According to Table 5.2, referring to "water" category, SVM provides 100% accuracy for both UA and PA. For "forest land", "fallow", and "low-density urban area" categories, all classification maps have high UA and PA with values greater than 85%, except for PA of "forest land" in MLC map. Comparatively, "fallow", "high-density urban area", "grassland" and "barren land" have lower UA and PA with most values around 80%. For MLC classification map, UA and PA are overall lower than other classification maps, which is consistent with the result of their overall accuracies. As for other three classifiers, they generate classification maps with high UA and PA generally. However, ANN generates less stable result in terms of some low values. For example, green cropland and barren land have low UA, which are 68.70% and 73.33% respectively; and grassland has low PA, which is 67.78%. As for SVM and RF, SVM generated classification maps with relatively more stable and higher UA and PA of the classes than RF.

All in all, SVM was selected for classification of all Landsat images to extract LULC information. To improve classification accuracy, post-classification processing was conducted on all classification maps. To demonstrate the improvement of classification result after this process, one example for 2006 image is shown as Figure 5.1 (e). Intra-class "salt and pepper" noise is reduced. According to Table 5.2, overall accuracy increases to 91.94%. UA and PA of high-density urban area and barren land are significantly improved. After all classification maps have been generated, change detection and urban growth monitoring were performed. Results are shown in the following sections.

5.2 Analysis of LULC Change

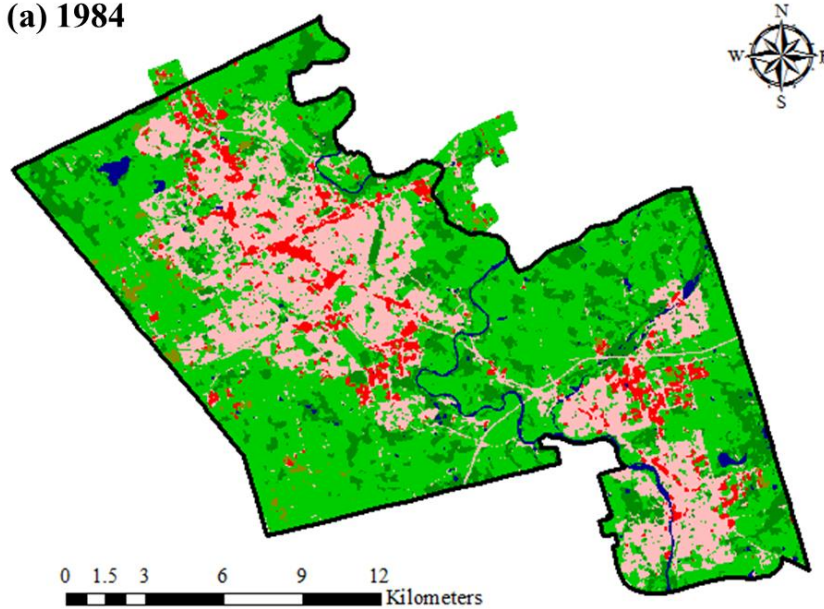
Classification was performed on all Landsat images of each year from 1984 to 2013 except for 1988, 2004, and 2012. Accuracy assessment result of each classification map is summarized in Appendix III. To increase the reliability of change detection result, green cropland, fallow, and grassland were combined into “vegetated area”. Other classes remained the same. Change detection analysis was conducted based on the classification results. To make the change detection results more meaningful from management perspective, statistics were extracted not from the entire study area, but from the municipality area of the cities. Results of bi-temporal, multi-temporal and time-serial change dynamics analysis are demonstrated in this section.

5.2.1 Bi-Temporal Change Detection Analysis

Classification maps of 1984 and 2013 are shown in Figure 5.2 with six classes, which are water, forest land, vegetated area, low-density urban area, high-density urban area, and barren land. There are two large and concentrated built-up areas which locations are isolated and can easily be distinguished in this study area in both two classification maps. The southeast urban area is located in Waterloo-Kitchener city area. And the other one is located in Cambridge city area. According to the maps, the most significant change occurred during this time period is caused by the expansion of urban built-up area. The sprawl of built-up area encroaches large area of vegetated area which includes agricultural land and grassland. As for other LULC types, just based on visual observation of the classification maps, forest lands almost remain the same; and water bodies are also well preserved. Some barren lands remain

the same, while some change to built-up area. To detect more specific changes occurred during this time period, the two classification maps are overlaid to extract the changes.

(a) 1984



(b) 2013

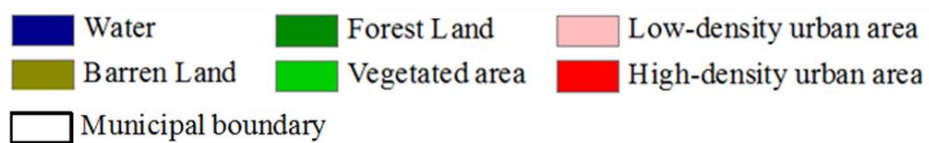
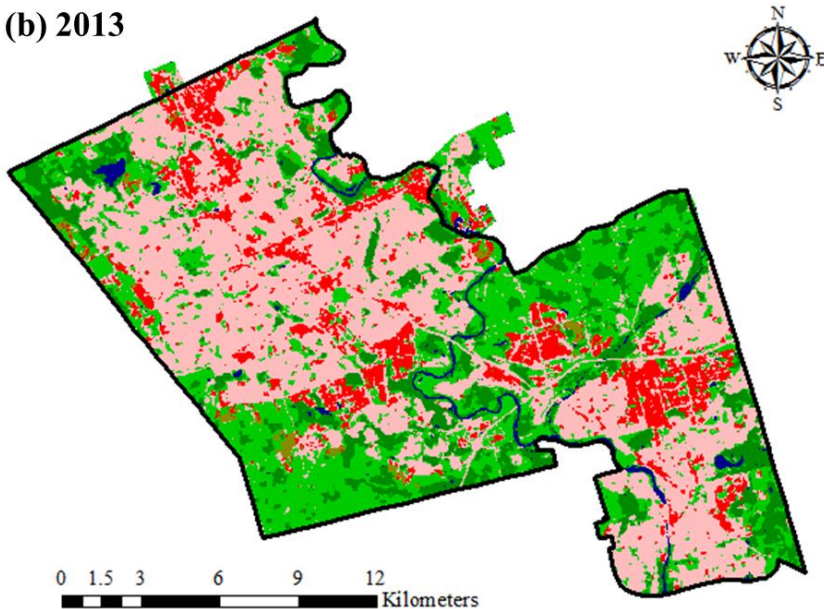


Figure 5.2 Classification maps of (a) 1984 and (b) 2013



Figure 5.3 Examples of real scenes of several LULC types

Overall accuracy of each map is shown in Appendix III. Reference samples were selected on Landsat images. Since 2013 is the most recent image, in order to make the result of accuracy assessment more reliable, a field trip was taken to checking the LULC type of several confusing pixels. Figure 5.3 shows some examples of photos taken for some LULC types. The field trips guaranteed the quality of reference samples.

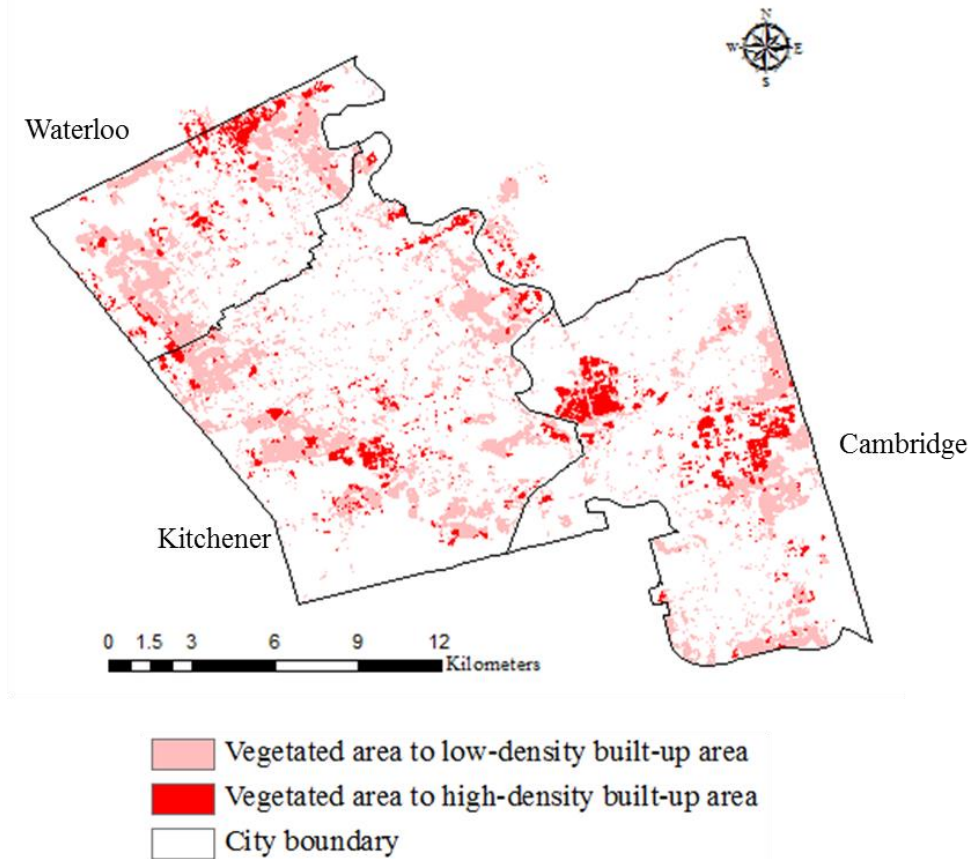


Figure 5.4 Change map showing alteration from vegetated area to built-up area

Based on the change detection result, important changes can be obtained. The most significant change is the alteration from vegetated area to built-up area. Figure 5.4 shows the spatial distribution of this type of change occurred over the recent 30 years. Low-density built-up area in Waterloo-Kitchener city area, represented as pink area, replaces large area of the greenfield surrounding the urban built-up area existing in 1984. As for Cambridge city area, low-density built-up area also increases and mainly occupies large amount of vegetation in the east and south part of Cambridge. For high-density built-up area which appears as red in Figure 5.4, result demonstrates that changes mainly occur in the north of Waterloo, in the south of Kitchener, and in the middle of Cambridge. Also, near the border of Kitchener and Cambridge, large area of high-density built-up area emerges that can be easily detected in the change map.

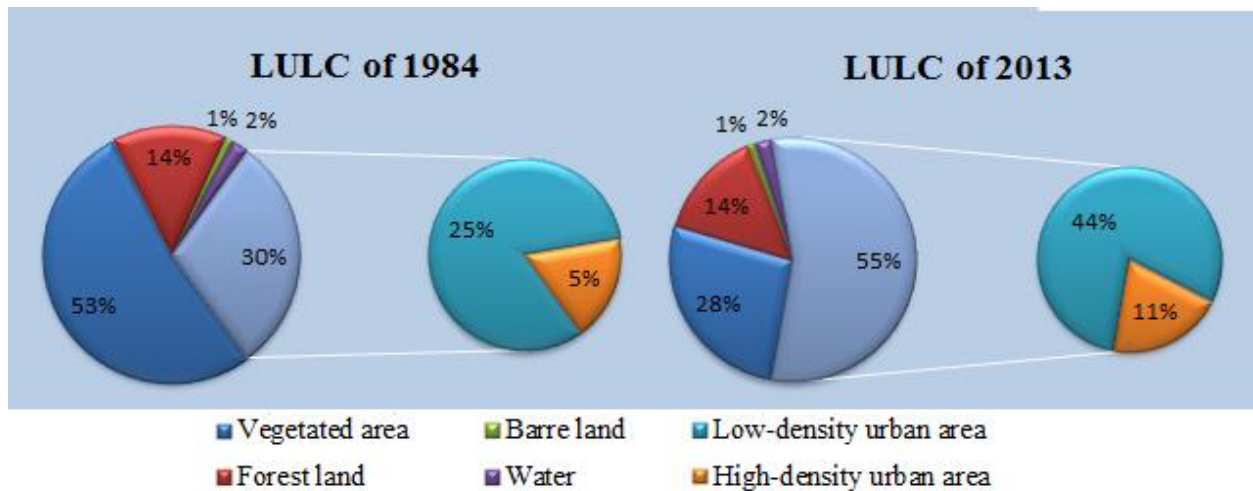


Figure 5.5 Pie chart of LULC coverage of 1984 and 2013

By counting the number of pixels of each class for each year, LULC coverage information can be obtained, which is shown as Figure 5.5. Taking the entire municipality area as a whole, forest land, water, and barren land don't experience significant change over the time period in general. The percentages of coverage of these three classes remain approximately 14%, 2%, and 1% respectively by coarsely estimated. However, as for vegetated area, the coverage shrinks dramatically from 53% to 28%, demonstrating that almost half of the vegetation excluding forest has disappeared by recent 30 years. Consistent with the decrease of vegetated area, coverage of urban built-up area increases significantly from 30% to 55%. Low-density area grows from 25% to 44%; and the coverage of high-density area in 2013 (11%) becomes more than twice as that in 1984 (5%).

Figure 5.5 only demonstrates the static state of each class in 1984 and 2013. In addition to the alteration from vegetated area to built-up area, other types of interclass changes also need to be detected for more comprehensive analysis. Specific "from-to" change information is obtained and summarized in Table 5.3. Values shown in the table represent the amount of change from one type detected in 1984 to another type detected in 2013. The amount of

changes is demonstrated by area (km²) and percentage (%) of the change class area detected in 1984. Observing the table, diagonal values represent the area with no change. Water, forest land, low-density urban area, and high-density urban are relatively stable classes that don't have significant change, keeping 72.46%, 68.68%, 89.15%, and 75.46% unchanged respectively. Only about 1.013 km² of water change to forest land and 0.36 km² change to vegetated area. 7.349 km² of forest land become vegetated area and 5.79 km² become low-density urban built-up area. As for low-density built-up area, a small portion (2.22 km²) of the area changes to vegetated area and another small portion (5.6 km²) changes to high-density built-up area. However, about 3.583 km² area of high-density built-up area changes to low-density built-up area according to the table.

Table 5.3 “From-to” change confusion matrix

1984 \ 2013	Water	Forest land	Vegetated area	Low-density urban area	High-density urban area	Barren land
	km ² (%)	km ² (%)	km ² (%)	km ² (%)	km ² (%)	km ² (%)
Water	4.651 (72.46)	0.704 (1.54)	0.574 (0.35)	0.116 (0.15)	0.001 (0.01)	0.000 (0.00)
Forest land	1.013 (15.77)	31.472 (68.68)	12.815 (7.78)	0.716 (0.89)	0.007 (0.04)	0.011 (0.34)
Vegetated area	0.356 (5.38)	7.349 (16.04)	72.094 (43.77)	2.222 (2.77)	0.433 (2.53)	1.058 (33.06)
Low-density urban area	0.401 (6.25)	5.794 (12.65)	60.106 (36.49)	71.619 (89.15)	3.583 (20.95)	1.387 (43.36)
High-density urban area	0.008 (0.13)	0.437 (0.95)	16.381 (9.95)	5.600 (6.97)	12.907 (75.46)	0.661 (20.65)
Barren land	0.000 (0.00)	0.067 (0.15)	2.737 (1.66)	0.061 (0.08)	0.175 (1.02)	0.083 (2.59)
Class changes	1.778 (27.55)	14.351 (31.32)	92.613 (56.23)	8.715 (10.85)	4.199 (24.55)	3.117 (97.41)

Comparatively, vegetated area experiences the most dramatic change. 60.106 km² and 16.381 km² of vegetated areas alter into low-density built-up area and high-density built-up

area, respectively. And 2.737 km² of the vegetated area are cleaned up to be barren land for establishing built-up area in the future. In total, about 56% of vegetated area detected in 1984 decreases for building purpose. As for barren land, about 1.387 km² and 0.661 km² of the area develop into low-density built-up area and high-density built-up area, respectively. However, the total area of barren land remains almost the same because a portion of vegetated area changes to it. Therefore, most of the barren land area can be considered as construction area that shows the intermediate transitional status from vegetation to buildings.

5.2.2 Multi-Temporal Change Detection Analysis

Based on the bi-temporal change detection method, LULC interclass changes can be detected according to their static states recorded by snapshots taken in 1984 and 2013. Result shows that the major change is the alteration from vegetation to built-up area caused by urban growth process. To detect relatively detailed change processes over the 30-year time period, multi-temporal change detection has been conducted with 6-year interval. Classification maps used in this analysis are of 1984, 1990, 1996, 2002, 2008, and 2013, which are displayed in sequence in Figure 5.6. Overall accuracy of each classification map is shown in Appendix III. All classification maps have high overall accuracy. The growth process of built-up area can be detected roughly by visual interpretation of the maps. It is obvious that both low-density built-up area and high-density built-up area expand outward in general. Low-density area grows surrounding the existing built-up area in Waterloo and Kitchener region, while it grows eastward and southward in Cambridge. As for high-density built-up area, significant growths occur in the north of Waterloo, in the south of Kitchener, and in the middle of Cambridge. Another emergence of high-density industrial area is detected near the boundary of Kitchener and Cambridge with rapid growth. In addition to outward growth, high-density built-up area

also has inward growth pattern which increases built-up density inside urban area. Correspondingly, the coverage of vegetated area shrinks. Some barren lands detected in earlier years are replaced by built-up area successively. And the newly emerged barren lands are mostly located on the fringe of the urban built-up area.

Table 5.4 Statistics of multi-temporal LULC net change

Time period		Water	Forest land	Vegetated area	Low-density urban area	High-density urban area	Barren land
1984 ~ 1990	km ²	-0.848	-1.981	-20.898	10.941	4.694	8.113
	%	-0.27	-0.62	-6.58	3.44	1.48	2.55
1990 ~ 1996	km ²	0.321	15.535	-28.716	9.937	5.633	-2.748
	%	0.10	4.89	-9.04	3.13	1.77	-0.87
1996 ~ 2002	km ²	-0.543	-4.541	-24.634	24.818	1.912	2.984
	%	-0.17	-1.43	-7.75	7.81	0.60	0.94
2002 ~ 2008	km ²	0.761	-6.430	-3.880	8.124	5.609	-4.252
	%	0.24	-2.02	-1.22	2.56	1.77	-1.34
2008 ~ 2013	km ²	0.046	-2.355	-3.040	8.756	1.042	-4.174
	%	0.01	-0.74	-0.96	2.76	0.33	-1.31
1984 ~ 2013	km ²	-0.263	0.228	-81.168	62.577	18.889	-0.077
	%	-0.08	0.07	-25.54	19.69	5.94	-0.02



Figure 5.6 Classification maps of (a) 1984, (b) 1990, (c) 1996, (d) 2002, (e) 2008, and (f) 2013

To detect specific change processes quantitatively, area and percentage of change of each class over each time interval are calculated and summarized in Table 5.4. Analyzing the table generally, only vegetated area experiences constant shrinkage during each time period with total loss of about 81 km². To the contrary, coverage of both low-density and high-density built-up area keeps increasing; the expanded areas are about 63 km² and 19 km² respectively. As for forest land, it only has gain in coverage during 1990 to 1996 period; and over other time period, the area decreases slightly and constantly. Comparatively, gain and loss of coverage of water and barren land are erratic. To more intuitively detect the change process of each class over this time span, area net changes represented by percentage in municipality area of each class are shown as graphic in Figure 5.7. Much of the change occurs during time period of 1990~1996 and 1996 to 2002, while least change occurs during 2008~2013 according to the figure. Gain in urban area is mainly cost by the loss of great amount of vegetated area and small portion of forest land. It is clearly shown that vegetated area experiences constant great loss from 1984 to 2002 with a decrease about 23% of the entire municipality area. Low-density built-up area increases most rapidly during 1996~2002 time period, gaining area of about 8%. During other four time periods, low-density urban area grows at similar rates which are about 3% in average. High-density urban area grows relatively slower than low-density urban area. The most rapid growth occurs during 1990~1996 and 2002~2008 time period, increasing area about 2%. Barren land fluctuates around gain and loss within the 30 years. And water experiences very subtle change that is not easy to detect.

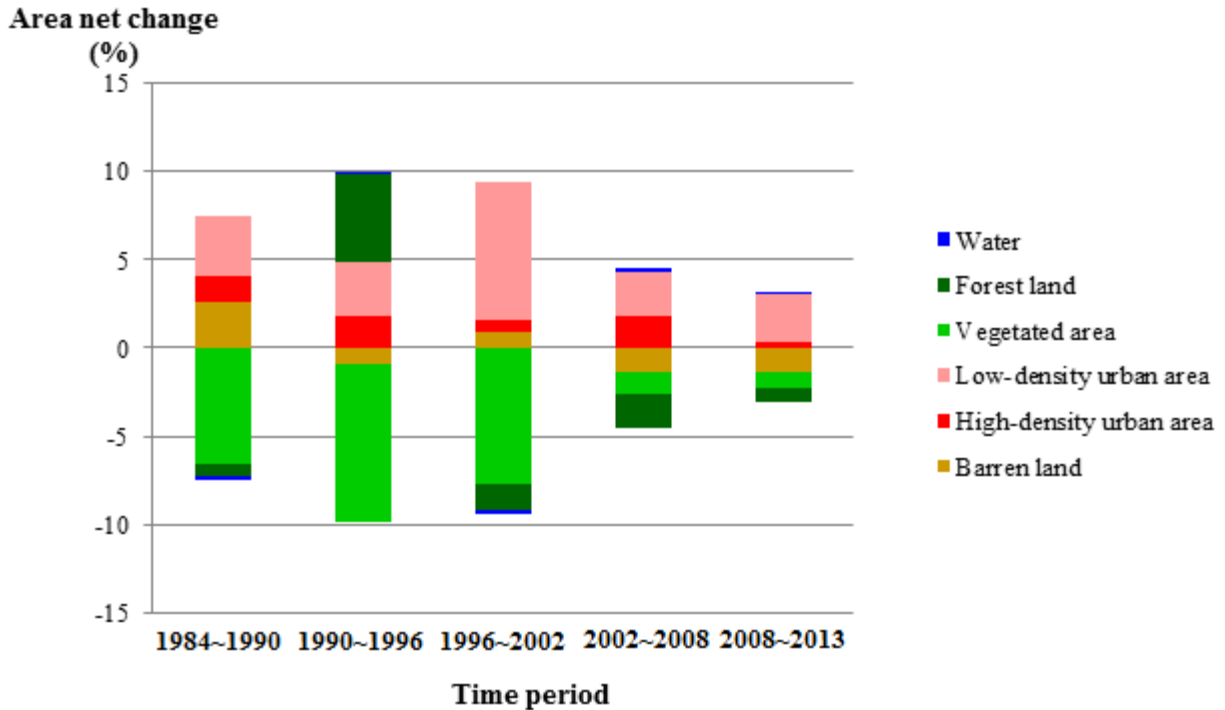


Figure 5.7 Normalized net change in municipality area by time period for each LULC class

5.2.3 Time-Serial Change Dynamics Analysis

In terms of coarsely multi-temporal change detection method, intermediate LULC classification maps generated with given time interval are used and analyzed to reveal the change processes during the time period. This analysis method shows more detailed change information than bi-temporal one. However, to detect more complex dynamics of LULC changes, all classification maps can be involved to accomplish time-serial analysis. . Statistics of the classes are calculated and recorded in Table 5.5. Trajectories of dynamic change of each class are illustrated in Figure 5.8.

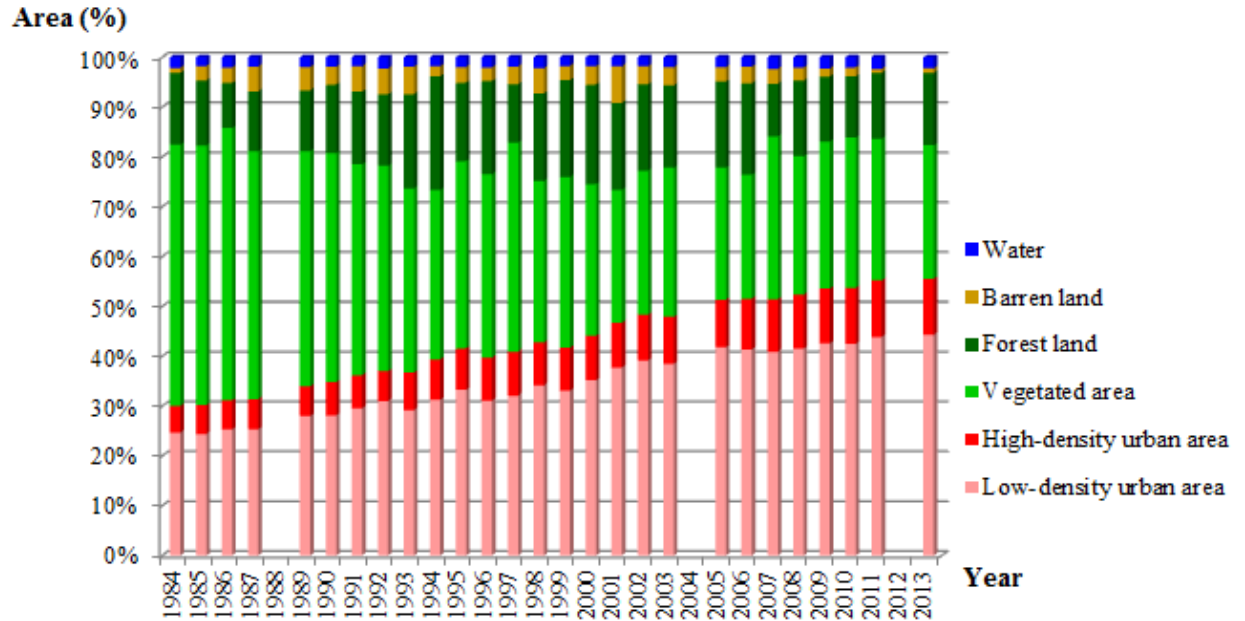


Figure 5.8 LULC dynamic change from 1984 to 2013

According to Figure 5.8, trajectory of change process of each class is clearly illustrated that dynamic change of each class can be easily observed. Obviously, urban built-up area experiences growth over the 30 years in general. However, based on the statistics recorded in Table 5.5, the overall trend of built-up area is increase, but the process is torturous. Area increases in one year but falls back slightly in next year and increases again in later years. For example, according to the table total percentage of built-up area is 48.3% in 2002, but the value decreases to 47.9% in 2003 and rebounds to 51.3% in 2005. The situation of vegetated area is similar as built-up area that the coverage decreases over the period but experiences fluctuation. As for forest land and barren land, they have erratic change throughout the years, while water cover keeps relatively stable values around 2%. Based on the observation of built-up area over the entire time span, Region of Waterloo has experienced relatively accelerating urbanization process in 1990s and in early 2000s.

In terms of the above change detection results, most of the changes are caused by the expansion of urban built-up area at the expense of vegetation area. Urbanization process can be monitored, and will be analyzed in the next section.

Table 5.5 Percentage of each class in municipality area for each year

Class Year	Water (%)	Forest land (%)	Vegetated area (%)	Low-density urban area (%)	High-density urban area (%)	Barren land (%)
1984	2.14	14.37	52.44	24.71	5.32	1.03
1985	1.75	13.06	52.09	24.42	5.79	2.88
1986	2.09	8.99	54.67	25.31	5.82	3.09
1987	1.84	12.02	49.79	25.35	5.98	5.03
1989	1.97	12.21	47.22	28.01	5.92	4.67
1990	1.89	13.71	45.95	28.09	6.74	3.64
1991	1.83	14.58	42.34	29.59	6.56	5.07
1992	2.22	14.31	41.21	30.97	6.03	5.21
1993	1.83	18.88	36.93	29.20	7.56	5.58
1994	1.78	22.83	33.99	31.26	8.09	2.03
1995	1.93	15.74	37.56	33.27	8.31	3.19
1996	2.03	18.65	36.83	31.11	8.61	2.77
1997	1.92	11.65	42.01	32.09	8.80	3.50
1998	2.18	17.57	32.41	34.17	8.64	5.04
1999	1.74	19.41	34.29	33.07	8.63	2.85
2000	1.79	19.97	30.43	35.21	8.87	3.70
2001	1.82	17.43	26.70	37.71	8.99	7.32
2002	1.82	17.31	28.92	39.14	9.19	3.62
2003	1.99	16.53	29.92	38.49	9.43	3.62
2005	2.01	17.28	26.51	41.83	9.51	2.83
2006	1.90	18.39	24.85	41.39	10.15	3.29
2007	2.35	10.53	32.72	40.91	10.50	2.98
2008	2.09	15.16	27.77	41.49	10.90	2.55
2009	2.25	13.03	29.49	42.55	11.03	1.63
2010	2.06	12.31	30.14	42.48	11.27	1.73
2011	2.32	13.25	28.44	43.89	11.32	0.78
2013	2.19	14.50	26.80	44.37	11.29	0.98

5.3 Urban Growth Analysis

5.3.1 Analysis of Urban Growth Pattern

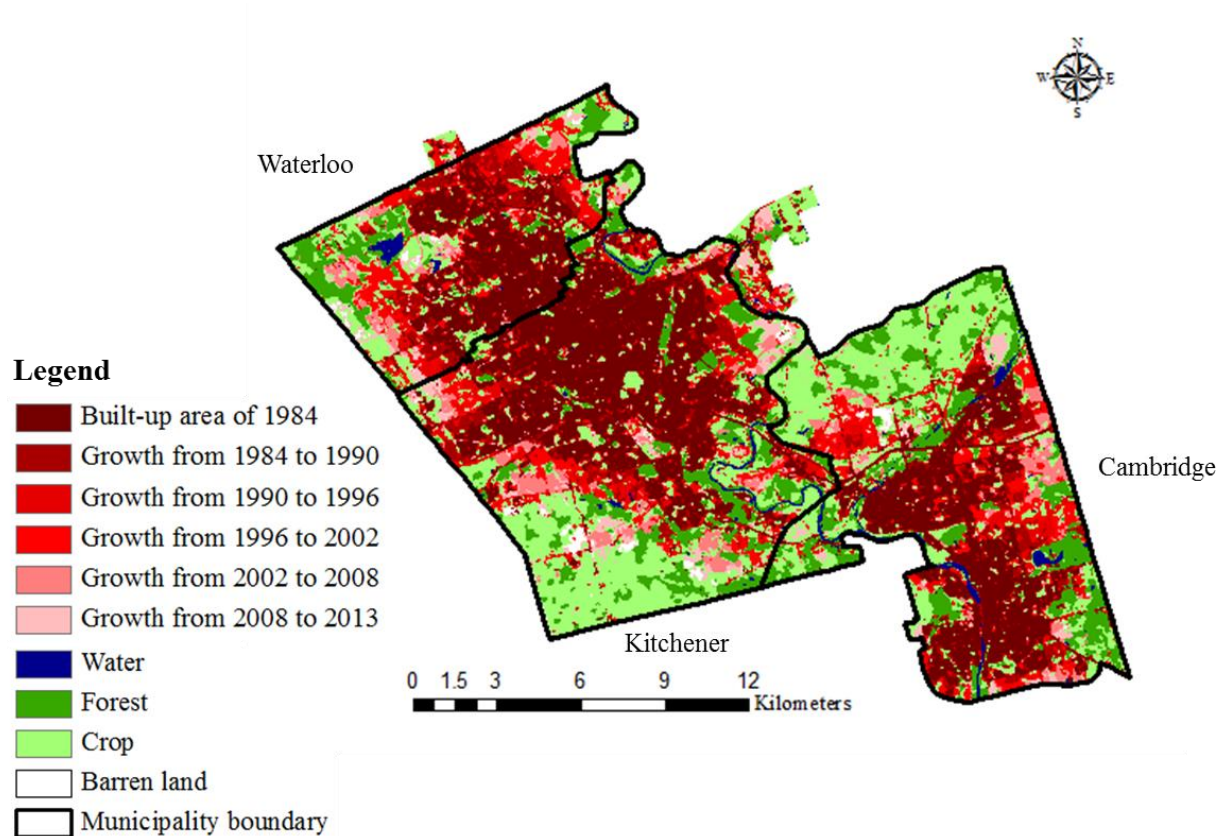


Figure 5.9 Map of the sprawl of urban built-up area

By extracting and overlaying the urban built-up area from the multi-temporal classification maps shown in Figure 5.6. Figure 5.9 shows the map that represents the urban expansion. The area appearing dark mahogany represents the built-up area in 1984. Other built-up area with colors changing gradually from dark red to pale red represents the growth occurred during different time periods, from earlier time periods to recent time periods. From spatial perspective, growth is unevenly distributed across the study area. Three types of urban growth patterns can be observed from this map. The dominant growth pattern over this recent 30-year time period is the exurban outward sprawl pattern that can be most easily detected.

Significant urban expansion in this pattern occurs in the northeast and southwest part of Waterloo, in the northeast and south part of Kitchener, and in the east and south part of Cambridge. As the Grand River flows through the urban area to the east of Waterloo and Kitchener and to the west of Cambridge, the rate of westward urban growth is faster than the eastward growth in Waterloo and Kitchener, while eastward growth is very dramatic and there is almost no westward growth in Cambridge. Examples of urban growth in outward sprawl pattern are shown in Figure 5.10 (a). It can be clearly observed that built-up area experiences steady outward growth over time.

The second type of urban growth pattern is growth in isolation. This can be considered as the initial emergence of built-up area which grows independently to other existing built-up area. One example of this type of growth is shown in Figure 5.10 (b). Referring to Figure 5.6 (a), this area is occupied with vegetation in the 1984 classification map. Then it experiences rapid growth in suburban area in isolation from neither main built-up area over the time period. Though this growth happens in suburban area, it is very close to the junction of Highway 8 and Highway 401.

The third type of growth pattern is inward growth which includes replacement of vegetation in central urban area and intensification of existing built-up area. One example of the previous inward growth is shown in Figure 5.10 (c). Large area of vegetation is gradually occupied by built-up area. As for the latter type of inward growth, the typical example is the change from low-density built-up area to high-density built-up area.

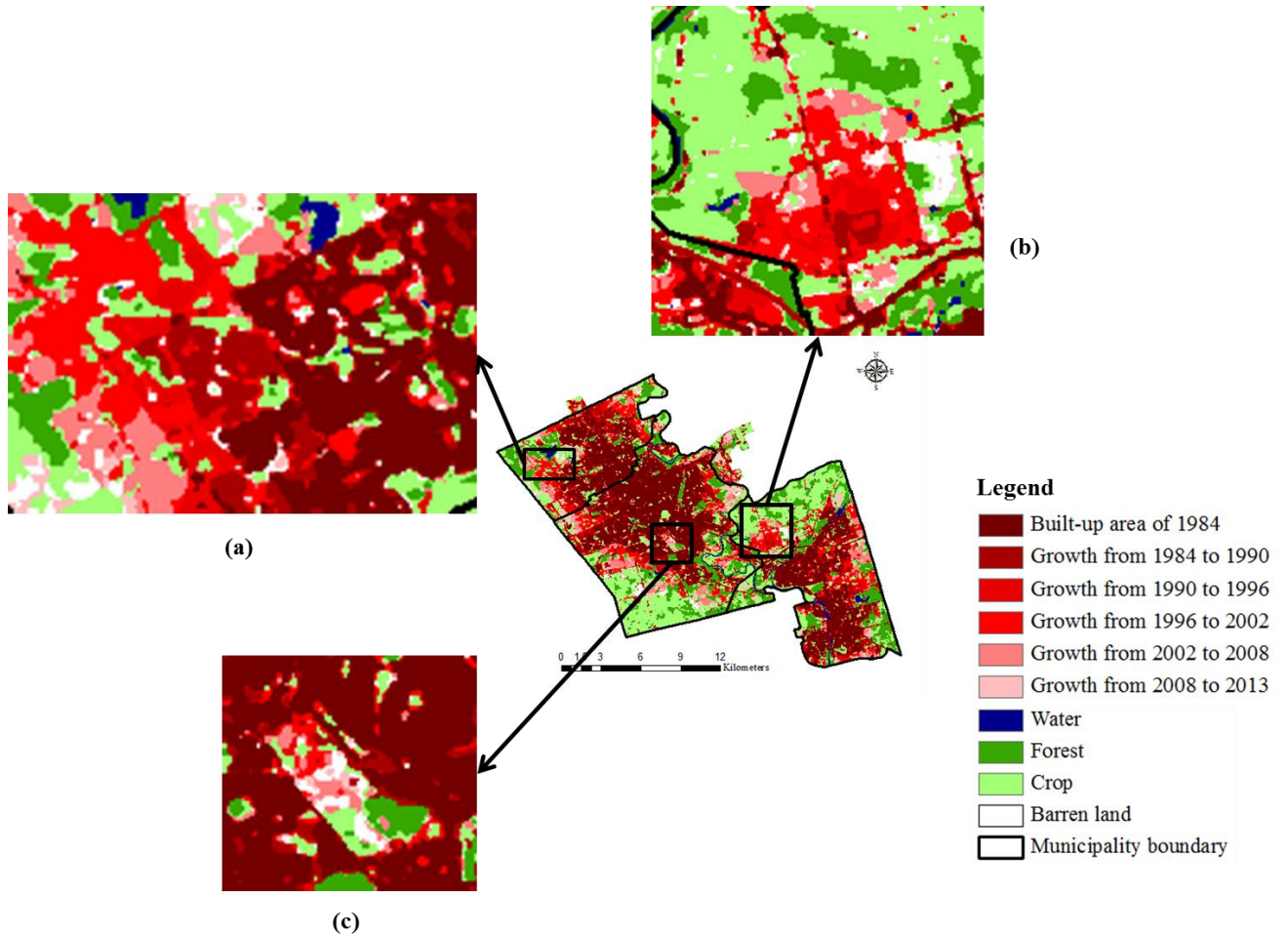


Figure 5.10 Examples of three urban growth patterns

5.3.2 Long-Term Processes of Population Growth and Urban Growth

According to the literature review, urban growth is mainly caused by population growth. To explore the long-term processes of population growth and urban growth of the Region of Waterloo, a double vertical axes chart, shown in Figure 5.11, was generated based on the census data and urban built-up area extracted from the classification maps of the corresponding years. The left hand side axis represents the area of total urban built-up area, while the right hand side axis is the population of the entire municipality area. According to this chart, both population and urban built-up area experiences a constant growth throughout the time period.

To further investigate the relationship between urban growth and population growth, Table 5.6 shows the growth rates of urban area and population for each time period respectively. For 1996~2001 and 2001 ~2006 period, urban built-up area experiences relatively higher growth rate than other time periods, with 17.58% and 10.36% respectively. Likewise, growth rates of population during these two time period are higher than other periods, which are 8.12% and 10.25% respectively. Based on Figure 5.11 and Table 5.6, it can be clearly demonstrated that urban area grows along with population growth in general.

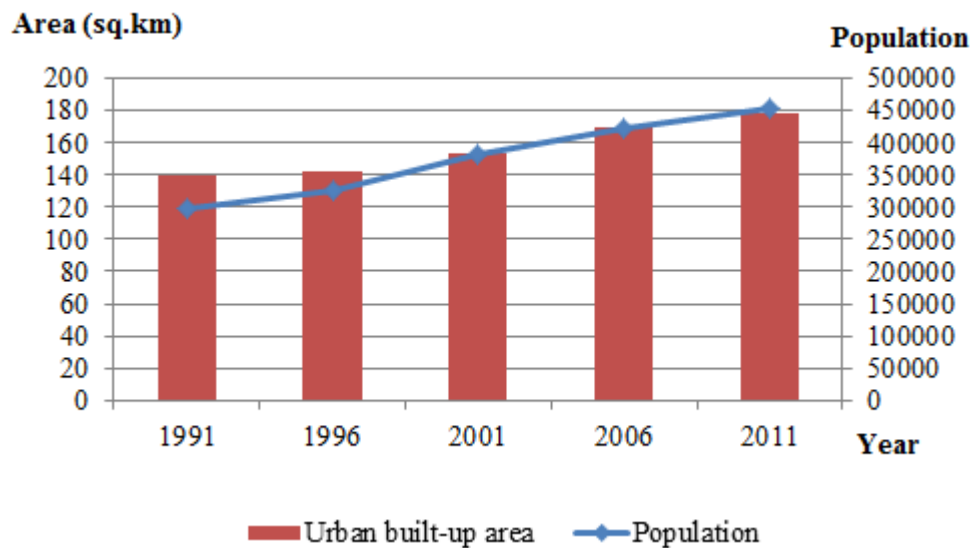


Figure 5.11 Population growth and urbanization process during recent 30 years

Table 5.6 Growth rates of population and urban area

Growth rate (%)	1991~1996	1996~2001	2001~2006	2006~2011
Population	1.18	8.12	10.25	5.25
Urban area	9.86	17.58	10.36	7.10

5.3.3 Linear Regression analysis of Urban Growth

Taking the entire built-up area as a whole object, qualitative growth pattern analysis can be conducted to discover the urbanization process roughly. However, in order to detect urban growth trend in a quantitative way, linear regression analysis was applied using annual urban built-up information. Since the urban area is comprised of three different cities, analysis was conducted on the statistics of each city respectively. Low-density built-up area, high-density built-up area, and total built-up area are also analyzed for each city respectively. Figure 5.12 to Figure 5.14 show the scatter plots and fitted lines of dynamic growth process of low-density built-up area, high-density built-up area, and total built-up area of Waterloo, Kitchener, and Cambridge, respectively, over the time period.

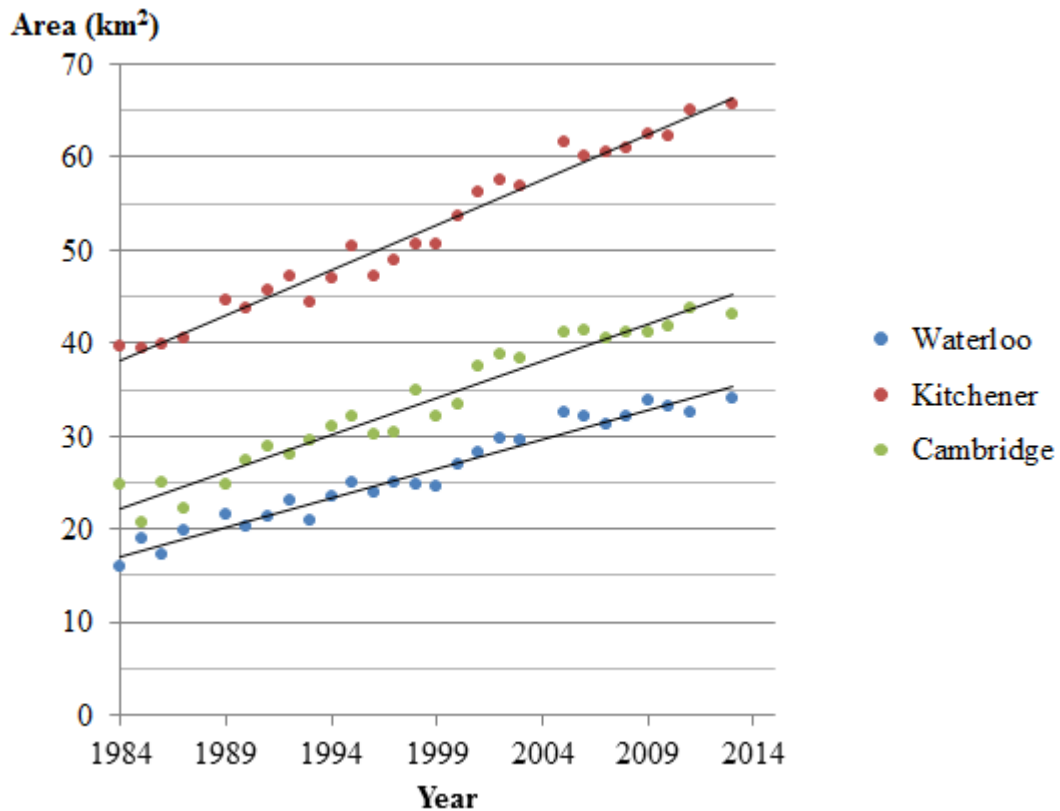


Figure 5.12 Dynamic change of low-density urban built-up area of Waterloo, Kitchener, and Cambridge from 1984 to 2013

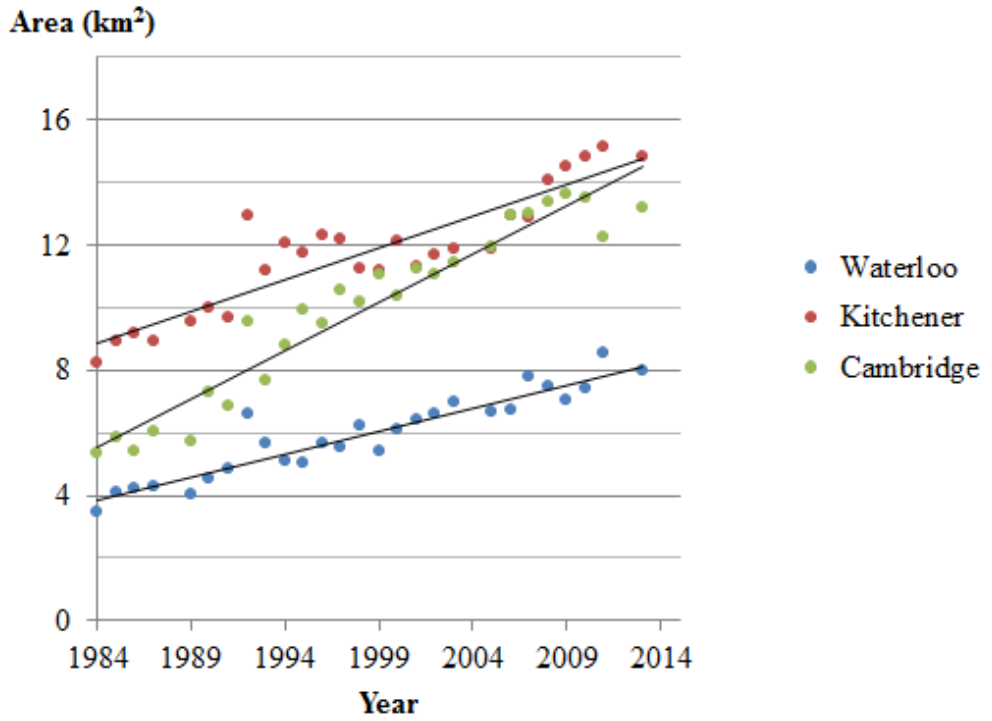


Figure 5.13 Dynamic change of high-density urban built-up area of Waterloo, Kitchener, and Cambridge from 1984 to 2013

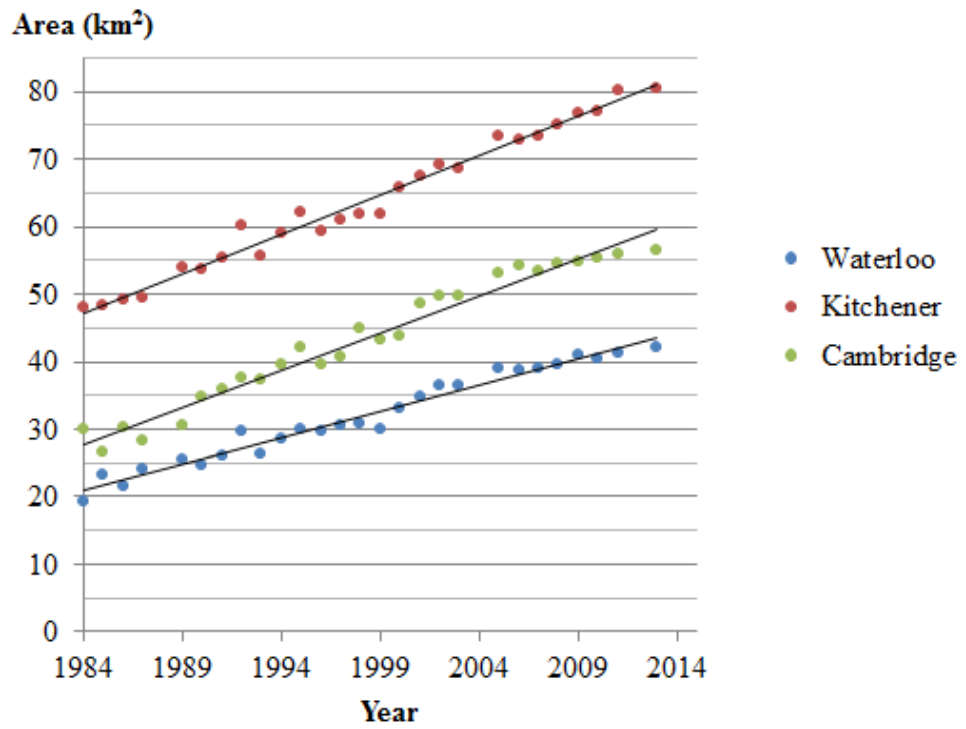


Figure 5.14 Dynamic change of total urban built-up area of Waterloo, Kitchener, and Cambridge from 1984 to 2013

It can be observed in these three figures that all cities experiences unstable built-up development based on the measured data. The linear fitted lines reveal the growth trend and growth rate of built-up area in each city. Regression coefficients and fit of linear regression model are summarized in Table 5.7. Nine linear models are generated. According to the values of R^2 , all of them are high values (greater than 0.8) and most of them are greater than 0.9, demonstrating that the trend of built-up area growth is well fitted by the linear model. By observing the figures, scatters representing low-density built-up area and total built-up area are mostly concentrated near the fitted lines, while the scatters representing high-density built-up area fluctuate relatively severe around the fitted lines than other measurements. In addition, significant level is another indicator of evaluating the model effectiveness. The values of significance are all less than 0.001 implying that the relationship between built-up area and its corresponding year is significant for all linear models.

Values under “Intercept” columns are the estimated area of low-density, high-density and total built-up area at year 1984 of each city by km^2 and percentage of its municipality area. Result shows that Kitchener has the largest area of both low-density and high-density types, which are $17.038 \pm 1.139 \text{ km}^2$ or $27.764 \pm 1.04\%$ and $8.898 \pm 0.083 \text{ km}^2$ or $6.451 \pm 0.61\%$ estimated at year 1984, respectively, while Waterloo has the smallest area. The rate of linear growth is observable referring to the “Slope” columns. The values show that Kitchener has greatest increase in low-density built-up area, at a rate of $0.969 \pm 0.033 \text{ km}^2/\text{year}$, or $0.703 \pm 0.02\%$ of the city area per year. Waterloo and Cambridge develop relatively slower, at a rate of $0.629 \pm 0.026 \text{ km}^2/\text{year}$ and $0.791 \pm 0.036 \text{ km}^2/\text{year}$, respectively. As for high-density built-up area, Cambridge develops much more rapid, with the area increasing at a rate of $0.309 \pm 0.017 \text{ km}^2/\text{year}$. Comparatively, Waterloo increases much slower, at a rate of $0.148 \pm 0.011 \text{ km}^2/\text{year}$,

and that of Kitchener, area increases at a rate of 0.203 ± 0.019 km²/year. Putting low-density and high-density built-up area together, Kitchener and Cambridge grows with similar rates, which are 1.172 ± 0.032 km²/year and 1.100 ± 0.041 km²/year respectively, while Waterloo increases relatively slower, at a rate of 0.777 ± 0.027 km²/year.

Table 5.7 Summary of regression coefficient and fit of linear regression model of urban built-up area over time from 1984 to 2013 for Waterloo, Kitchener, Cambridge

Municipality		Intercept (estimated at year 1984)			Slope			R ²
		km ² (S.E.)	% (S.E.)	Sig.	km ² /year (S.E.)	%/year (S.E.)	Sig.	
Low-density	Waterloo	17.038 (1.139)	26.33 (1.76)	.000	0.629 (0.026)	0.97 (0.04)	.000	0.959
	Kitchener	38.293 (1.430)	27.76 (1.04)	.000	0.969 (0.033)	0.70 (0.02)	.000	0.973
	Cambridge	22.246 (1.593)	19.33 (1.38)	.000	0.791 (0.036)	0.69 (0.03)	.000	0.950
High-density	Waterloo	3.774 (0.466)	5.83 (0.72)	.000	0.148 (0.011)	0.23 (0.02)	.000	0.886
	Kitchener	8.898 (0.843)	6.45 (0.61)	.000	0.203 (0.019)	0.15 (0.01)	.000	0.816
	Cambridge	5.524 (0.761)	4.80 (0.66)	.000	0.309 (0.017)	0.27 (0.02)	.000	0.927
Total	Waterloo	20.970 (1.195)	32.40 (1.85)	.000	0.777 (0.027)	1.20 (0.04)	.000	0.970
	Kitchener	47.151 (1.405)	34.19 (1.02)	.000	1.172 (0.032)	0.85 (0.02)	.000	0.982
	Cambridge	27.800 (1.792)	24.16 (1.56)	.000	1.100 (0.041)	0.96 (0.04)	.000	0.967

(S.E. = standard error; Sig. = significance)

5.4 Chapter Summary

This chapter shows the major results obtained based on the methodology. Classification maps generated by four classifiers were compared in terms of accuracy assessment. According to the comparison result, machine learning classifiers provided better results than MLC. And finally SVM classifier was selected as the most appropriate classifier to process all Landsat

images in this study. Subsequently, based on LULC information extracted from the classification maps, bi-temporal, multi-temporal, and time-serial change detection analysis were conducted to comprehensively explore the change process both qualitatively and quantitatively. Result shows that urbanization is the major cause that leads to change, replacing large area of vegetation. The most significant change occurred during 1996 to 2002 time period. More detailed dynamic change process can be detected by time-serial analysis.

Urban growth analysis is also included in this chapter. Three urban growth patterns, which are outward urban sprawl, growth in isolation, and inward expansion, were detected by observing classification maps spatially. The dominant growth pattern is the outward growth. In addition, growth trend and growth rate of Waterloo, Kitchener, and Cambridge were analyzed as well. Simple linear regression model was applied to the data representing the area of built-up area obtained from the high-frequent classification maps. Strong relationship was shown between the area and the year detected. Kitchener experiences highest growth rate of low-density built-up area, while high-density built-up area increases most rapidly in Cambridge. In total, Kitchener and Cambridge grow relatively faster than Waterloo over this time period.

Chapter 6 Conclusions and Recommendations

In this study, LULC change dynamics and urban growth trend of the Region of Waterloo were successfully detected by using long-term Landsat archive data. In this chapter, key findings, significance and contributions of this study will be summarized. Moreover, some limitations and uncertainties of this study will be considered as well. Potential future studies will be conceived and proposed in the end.

6.1 Key Findings of the Study

This study aims to detect the LULC change dynamics and monitor urban growth process of the urban area of Region of Waterloo using long-term Landsat record. By discussing the fulfillment of the objectives defined in the beginning, key findings and contributions of this study will be summarized.

6.1.1 Performance of Classifiers

There are several key findings of this study. First of all, classification is the most important process that determines the reliability of the results. SVM outperformed MLC, ANN, and RF based on its highest overall accuracy in this study. However, it is insufficient to indicate that SVM is the best classifier among the four classifiers. Each classifier has its own advantages and disadvantages. Based on the overall accuracy, all classifiers can generate acceptable results. MLC obtained result with the lowest accuracy in this study, but the idea behind the algorithm is easy to understand and it needs the least parameters to be tuned and least operation time. Among the machine learning classifiers, the running time of ANN classification was the longest, while the time of RF classification was the shortest. Also, there were more parameters that need to be defined when using ANN classifier. ANN is sensitive to

the number of hidden layer and the type of activation function. Compared to SVM, RF is less sensitive to the input parameters. Additionally, RF also can provide intermediate OOB estimate of error rate during training process to demonstrate whether the defined parameters are the most appropriate or not.

As a whole, machine learning classifiers performed much better than traditional MLC algorithms when dealing with digital satellite data of complex urban area landscape. When selecting training samples, some mixed urban pixels might be selected. Especially for low-density built-up area, many pixels are not pure pixels that only represent built-up land cover type. The mixed pixels might contain land cover type of grassland or soil/barren land. Moreover, due to the phenological effect, some pixels representing green cropland and grassland have very similar spectral signature so that they are hard to be distinguished from each other. Based on their performance, machine learning classifiers exhibit their robustness in dealing with such complex situation. Furthermore, the robustness of SVM was also verified by using long-term Landsat dataset. High overall accuracy of the classification maps can be guaranteed.

6.1.2 LULC Change Dynamics of Urban Area of Region of Waterloo

With the free access to Landsat archive data, LULC change dynamics can be completely detected by extracting LULC information from the temporally dense and extensive time-serial classification maps. Complexities of LULC change of urban systems of Region of Waterloo can be successfully detected. One major finding was obtained from the time-serial trajectory analysis that LULC change processes of urban area of Region of Waterloo were very complex, not simply increasing or decreasing all the way. Taking built-up area as an example, it experienced dramatic growth over the time period, but the coverage still had irregular

fluctuation up and down during the process. Water and forest, which was not supposed to change too much, also experienced observable fluctuation during this time period.

Apart from the real change, those fluctuations might be resulted from other two aspects. One is the classification error which cannot be completely eliminated because of the medium spatial resolution of Landsat data and atmospheric noise. The other one might be the phenological effects that influence the classification results. Under this circumstance, the use of long-term dense datasets reveals its superiority of reducing the impacts caused by those factors. Time-series trajectory analysis detects the long-term change of complex ecosystems in a macroscopic view, reducing reliance on one single classification map. For example, it can be detected that there was an acceleration of urban built-up area growth of Region of Waterloo in 1990s and a deceleration in late 2000s. Such valuable information of change complexities, which are required by environmental researchers and decision makers, cannot be detected by bi-temporal method or multi-temporal method.

6.1.3 Urban Growth Monitoring of the Region of Waterloo

In this study, the predominant change is urban growth. One important finding is that the growth of urban built-up area of Region of Waterloo presents three types of pattern. The major growth pattern is the outward sprawl mainly caused by the expansion of low-density built-up (residential) area towards suburban area. The second type of urban growth is the inward intensification, occupying some vegetated area inside the city. The third pattern is the growth in isolation, which is mainly due to industrial development.

Another finding of this study is that the urban growth trend and growth rate of each city can be truthfully presented and estimated based on the built-up area trajectories. Cambridge experienced dramatic growth of high-density built-up area with fastest growth rate among the

three cities. Kitchener had the most rapid growth rate of low-density built-up area and of total built-up area. Meanwhile, Waterloo had the slowest growth rate of both low-density and high-density built-up areas. The regression model based on the dense dataset can generate more reliable result than sparse dataset. Likewise, the limitation of data spatial resolution, the effect of phenological change, and the atmospheric noise introduced by satellite images can be reduced by using such high dense dataset. The results are very valuable for the regional governments to make decisions of regional development in the future.

In summary, this study has several contributions. First of all, this study verifies SVM as a robust classifier for urban area classification, which is tested by using long-term Landsat data. Second, since this study used the most recent 2013 Landsat 8 data, the change detection results of the urban area of Region of Waterloo are the most up-to-date. The third contribution is that this is the first attempt to conduct long-term analysis of change dynamics and urban growth Region of Waterloo. The results are of great value for environmental researchers to perform further environmental studies, and for policy makers and planners of Region of Waterloo for better environmental management and urban planning purposes. Moreover, the methods of long-term change dynamics analysis and urban growth trend monitoring used in this study can inform further studies in various remote sensing fields by using long-term temporally dense and extensive datasets with the booming of remote sensing data volume.

6.2 Limitations and Uncertainties of This Study

This study has focused on change detection and urban growth analysis using high-frequency Landsat dataset. There are some limitations and uncertainties in this study. From data perspective, in order to detect long-term dynamic change and generate linear regression model of urban built-up area, remote sensing data which are sufficiently dense and extensive in time

are required. With the long-term record and free open policy, Landsat archive data are the best choice for this study. However, Landsat data with medium spatial resolution (30m * 30m) cannot detect very subtle objects on land surface. Therefore, classification errors will be introduced and cannot be eliminated. Moreover, from classification perspective, in this study, classification was performed on each Landsat image taken from 1984 to 2013 except for 1988, 2004, and 2012. Training samples were selected for each year. In this way, the quality of classification maps can be guaranteed because the training samples are sufficient. However, for high dense dataset, selecting training samples for each year was a huge task in this study. The work might become more burdensome when the study area is large. Additionally, it is hard to control all sets of training samples with the same quality. Therefore, effective image normalization methods should be developed to let training sample selection process much easier. During classification process, parameters determination is critical for obtaining the best result. However, when employing machine learning classifiers, it is difficult to determine which combination of the parameter setting is the most superior.

Furthermore, in terms of the result of linear regression analysis of urban built-up area, the regression lines were well fitted by the extracted built-up area information from the classification maps. Though the fitted lines can well represent the growth trend of each city, it cannot be concluded that the linear model is the best model that exactly reflect the real urbanization process of Region of Waterloo. It only can be concluded that the linear model can successfully reflect the general trend of urban growth during 1984 to 2013 time period. Since urbanization is a very long and complex process, urban growth model can be very complicated. In order to detect the urban growth trend more accurate, the entire time span should be extended and more statistical growth models should be generated and employed.

6.3 Recommendations for Future Studies

Based on both the superiorities and limitations of this study, some potential future studies are proposed here. With the global coverage of Landsat data, the time-serial change detection method can also be applied to other cities or metropolitan areas or even global scale to detect the LULC dynamic change. As for urban area analysis using remote sensing data, efforts also can be put into improving the urban area classification result. Since machine learning classifiers can deal with high dimensional dataset, various input features can be integrated together to investigate their effectiveness of improving the classification result. Also, studies can be focused on feature selection using RF algorithm to select useful features obtained from not only different remote sensing data, but also environmental variables and geographical parameters for urban area classification improvement. Moreover, in addition to time-serial remote sensing data, GIS data and socio-economic data can be also incorporated to generated more accurate urban growth model. Furthermore, the accessibility of long-term Landsat record also makes it possible to detect time-serial dynamic change of different land cover types, such as dynamic change of forest cover, glacier, watershed, coastline, etc.

References

- Abd El-Kawy, O. R., Rød, J. K., Ismail, H. a., & Suliman, a. S. (2011). Land use and land cover change detection in the western Nile delta of Egypt using remote sensing data. *Applied Geography*, 31(2), 483-494.
- Afify, H. a. (2011). Evaluation of change detection techniques for monitoring land-cover changes: A case study in new Burg El-Arab area. *Alexandria Engineering Journal*, 50(2), 187-195.
- Akar, Ö., & Güngör, O. (2012). Classification of multispectral images using Random Forest algorithm. *Journal of Geodesy and Geoinformation*, 1(2), 105-112.
- Alumutairi, A., & Warner, T. A. (2010). Change detection accuracy and image properties: a study using simulated data. *Remote Sensing*, 2, 1508-1529.
- Alphan, H. (2011). Comparing the utility of image algebra operations for characterizing landscape changes: the case of the Mediterranean coast. *Journal of Environmental Management*, 92(11), 2961-71.
- Anderson, J. R., Hardy, E. E., Roach, J. T., & Witmer, R. E. (1976). A land use and land cover classification system for use with remote sensor data. United States Government Printing Office, Washington: 1976.
- Benediktsson, J. A., Chanussot, J., & Fauvel, M. (2007). Multiple classifier systems in remote sensing : from basics to recent developments. *MCS 2007, LNCS 4472*, 501-512.
- Bhatta, B. (2010). Analysis of urban growth and sprawl from remote sensing data. ISBN: 978-3-642-05298-9. Springer.

- Bischof, H., Schneider, W., & Pinz, A. J. (1992). Multispectral classification of Landsat-Images using neural networks. *IEEE Transactions on Geoscience and Remote Sensing*, 30 (3), 482-490.
- Breiman, L. (2001). Random Forests. *Machine Learning*, 45, 5-32.
- Breiman L. (2002), Manual on setting up, using, and understanding random forests V3.1.
Retrieved from: http://oz.berkeley.edu/users/breiman/Using_random_forests_V3.1.pdf
- Byrne, G. F., Crapper, P. F., & Mayo, K. K. (1980). Monitoring land-cover change by principal component analysis of multitemporal landsat data. *Remote Sensing of Environment*, 10(3), 175-184.
- Canada's Technology Triangle. (2013). Community profile 2013. Retrieved from:
<http://www.techtriangle.ca/en/ataglance/AtAGlanceWaterlooRegion.asp>
- Congalton, R. (1991). A review of assessing the accuracy of classifications of remotely sensed data. *Remote Sensing of Environment*, 46, 35-46.
- Congalton, R. G., & Green, K. (1999). *Assessing the Accuracy of Remotely Sensed Data: Principles and Practices*. ISBN 0-87371-986-7. CRC Press.
- Coppin, P., Jonckheere, I., Nackaerts, K., Muys, B., & Lambin, E. (2004). Digital change detection methods in ecosystem monitoring: a review. *International Journal of Remote Sensing*, 25(9), 1565-1596.
- Dawelbait, M., & Morari, F. (2012). Monitoring desertification in a Savannah region in Sudan using Landsat images and spectral mixture analysis. *Journal of Arid Environments*, 80, 45-55.
- Deng, J.-S., Wang, K., Li, J., & Deng, Y.-H. (2009). Urban land use change detection using multisensor satellite images. *Pedosphere*, 19(1), 96-103.

- Estes, A. B., Kuemmerle, T., Kushnir, H., Radeloff, V. C., & Shugart, H. H. (2012). Land-cover change and human population trends in the greater Serengeti ecosystem from 1984–2003. *Biological Conservation*, *147*(1), 255-263.
- Fitzgerald, R. W., & Lees, B. G. (1994). Assessing the classification accuracy of multisource remote sensing data. *Remote Sensing of Environment*, *47*, 362-368.
- Frohn, R., & Arellano-Neri, O. (2005). Improving artificial neural networks using texture analysis and decision trees for the classification of land cover. *GIScience & Remote Sensing*, *42*(1), 44-65.
- Geomatica. (2013). Atmospheric correction (with ATCOR). Retrieved from: <http://www.pcigeomatics.com/pdf/AtmosphericCorrection.pdf>
- Gillanders, S. N., Coops, N. C., Wulder, M. a., & Goodwin, N. R. (2008). Application of landsat satellite imagery to monitor land-cover changes at the Athabasca Oil Sands, Alberta, Canada. *Canadian Geographer*, *52*(4), 466-485.
- Gislason, P. O., Benediktsson, J. A., & Sveinsson, J. R. (2006). Random Forests for land cover classification. *Pattern Recognition Letters*, *27*(4), 294-300.
- Hadjimitsis, D. G., Papadavid, G., Agapiou, A., Themistocleous, K., Hadjimitsis, M. G., & Retalis, A. (2010). Atmospheric correction for satellite remotely sensed data intended for agricultural applications : impact on vegetation indices. *Natural Hazards and Earth System Sciences*, *10*, 89-95.
- Hansen, M. C., & Loveland, T. R. (2012). A review of large area monitoring of land cover change using Landsat data. *Remote Sensing of Environment*, *122*, 66-74.

- Hayes, D. J., & Sader, S. A. (2001). Comparison of change detection techniques for monitoring tropical forest clearing and vegetation regrowth in a time series. *Photogrammetric Engineering & Remote Sensing*, 67(9), 1067-1075.
- Hodge, G., & Gordon, D. L. A. (2008). *Planning Canadian Communities: An Introduction to the Principles, Practice, and Participants*, 5th Edition. Thomson Canada.
- Huang, C., Davis, L. S., & Townshend, J. R. G. (2002a). An assessment of support vector machines for land cover classification. *International Journal of Remote Sensing*, 23(4), 725-749.
- Huang, C., Davis, L. S., & Townshend, J. R. G. (2002b). An assessment of support vector machines for land cover classification. *International Journal of Remote Sensing*, 23(4), 725-749.
- Huang, Y., Fipps, G., Lacey, R. E., & Thomson, S. J. (2011). Landsat satellite multi-Spectral image classification of land cover and land use changes for GIS-based urbanization analysis in irrigation districts of Lower Rio Grande Valley of Texas. *Applied Remote Sensing Journal*, 2(1), 27-36.
- Huiping, Z., Hong, J., & Qinghua, H. (2011). Landscape and water quality change detection in urban wetland: a post-classification comparison method with IKONOS Data. *Procedia Environmental Sciences*, 10, 1726-1731.
- Im, J., Jensen, J. R., & Tullis, J. a. (2008). Object-based change detection using correlation image analysis and image segmentation. *International Journal of Remote Sensing*, 29(2), 399-423.

- Immitzer, M., Atzberger, C., & Koukal, T. (2012). Tree species classification with random forest using very high spatial resolution 8-band WorldView-2 Satellite Data. *Remote Sensing*, 4(12), 2661-2693.
- IRS (2013). ITC's database of satellites and sensors. Faculty of Geo-Information Science and Earth Observation (ITC). University of Twente. Retrieved from: <http://www.itc.nl/research/products/sensordb/AllSatellites.aspx>
- Japan Association of Remote Sensing (JARS). (1999). Remote sensing notes. Retrieved from: <http://wtlab.iis.u-tokyo.ac.jp/~wataru/lecture/rsgis/index.htm>
- Jensen, J. R. (2005). *Introductory of Digital Image Processing: A Remote Sensing Perspective*, 3rd Edition. Pearson Education. ISBN 0-13-145361-0.
- Jensen, J. R. (2006). *Remote Sensing of the Environment: An Earth Resource Perspective*, 2nd Edition. Pearson Education. ISBN 0-13-188950-8.
- Jha, C. S., & Unni, N. V. M. (1994). Digital change detection of forest conversion of a dry tropical Indian forest region. *International Journal of Remote Sensing*, 15(13), 2543-2552.
- Jieli, C., Manchun, L. I., Yongxue, L. I. U., Chenglei, S., & Wei, H. U. (2008). Extract residential areas automatically by new built-up index. School of Geographic & Oceanographic Science. Nanjing University.
- Kaufmann, R. K., & Seto, K. C. (2001). Change detection, accuracy, and bias in a sequential analysis of Landsat imagery in the Pearl River Delta, China: econometric techniques. *Agriculture, Ecosystems & Environment*, 85(1-3), 95-105.
- Kennedy, R. E., Townsend, P. a., Gross, J. E., Cohen, W. B., Bolstad, P., Wang, Y. Q., & Adams, P. (2009). Remote sensing change detection tools for natural resource

- managers: Understanding concepts and tradeoffs in the design of landscape monitoring projects. *Remote Sensing of Environment*, 113(7), 1382-1396.
- Kleynhans, W., Olivier, J. C., Wessels, K. J., Salmon, B. P., van den Bergh, F., & Steenkamp, K. (2011). Detecting land cover change using an extended Kalman filter on MODIS NDVI time-series data. *IEEE Geoscience and Remote Sensing Letters*, 8(3), 507-511.
- Kontoos, C. C. (2008). Operational land cover change detection using change vector analysis. *International Journal of Remote Sensing*, 29(16), 4757-4779.
- Kotsiantis, S. B. (2007). Supervised machine learning : a review of classification techniques. *Informatica* 31, 249-268.
- Liaw, A., & Wiener, M. (2002). Classification and regression by random forest. *R News*, 2(3), 18-22.
- Lu, D., Batistella, M., Moran, E., & Mausel, P. (2004). Application of spectral mixture analysis to Amazonian land-use and land-cover classification. *International Journal of Remote Sensing*, 25(23), 5345-5358.
- Lu, D., Mausel, P., Brondizio, E., & Moran, E. (2004). Change detection techniques. *International Journal of Remote Sensing*, 25(12), 2365-2407.
- Lu, D., Mausel, P., Batistella, M., & Moran, E. (2005). Land-cover binary change detection methods for use in the moist tropical region of the Amazon: a comparative study. *International Journal of Remote Sensing*, 26(1), 101-114.
- Lu, D., & Weng, Q. (2007). A survey of image classification methods and techniques for improving classification performance. *International Journal of Remote Sensing*, 28(5), 823-870.

- Lu, D., Moran, E., & Hetrick, S. (2011). Detection of impervious surface change with multitemporal Landsat images in an urban-rural frontier. *ISPRS Journal of Photogrammetry and Remote Sensing*, 66(3), 298-306.
- Lu, D., & Weng, Q. (2004). Spectral mixture analysis of the urban landscape in Indianapolis with Landsat ETM+ imagery. *Photogrammetric Engineering & Remote Sensing*, 70(9), 1053-1062.
- Lu, D., & Weng, Q. (2005). Urban classification using full spectral information of Landsat ETM+ imagery in Marion County , Indiana. *Photogrammetric Engineering & Remote Sensing* 71(11), 1275-1284.
- Lu, D., & Weng, Q. (2006). Use of impervious surface in urban land-use classification. *Remote Sensing of Environment*, 102(1-2), 146-160.
- Lunetta, R. S., & Elvidge, C. D. (1998). *Remote Sensing Change Detection: Environmental Monitoring Methods and Applications*. Sleeping Bear Press. ISBN 1-57504-037-9.
- Lunetta, R. S., Johnson, D. M., Lyon, J. G., & Crotwell, J. (2004). Impacts of imagery temporal frequency on land-cover change detection monitoring. *Remote Sensing of Environment*, 89, 444-454.
- Macleod, R. D., & Congalton, R. G. (1998). A quantitative comparison of change-detection algorithms for monitoring eelgrass from remotely sensed data. *Photogrammetric Engineering & Remote Sensing*, 64(3), 207-216.
- Manavalan, P., Kesavasamy, K., & Adiga, S. (1995). Irrigated crops monitoring through seasons using digital change detection analysis of IRS-LISS 2 data. *International Journal of Remote Sensing*, 16(4), 633-640.

- Masek, J. G., Lindsay, F. E., & Goward, S. N. (2000). Dynamics of urban growth in the Washington DC metropolitan area, 1973-1996, from Landsat observations. *International Journal of Remote Sensing*, 21(18), 3473-3486.
- Mellor, A., Haywood, A., Stone, C., & Jones, S. (2013). The performance of random forests in an operational setting for large area sclerophyll forest classification. *Remote Sensing*, 5(6), 2838-2856.
- Meyers, L. S., Gamst, G., & Guarino, A. J. (2006). *Applied Multivariate Research: Design and Interpretation*. ISBN 1-4129-0412-9. Sage Publications.
- Munthali, K. G., & Murayama, Y. (2011). Land use/cover change detection and analysis for Dzalanyama forest reserve, Lilongwe, Malawi. *Procedia Social and Behavioral Sciences*, 21, 203-211.
- Nemmour, H., & Chibani, Y. (2011). Support vector machines for automatic multi-class change detection in Algerian Capital using landsat TM imagery. *Journal of the Indian Society of Remote Sensing*, 38(4), 585-591.
- Pal, M. (2005). Random forest classifier for remote sensing classification. *International Journal of Remote Sensing*, 26(1), 217-222.
- Pal, M., & Mather, P. M. (2005). Support vector machines for classification in remote sensing. *International Journal of Remote Sensing*, 26(5), 1007-1011.
- Parra, G. A., Mouchot, M. C., & Roux, C. (1996). A multitemporal land-cover change analysis tool using change vector and principal components analysis. *IEEE 0-7803-3068-4/96*, 1753-1755.

- Patino, J. E., & Duque, J. C. (2013). A review of regional science applications of satellite remote sensing in urban settings. *Computers, Environment and Urban Systems*, 37, 1-17.
- Peiman, R. (2011). Pre-classification and post-classification change-detection techniques to monitor land-cover and land-use change using multi-temporal Landsat imagery: a case study on Pisa Province in Italy. *International Journal of Remote Sensing*, 32(15), 4365-4381.
- Powell, R., Roberts, D., Dennison, P., & Hess, L. (2007). Sub-pixel mapping of urban land cover using multiple endmember spectral mixture analysis: Manaus, Brazil. *Remote Sensing of Environment*, 106(2), 253-267.
- Prakash, A., & Gupta, R. P. (1998). Land-use mapping and change detection in a coal mining area --- a case study in the Jharia coalfield, India. *International Journal of Remote Sensing*, 19(3), 391-410.
- Qluch, R. (2002). Urban growth detection using texture analysis on merged Landsat TM and SPOT-P data. *Photogrammetric Engineering & Remote Sensing*, 68(12), 1283-1288.
- Region of Waterloo. (2006). Regional Growth Management Strategy (RGMS). Retrieved from: <http://www.regionofwaterloo.ca/en/aboutTheEnvironment/resources/RegionalGrowthManagement.pdf>
- Region of Waterloo. (2006). Regional Growth Management Strategy (RGMS) highlights brochure. Retrieved from: <http://www.regionofwaterloo.ca/en/aboutTheEnvironment/resources/FINALRGMSBrochure2006.pdf>
- Region of Waterloo. (2010). Regional Official Plan (ROP). Retrieved from:

<http://www.regionofwaterloo.ca/en/regionalGovernment/PreviousROP.asp>

- Ridd, M. K., & Hipple, J. D. (2006). *Remote Sensing of Human Settlements: Manual of Remote Sensing, 3rd Edition*. American Society for Photogrammetry and Remote Sensing. ISBN 1-57083-077-0.
- Rogan, J., & Chen, D. (2004). Remote sensing technology for mapping and monitoring land-cover and land-use change. *Progress in Planning*, 61(4), 301-325.
- Rozenstein, O., & Karnieli, A. (2011). Comparison of methods for land-use classification incorporating remote sensing and GIS inputs. *Applied Geography*, 31(2), 533-544.
- Sexton, J. O., Urban, D. L., Donohue, M. J., & Song, C. (2013). Long-term land cover dynamics by multi-temporal classification across the Landsat-5 record. *Remote Sensing of Environment*, 128, 246-258.
- Sexton, J. O., Song, X., Huang, C., & Channan, S. (2013). Urban growth of the Washington, D.C.-Baltimore, MD metropolitan region from 1984 to 2010 by annual, landsat-based estimates of impervious cover. *Remote Sensing of Environment*, 129, 42-53.
- Singh, A. (1989). Digital change detection techniques using remotely-sensed data. *International Journal of Remote Sensing*, 10 (6), 989-1003.
- Sleeter, B.M., Wilson, T.S., & Acevedo, W. (2012). Status and trends of land change in the Western United States—1973 to 2000: USGS Professional Paper 1794–A, 324 p. Retrieved from: <http://pubs.usgs.gov/pp/1794/a/>.
- Slonecker, E. T., Jennings, D. B., & Garofalo, D. (2001). Remote sensing of impervious surfaces: A review. *Remote Sensing Reviews*, 20(3), 227-255.
- Somers, B., Asner, G. P., Tits, L., & Coppin, P. (2011). Endmember variability in Spectral Mixture Analysis: A review. *Remote Sensing of Environment*, 115(7), 1603-1616.

- Song, X., Duan, Z., & Jiang, X. (2012). Comparison of artificial neural networks and support vector machine classifiers for land cover classification in Northern China using a SPOT-5 HRG image. *International Journal of Remote Sensing*, 33(10), 3301-3320.
- Statistics Canada. (2011). Focus on geography series, 2011 census. Retrieved from: <http://www12.statcan.gc.ca/census-recensement/2011/as-sa/fogs-spg/Facts-pr-eng.cfm?Lang=Eng&GK=PR&GC=35>
- Sundarakumar, K., Harika, M., Begum, S. K. A., Yamini, S., & Balakrishna, K. (2012). Land use and land cover change detection and urban sprawl analysis of Vijayamada city using multitemporal Landsat data. *International Journal of Engineering Science and Technology*, 4(01), 170-178.
- Tan, K. C., Lim, H. S., MatJafri, M. Z., & Abdullah, K. (2009). Landsat data to evaluate urban expansion and determine land use/land cover changes in Penang Island, Malaysia. *Environmental Earth Sciences*, 60(7), 1509-1521.
- Tang, J., Wang, L., & Yao, Z. (2008). Analyses of urban landscape dynamics using multi-temporal satellite images: A comparison of two petroleum-oriented cities. *Landscape and Urban Planning*, 87(4), 269-278.
- Thapa, R. B., & Murayama, Y. (2009). Urban mapping, accuracy, & image classification: A comparison of multiple approaches in Tsukuba City, Japan. *Applied Geography*, 29(1), 135-144.
- Thompson, S. K. (1992). *Sampling*. ISBN 0-471-54045-5. John Wiley & Sons, Inc.
- Tian, G., Jiang, J., Yang, Z., & Zhang, Y. (2011). The urban growth, size distribution and spatio-temporal dynamic pattern of the Yangtze River Delta megalopolitan region, China. *Ecological Modelling*, 222(3), 865-878.

- USGS. (2013). Landsat 8. Fact sheet 2013-3060. Retrieved from:
<http://pubs.er.usgs.gov/publication/fs20133060>
- USGS. (2013). Landsat---A global land-imaging mission. Fact sheet 2012-3072. Retrieved from: <http://pubs.usgs.gov/fs/2012/3072/fs2012-3072.pdf>
- USGS. (2013). Landsat 8. Retrieved from: <http://landsat.usgs.gov/landsat8.php>
- USGS. (2013). Landsat project statistics. Retrieved from:
http://landsat.usgs.gov/Landsat_Project_Statistics.php
- USGS. (2013). Landsat project description. Retrieved from:
http://landsat.usgs.gov/about_project_descriptions.php
- USGS. (2013). Landsat processing details. Retrieved from:
http://landsat.usgs.gov/Landsat_Processing_Details.php
- Walter, V. (2004). Object-based classification of remote sensing data for change detection. *ISPRS Journal of Photogrammetry and Remote Sensing*, 58(3-4), 225-238.
- Waqar, M. M., Mirza, J. F., Mumtaz, R., & Hussain, E. (2012). Development of New Indices for Extraction of Built-Up Area & Bare Soil. *Open Access Scientific Reports*, 1(1), 1-4.
- Weng, Q. (2012). Remote sensing of impervious surfaces in the urban areas: Requirements, methods, and trends. *Remote Sensing of Environment*, 117, 34-49.
- Wulder, M. A., White, J. C., Masek, J. G., Dwyer, J., & Roy, D. P. (2011). Continuity of Landsat observations: short term considerations. *Remote Sensing of Environment*, 115, 747-751.
- Xiaolu, S., & Bo, C. (2011). Change detection using change vector analysis from Landsat TM images in Wuhan. *Procedia Environmental Sciences*, 11, 238-244.

- Xu, H. (2007). Extraction of Urban Built-up Land Features from Landsat Imagery Using a Thematic- oriented Index Combination Technique, *Photogrammetric Engineering & Remote Sensing*, 73(12), 1381-1391.
- Xu, H. (2010). Analysis of impervious surface and its impact on urban heat environment using the normalized difference impervious surface index (NDISI). *Photogrammetric Engineering & Remote Sensing*, 76(5), 557-565.
- Yang, L., Xian, G., Klaver, J. M., & Deal, B. (2003). Urban land-cover change detection through sub-pixel imperviousness mapping using remotely sensed data. *Photogrammetric Engineering & Remote Sensing*, 69(9), 1003-1010.
- Yang, X. (2002). Satellite monitoring of urban spatial growth in the Atlanta Metropolitan Area. *Photogrammetric Engineering & Remote Sensing*, 68(7), 725-734.
- Yang, X. (2011). *Urban Remote Sensing: Monitoring, Synthesis and Modeling in the Urban Environment*. John Wiley & Sons.
- Yin, J., Yin, Z., Zhong, H., Xu, S., Hu, X., Wang, J., & Wu, J. (2011). Monitoring urban expansion and land use/land cover changes of Shanghai metropolitan area during the transitional economy (1979-2009) in China. *Environmental Monitoring and Assessment*, 177(1-4), 609-621.
- Yuan, F., Sawaya, K. E., Loeffelholz, B. C., & Bauer, M. E. (2005). Land cover classification and change analysis of the Twin Cities (Minnesota) Metropolitan Area by multitemporal Landsat remote sensing. *Remote Sensing of Environment*, 98(2-3), 317-328.

Zha, Y., Gao, J., & Ni, S. (2003). Use of normalized difference built-up index in automatically mapping urban areas from TM imagery. *International Journal of Remote Sensing*, 24(3), 583-594.

Zhao, H., Chen, X., & Area, A. S. (2005). Use of normalized difference bareness index in quickly mapping bare areas from TM / ETM+. *IEEE Transactions on Geoscience and Remote Sensing* 4(5), 1666-1668.

Appendix I

Equations of parameters of linear regression analysis

$$S_{\widehat{\beta}_1} = \sqrt{\frac{\frac{1}{n-2} \sum_{i=1}^n \widehat{\varepsilon}_i^2}{\sum_{i=1}^n (x_i - \bar{x})^2}}$$

$$S_{\widehat{\beta}_0} = S_{\widehat{\beta}_1} \sqrt{\frac{1}{n} \sum_{i=1}^n x_i^2}$$

$S_{\widehat{\beta}_1}$ is the standard error of estimated β_1 ; $S_{\widehat{\beta}_0}$ is the standard error of estimated β_0 .

$$R^2 = \frac{SSR}{SST} = 1 - \frac{SSE}{SST}$$

SST is the total sum of squares; SSR is the residual sum of squares; and SSE is the sum of squared errors.

$$SST = \sum_{i=1}^n (Y_i - \bar{Y})^2$$

$$SSR = \sum_{i=1}^n (\widehat{Y}_i - \bar{Y})^2$$

$$SSE = \sum_{i=1}^n (Y_i - \widehat{Y}_i)^2$$

\bar{Y} is the mean of Y_i .

Appendix II

The R script for random forest classification

###Invoking the R packages

```
library(sp)
library(maptools)
library(randomForest)
library(raster)
library(rgdal)
```

###Reading the .txt files of each band and the training data

```
train = scan('D:/RF classification/txt/roi.txt')
b1 = scan('D:/RF classification/txt/b1.txt')
b2 = scan('D:/RF classification/txt/b2.txt')
b3 = scan('D:/RF classification/txt/b3.txt')
b4 = scan('D:/RF classification/txt/b4.txt')
b5 = scan('D:/RF classification/txt/b5.txt')
b7 = scan('D:/RF classification/txt/b7.txt')
```

###Store all layers into one dataframe

```
data_all = data.frame(class = train, t.1 = b1, t.2 = b2, t.3 = b3, t.4 = b4, t.5 = b5, t.6 = b7)
```

###Eliminate all data with value of 0

```
data <- data_all[data_all$class != 0, ]
data$class <- factor(data$class)
```

###Training using random forest

```
rf <- randomForest(class~., data = data, ntree = 500, mtry = 3, importance = T, proximity = T)
importance(rf)
print(rf)
varImpPlot(rf)
```

###Read the image and store the classification data as .tif file

```
satImage <- stack('D:/RF classification/t.tif')
outImage <- 'D:/RF classification/t_RF.tif'
```

###Classification

```
predict(satImage, rf, filename=outImage, progress='text', format='GTiff', datatype='INT1U',
type='response', overwrite=TRUE)
```

###Read reference data and classification data

```
ref = scan('D:/RF classification/txt/ref.txt')
t_RF = scan('D:/RF classification/txt/t_RF.txt')
```

###Accuracy assessment

```
acc_data = data.frame(ref, t_RF)
acc_data = acc_data[!acc_data$ref == 0,]
```

###Error matrix

```
acc = table(acc_data$t_RF, acc_data$ref)
acc
```

###Kappa coefficient

```
library(psych)
wkappa(acc)
```

Appendix III

Accuracy assessment of classification maps

	1984	1990	1996	2002	2008	2013
Overall accuracy (%)	90.37	92.90	88.67	88.55	92.08	92.84
Kappa coefficient	0.89	0.92	0.89	0.87	0.91	0.92